INFORMATION TO USERS

This manuscript has been reproduced from the microfilm master. UMI films the text directly from the original or copy submitted. Thus, some thesis and dissertation copies are in typewriter face, while others may be from any type of computer printer.

The quality of this reproduction is dependent upon the quality of the copy submitted. Broken or indistinct print, colored or poor quality illustrations and photographs, print bleedthrough, substandard margins, and improper alignment can adversely affect reproduction.

In the unlikely event that the author did not send UMI a complete manuscript and there are missing pages, these will be noted. Also, if unauthorized copyright material had to be removed, a note will indicate the deletion.

Oversize materials (e.g., maps, drawings, charts) are reproduced by sectioning the original, beginning at the upper left-hand corner and continuing from left to right in equal sections with small overlaps.

Photographs included in the original manuscript have been reproduced xerographically in this copy. Higher quality 6" x 9" black and white photographic prints are available for any photographs or illustrations appearing in this copy for an additional charge. Contact UMI directly to order.

Bell & Howell Information and Learning
300 North Zeeb Road, Ann Arbor, MI 48106-1346 USA

UMI®
800-521-0600

A New Sufficient-Order Blind Equalization Scheme

Vijay Jain

A Thesis

in

The Department

of

Electrical and Computer Engineering

Presented in Partial Fulfillment of the Requirements

for the Degree of Master of Applied Science at

Concordia University

Montréal, Québec, Canada

August 1999

National Library
of Canada

Acquisitions and
Bibliographic Services

395 Wellington Street
Ottawa ON K1A 0N4
Canada

Bibliothèque nationale
du Canada

Acquisitions et
services bibliographiques

395, rue Wellington
Ottawa ON K1A 0N4
Canada

Your file Votre référence

Our file Notre référence

0-612-43652-7

Canada

ABSTRACT

A New Sufficient-Order Blind Equalization Scheme

Vijay Jain

The data throughput or bandwidth efficiency of high-speed digital transmission over band-limited channels can be increased by employing a blind equalizer. The traditional blind equalization schemes, employing only adaptive finite impulse response (FIR) filter-based structures, perform poorly for maximum-phase communication channels having deep spectral nulls. This problem is due to the difficulty in modeling the inverse of the maximum-phase communication channel with a finite-length adaptive FIR filter. Attempts have been made to solve this problem by including both infinite impulse response (IIR) and FIR filters in the equalizer structure. However, these techniques are computationally demanding and are very complex for a hardware implementation. In this thesis a new sufficient-order blind equalization scheme is proposed that attempts to address some of the problems of the existing techniques.

The proposed sufficient-order blind equalization scheme is based on a structure that makes use of an adaptive IIR predictor, an FIR filter, an adaptive FIR filter, and two block-based time reversers. New algorithms for the adaptation of IIR predictor and FIR filter are proposed. The adaptation algorithm for the IIR predictor is derived based on the well known least mean square error criterion using a gradient method, and for the adaptation of the FIR filter, a constant modulus adaptive algorithm is proposed. It is shown that the proposed blind equalization scheme requires a substantially less amount of computations and is easy to implement.

The proposed sufficient-order blind equalization scheme is applied to various linear and deep-null minimum-phase, maximum-phase, and mixed-phase communication channels. From the experimental results, it is demonstrated that the proposed scheme estimates the unknown channels correctly and provides a better performance as compared to the existing schemes, in terms of the channel estimation, symbol error rate, and spectral response.

Bahubali Bhagwan ko Samarpit

ACKNOWLEDGMENTS

I would like to express my sincere gratitude to my supervisors, Dr. M. O. Ahmad and Dr. P. Jain, for providing the guidance and support that made this work possible. I am grateful for their extremely careful and thorough review of my thesis, and for their inspiration throughout the course of this work. I feel privileged for having the opportunity to work with them. I would also like to thank the members of my examination committee, Dr. M. N. S. Swamy, Dr. T. Fancott, and Dr. A. K. Elhakeem, for their helpful comments and suggestions.

I would like to express my deepest gratitude to my wife Tanu, for her love, patience, and sacrifices. I am heartily grateful to my parents for their love, support and sacrifices that they made in bringing me up.

I would also like to express my gratitude to my father-in-law and mother-in-law for their love and motivation. Many thanks are due to my brother-in-law Anupam, sister Meenakshi, brother Ajay, his wife Ritu, sister-in-law Piyu, and nieces Winnie and Nuppi for their indisputable love.

Thanks are also due to my friends for their help and advice.

Contents

List of Figures

List of Tables

List of Symbols

$\mathbf{a}(n)$	IIR predictor tap weight vector
b_n	Binary data sequence
$c(n)$	Convolutional noise
$dec(.)$	Decision function operator
$e(n)$	Estimation error
$f_X(x)$	Probability density function of data symbol $x(n)$
$g(.)$	Non-linear function operator
$\mathbf{h}$	Channel estimation vector
$h(n)$	Impulse response of the communication channel
n_c	Order of the channel
n_r	Length of the IIR predictor
$sgn(.)$	Signum function
$u(n)$	Equalizer input
$v(n)$	Additive white Gaussian noise
$\mathbf{w}(n)$	FIR filter tap weight vector
$w_i(n)$	Coefficients of the FIR filter
$\widehat{w}_i(n)$	Estimate of the FIR filter coefficients
$x(n)$	Channel input
$\widehat{x}(n)$	Estimate of the channel input
$\mathbf{z}(n)$	Input data vector of the FIR filter
E	Statistical expectation operator

G	Gain of the blind equalizer
J	Ensemble averaged cost function
$\widehat{J}$	Estimate of ensemble averaged cost function
N	Length of the FIR filter
R_p	Positive real constant
R_u	Autocorrelation function of the received signal $u(t)$
R_X	Autocorrelation function of a random process $X(t)$
T_b	Bit duration
δ_l	Kronecker delta
$\phi(t)$	Shaping pulse
γ	Adaptation constant for the estimation of output power of IIR predictor
μ	Step-size parameter
σ^2	Output power of the IIR predictor
ξ_i^l	ith coefficient of the minimum-phase communication channel
ξ_j^o	jth coefficient of the maximum-phase communication channel
$\psi(y)$	Dependence of the estimation error on the transversal filter output $y(n)$ in the least mean square algorithm
$\Psi(n)$	Input data vector of the IIR predictor

List of Acronyms

AR	Auto Regressive
ARMA	Auto Regressive Moving Average
ARMA-FOC	Auto Regressive Moving Average Fourth-Order Cumulants
AWGN	Additive White Gaussian Noise
BER	Bit Error Rate
CMA	Constant Modulus Adaptive
CTEA	Cross-Tricepstrum Equalization Algorithm
ETEA	Extended Tricepstrum Equalization Algorithm
FIR	Finite Impulse Response
HOS	Higher Order Statistics
iid	Independently and Identically Distributed
IIR	Infinite Impulse Response
ISI	Inter Symbol Interference
LLS-EA	Linear Least-Squares-Estimation Algorithm
LMS	Least Mean Square
MA	Moving Average
NLS-CF	Nonlinear Least-Squares-Cumulants Fitting
NLS-EA	Nonlinear Least-Squares-Estimation Algorithm
NPG	Nonminimum-Phase system identification with Gradient type algorithm
PAM	Pulse Amplitude Modulation
pdf	Probability Density Function

POPREA	Polyspectra and Prediction Equalization Approach
POTEA	Power Cepstrum and Tricoherence Equalization Algorithm
QAM	Quadrature Amplitude Modulation
SEMP	Spectrally Equivalent Minimum-Phase
SIMO	Single Input Multiple Output
SISO	Single Input Single Output
Std	Standard Deviation
TEA	Tricepstrum Equalization Algorithm

Chapter 1

Introduction

1.1 General

A communication channel well suited for the transmission of digital data (e.g., computer data) is the telephone channel that generally has a high signal-to-noise ratio. However, a practical deficiency of the telephone channel is the fact that it is bandwidth-limited [1]. There are two basic signal processing operations for the transmission of digital data on bandwidth-limited communication channels.

1. Discrete Pulse Amplitude Modulation (PAM) in which the amplitudes of successive pulses in a periodic pulse train with a discrete set of possible amplitude level are coded.

2. A linear modulation scheme in which a bandwidth conservation is performed.

When data are transmitted over the channel by means of a discrete PAM combined with a linear modulation scheme (e.g., quadriphase-shift keying), the number of detectable levels that the telephone channel can support is essentially limited by inter symbol interference (ISI) rather than by additive noise. ISI arises because of the "spreading" of a transmitted pulse due to the dispersive nature of the channel, which results in an overlap of adjacent pulses. If ISI is left unchecked, it can produce an error in the reconstructed data stream at the receiver output. In principle, if the channel is known precisely, it is virtually always possible to make the ISI arbitrarily small by using a suitable pair of transmitting and receiving filters. The transmitting filter is placed directly before the modulator, whereas

the receiving filter is placed directly after the demodulator [2]. Thus, insofar as ISI is concerned, we may consider the data transmission as being essentially bandwidth limited.

In a switched telephone network, there are two factors that contribute to the distribution of pulse distortion on different link connections:

1. Differences in the transmission characteristics of the individual links that may be switched together.

2. Differences in the number of links in a connection.

As a result, the telephone channel is random in the sense of being one of an ensemble of possible channels [2]. Consequently, the use of a fixed pair of transmitting and receiving filter designed on the basis of average channel characteristics may not adequately reduce inter symbol interference. Therefore, it is appropriate to assume that the actual channel used for transmission, which is well modeled as a linear system, is unknown to the receiver that must recover the digital information. In such a case, the problem is to design a corrective system which, when cascaded with the original system, produces an output that, in some sense, corrects the distortion caused by the channel and thus yields a replica of the desired transmitted signal. In digital communications such a corrective system is called an equalizer. Therefore, the system degradation due to ISI can be combatted by placing an equalizer in cascade with the channel as shown in Fig. 1.1.

Among the philosophies for adaptive equalization of data transmission systems, we may have a prechannel equalization at the transmitter or a post channel equalization at the receiver. Because the first approach requires a feedback channel, systems with adaptive equalization at the receiving end are generally preferred.

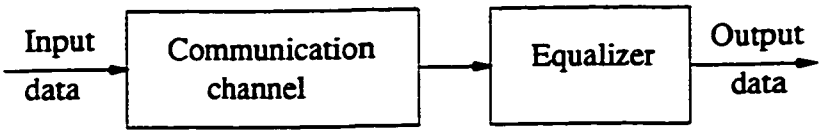

Figure 1.1: Block diagram of equalized channel.

In the context of linear system theory, we call the corrective system an inverse system, since it has a frequency response that is essentially the reciprocal of the frequency response of the system that causes the distortion. Some important elements of a baseband system are discussed in the following two sections.

1.2 Baseband PAM System

The basic elements of a baseband binary PAM system are shown in Fig. 1.2. The signal applied to the input of the system consists of a binary data sequence $\{b_n\}$ with a bit duration of T_b seconds; b_n has a binary value, 1 or 0. This signal is applied to a pulse generator, producing the pulse waveform

$$x(t) = \sum_{n=-\infty}^{\infty} x_n \phi(t - nT_b) \tag{1.1}$$

where $\phi(t)$ denotes the shaping pulse that is normalized, such that

$$\phi(0) = 1 \tag{1.2}$$

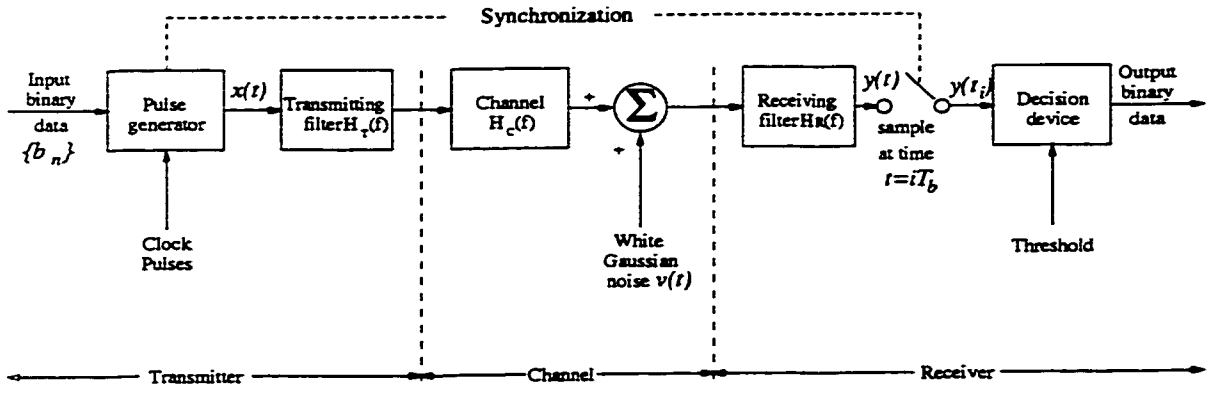

Figure 1.2: Baseband binary data transmission system.

The amplitude x_n in Eq. (1.1) depends on the identity of the input bit b_n; specifically, we assume that

$$x_n = \begin{cases} +K, & \text{if the input bit } b_n \text{ is represented by symbol 1} \\ -K, & \text{if the input bit } b_n \text{ is represented by symbol 0} \end{cases}$$

The PAM signal $x(t)$ is passed through a transmitting filter with transfer function $H_T(f)$. The resulting filter output defines the transmitted signal, which is modified in a deterministic fashion as a result of transmission through the channel with transfer function $H_C(f)$. In addition, the channel adds random noise to the transmitted signal at the receiver input. Then the noisy signal is passed through a receiving filter with transfer function $H_R(f)$. This filter output is sampled synchronously with the transmitter , with the sampling instants being determined by a clock or timing signal that is usually extracted from the receiving filter output. Finally, the sequence of samples thus obtained is used to reconstruct the original data sequence by means of a decision device. The amplitude of each sample is compared to a threshold. If the threshold is exceeded, a decision is made in favor of symbol, say, 1 . If the threshold is not exceeded, a decision is made in favor of symbol 0. If the sample amplitude equals the threshold exactly, the flip of a fair coin will determine which symbol was transmitted [2]. The receiving filter output may be written as

$$y(t) = \sum_{n=-\infty}^{\infty} A_n r(t - nT_b) + c(t) \tag{1.3}$$

where A_n is the amplitude, and $r(t)$ a pulse normalized such that

$$r(0) = 1 \tag{1.4}$$

The pulse $A_n r(t)$ is the response of the cascade connection of the transmitting filter, the channel, and the receiving filter which is produced by the pulse $x_n \phi(t)$ applied to the input of this cascade connection. Therefore, we may relate $r(t)$ to $\phi(t)$ in the frequency domain as

$$A_n R(f) = a_n \Phi(f) H_T(f) H_C(f) H_R(f) \tag{1.5}$$

where $R(f)$ and $\Phi(f)$ are the Fourier transforms of $r(t)$ and $\phi(t)$, respectively. Finally,

the term $c(t)$ in Eq. (1.3) is the noise produced at the output of the receiving filter due to the additive noise $v(t)$ at the receiver input. It is customary to model $v(t)$ as a white Gaussian noise of zero mean.

The receiving filter output y(t) is sampled at time $t = iT_b$ (where i is an integer), yielding

$$\begin{aligned} y(t_i) &= \sum_{n=-\infty}^{\infty} A_n r[(i-n)T_b] + c(t_i) \\ &= A_i + \sum_{n=-\infty; n\neq i}^{\infty} A_n r[(i-n)T_b] + c(t_i) \end{aligned} \tag{1.6}$$

1.2.1 Inter Symbol Interference (ISI)

In Eq. (1.6), the first term A_i represents the ith transmitted bit. The second term represents the residual effect of all other transmitted bits on the decoding of the ith bit; this residual effect is called the inter symbol interference (ISI). The last term $c(t_i)$ represents the noise sample at time t_i. In the absence of ISI and noise, we can see from Eq. (1.6) that

$$y(t_i) = A_i \tag{1.7}$$

which shows that, under these conditions, the ith transmitted bit can be decoded correctly. The unavoidable presence of ISI and noise in the system, however , introduces errors in the decision device at the receiver output. Therefore, in the design of the transmitting and receiving filters, the objective is to minimize the effects of noise and ISI, and thereby deliver the digital data to its destination with the smallest error rate possible [2].

1.2.2 M-ary PAM System

In the binary PAM system of Fig. 1.2, the output of the pulse generator consists of binary pulses, that is, pulses with one of two possible amplitude levels. On the other hand, in a baseband M-ary PAM system, the output of the pulse generator takes on one of the M possible amplitude levels, with $M > 2$, as illustrated in Fig. 1.3 for the case of quaternary ($M = 4$) system. The corresponding electrical representation for each of the four possible dibits is shown in Table 1.1. In an M-ary system, the information source emits a sequence of symbol from an alphabet that consists of M symbols. Each amplitude level at the pulse generator output corresponds to a distinct symbol, so that there are M distinct amplitude levels to be transmitted [1].

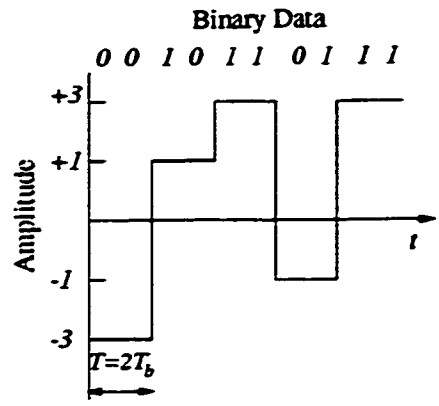

Figure 1.3: Output waveform of a quartenary system.

Table 1.1: Representation of the 4 possible dibits.

Dibit	Amplitude
00	−3
01	−1
10	+1
11	+3

1.2.3 Baud Rate

In an M-ary PAM system with a signal alphabet that contains M equally likely and statistically independent symbols, we may denote the symbol duration by T seconds. We refer to $1/T$ as the signaling rate of the system, which is expressed in symbols per second or bauds. It is important to relate the signaling rate of this system to that of an equivalent binary PAM system for which the value of M is 2 and the binary symbols 1 and 0 are equally likely and statistically independent, with the duration of either symbol denoted by T_b seconds. For a zero memory binary source, with symbols 1 and 0 equally likely and successive symbols statistically independent, the entropy equals one bit. Hence, the binary PAM system produces information at the rate of $1/T_b$ bits per second. In the case of the quaternary PAM system, each symbol represents 2 bits of information, and 1 baud is equal to 2 bits per second. We may generalize this result by stating that in an M-ary PAM system, 1 baud is equal to $log_2 M$ bits per second, and the symbol duration T of the M-ary PAM system is related to the bit duration T_b of the equivalent binary PAM system as

$$T = T_b log_2 M \tag{1.8}$$

Therefore, for a given channel bandwidth, it is found that by using an M-ary PAM system, we are able to transmit information at a rate that is $log_2 M$ faster than the corresponding binary PAM system. However, in order to realize the same average probability of symbol error, an M-ary PAM system requires more transmitted power. For M much larger than 2 and an average probability of symbol error smaller compared to 1, the transmitted power must be increased by a factor of $M^2/log_2 M$, compared to a binary PAM system. Also the designs of the pulse generator and the decision making device in an M-ary PAM systems are more complex than those in a binary PAM system [2].

1.3 Adaptive Equalization

In digital communications, considerable effort has been devoted to the study of data transmission systems that utilize the available channel bandwidth [1]. The objective is to design a system that accommodates the highest possible rate of data transmission, subject to a specified reliability that is usually measured in terms of the error rate or average probability of symbol error. The transmission of digital data through a linear communication channel is limited by two factors, inter symbol interference as discussed earlier and thermal noise, generated by the receiver at its front end. For bandwidth-limited channels (e.g., voice-grade telephone channels), we usually find that ISI is one of the most crucial factors in the design of high-data-rate transmission systems.

The basic operation of an adaptive filtering is shown in Fig. 1.4. An adaptive filtering algorithm requires the knowledge of the "desired" response so as to form the error signal needed for the adaptive process to function. In theory, the transmitted sequence (originating at the transmitter output) is the "desired" response for adaptive equalization. In practice, however, with the adaptive equalizer located in the receiver, the equalizer is physically separated from the origin of its ideal desired response. There are two modes that are applied to produce the replica of the desired response locally in the receiver.

1. *Training method:* In this method, a replica of the desired response is stored in the receiver. The generator of this stored reference is electronically synchronized with the known transmitted sequence.

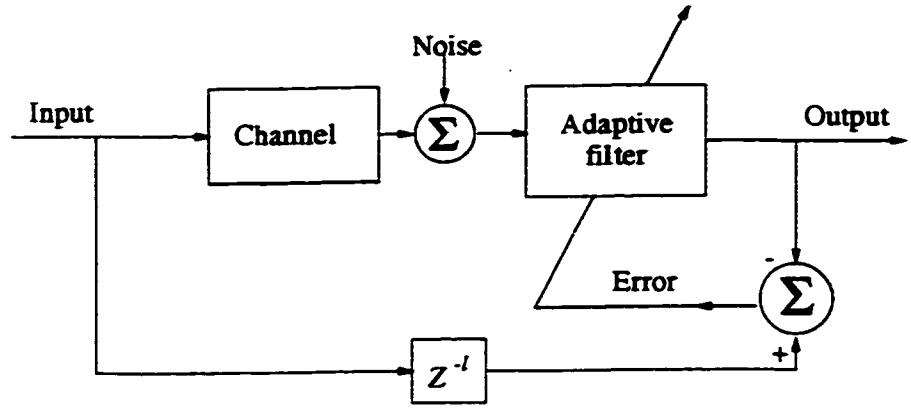

Figure 1.4: Basic adaptive filter.

2. *Decision-directed method:* Under normal operating conditions, a good replica of the transmitted sequence is produced at the output of the decision device in the receiver. Accordingly, if this output were the correct transmitted sequence, it may be used as the "desired" response for the purpose of adaptive equalization. Such a method of learning is said to be decision directed, because the receiver attempts to learn by employing its own decisions [3].

With a known training sequence, as in the first mode, the adaptive filtering algorithm used to adjust the equalizer coefficients corresponds mathematically to searching for the unique minimum of a quadratic error performance surface. The unimodal nature of this surface assures convergence of the algorithm. In the decision-directed method, on the other hand, the use of estimated and unreliable data modifies the error performance into a multi-modal one, in which case a complex behavior may result. Specifically, the error performance surface now exhibits two types of local minima:

1. Desired local minima, whose positions correspond to coefficient (tap weight) settings that yield the same performance as that obtained with a known training sequence.

2. Undesired (extraneous) local minima, whose positions correspond to coefficient settings that yield inferior equalizer performance.

A poor choice of the initial coefficient settings may cause the adaptive equalizer to converge to an undesirable local minimum and stay there. The most significant point to note

is that, in general, a linear adaptive equalizer must be trained before it is switched to the decision-directed mode of operation, if we are to be sure of delivering a high performance.

1.3.1 Eye Pattern

A popular experimental technique for assessing the performance of a data transmission system involves the use of an eye pattern [2]. This pattern is obtained by applying the received wave to the vertical deflection plates of an oscilloscope, and a sawtooth wave at the transmitted symbol rate to the horizontal deflection plates. The resulting display is called an eye pattern because of its resemblance to the human eye. Thus, in a system using adaptive equalization, the equalizer attempts to correct for inter symbol interference in the system and thereby open the eye pattern as far as possible.

1.4 Blind Equalization

In the case of a highly nonstationary communication environment (e.g., digital mobile communications), it is impractical to consider the use of a training sequence. In such a situation, the adaptive filter has to equalize the communication channel in a self- organized (unsupervised) manner, and the resulting operation is referred to as blind equalization. Design of a blind equalizer is more difficult than a conventional adaptive equalizer, because it has to make up for the absence of a training sequence by some practical means. A conventional adaptive equalizer relies on second-order statistics of the input data; however, a blind equalizer relies on additional information about the environment. This additional information may take one of the two basic forms:

1. *Higher-order statistics (HOS)*, the extraction of which is implicitly or explicitly built into the design of the blind equalizer. For this to be possible, the input data must be non-Gaussian, and the equalizer must include some form of nonlinearity.

2. *Cyclostationarity*, which arises when the amplitude, phase, or frequency of a sinusoidal carrier is varied in accordance with an information bearing signal. In this case, design of the blind equalizer is based on second-order cyclostationary statistics of the input data, and the use of nonlinearity is no longer a requirement.

These blind equalization schemes employ only adaptive FIR filter-based structures and perform poorly for maximum-phase communication channels having deep spectral nulls.

This problem is due the difficulty of modeling the inverse of the maximum-phase communication channel with a finite length adaptive FIR filter. A blind equalizer which can estimate such channels is known as a sufficient-order blind equalizer.

In [16]-[18] attempts have been made to solve this problem by using a blind equalization structure which makes use of an adaptive IIR predictor and an all-pass filter. This technique employs a fourth-order norm to estimate the unknown channel, thus requiring an extremely high computational complexity. A further attempt has been made in [12], to reduce this high computational complexity by using two block-based time reversers, in addition to IIR and FIR filters. However, this scheme reduces the computational complexity only to a certain extent. Moreover, the adaptive algorithm used for the adaptation of the IIR predictor, may converge to an arbitrary point on the mean square output error surface, if the denominator polynomial transfer function of the IIR predictor does not satisfy a strictly positive real condition. This scheme also requires swapping of the IIR and adaptive FIR filters, for it to work satisfactorily at low levels of signal-to-noise ratio.

1.5 Scope and Organization of the Thesis

The objective of this thesis is to investigate the problem of blind equalization and propose a scheme that is simple, computationally efficient and performs well in the environment of maximum-phase communication channels having deep spectral nulls. Emphasis is put to reduce or eliminate some of the undesirable features of the existing schemes and yet to provide a performance that is generally superior in terms of the convergence rate and symbol error rate.

In Chapter 2, the underlying theory behind the HOS-based and cyclostationary statistics-based blind equalization schemes is discussed. Some widely used blind equalizer structures are presented and the limitations of these schemes to estimate the maximum-phase deep spectral null channels are discussed.

In Chapter 3, the theory of adaptive IIR predictor and all-pass filter based blind equalization technique along with the one that, in addition, uses two block-based time reversers is briefly discussed. A new sufficient-order blind equalization scheme is then proposed by developing adaptation algorithms for the IIR predictor and the FIR filter. An analysis

of the proposed and the existing schemes is carried out to show the advantages of the proposed scheme in terms of computational complexity, hardware implementation, and stability of the IIR predictor.

In Chapter 4, experimental results obtained by using the proposed blind equalization scheme for minimum-phase communication channels in terms of the convergence of the adaptation coefficients and the symbol error rate are presented and discussed in detail. A comparison is made with the results obtained by using the scheme of [12].

In Chapter 5, experimental results for maximum-phase and mixed-phase channels in terms of convergence of the adaptation coefficients and symbol error rate are presented and discussed in detail. Results on spectral performance of the proposed blind equalization scheme for a maximum-phase deep-null channel is also given.

Finally, Chapter 6 concludes the thesis by pointing out the contribution of the proposed investigation and suggesting some related problems for future investigation.

Chapter 2

Blind Equalization Theory

2.1 Introduction

The most important approach followed in the adaptive equalization of digital communication channels is to use known training sequences [1]. The equalizer is typically a linear transversal FIR filter. The coefficients of this filter are adjusted to minimize the mean-square error. Once an initial training of the filter is done, the equalizer is switched to a decision-directed mode. The detected symbols are then considered as the transmitted ones, and the error so obtained is used to adjust the equalizer gains as it is done during the training mode. In some cases the inter symbol interference and the noise are sufficiently small so that the eye of the "eye pattern" is widely open [1]. In such cases decision-directed equalization is possible even without an initial training sequence. However, in the cases where the presence of inter symbol interference is sufficiently large and the training sequence is not available, some other solutions are required. Generally, in the situation where initial training sequence is not available at the receiver, the problem of equalization is referred to as a blind equalization problem.

Most of the existing works on blind equalization use nonquadratic cost functions, and recursively minimize these functions with respect to the equalizer's parameters. Generally, the adaptation is done by gradient-type algorithms, e.g., the least mean square (LMS) or its numerous variations [10]. Some important works on the blind equalization problem can be found in [4]-[9]. In a broad sense, blind equalizers can be grouped into two categories.

1. *Higher-order statistics (HOS)-based algorithms*: In this family of blind equalization the extraction of statistics is built into the design of the blind equalizer. This class of the blind equalization technique can be further subdivided into two groups as follows:

   (a) *Implicit HOS-based algorithms*: These algorithms exploit higher-order statistics of the received signal in an implicit sense. This group of blind equalization algorithms includes the most popular Bussgang algorithm [1].

   (b) *Explicit HOS-based algorithms*: These algorithms explicitly use higher-order cumulants or their discrete Fourier transforms, known as polyspectra [1]. The property of polyspectra to preserve phase information makes them well suited for blind deconvolution.

2. *Cyclostationary statistics-based algorithms*: These algorithms exploit the second-order cyclostationary statistics of the received signal; the property of cyclostationarity arises in a modulated signal resulting from varying the amplitude, phase, or frequency of a sinusoidal carrier [1].

In this chapter, some of the most widely used blind equalization structures are discussed. Since the proposed new algorithm belongs to the category of higher-order statistics-based algorithms, a greater emphasis is put on the discussion of such algorithms. In Section 2.2, the blind equalization problem is defined. In Section 2.3, the basic algorithm for Bussgang algorithm is discussed in detail. Two important cases of the Bussgang algorithm, namely Sato and Godard algorithms, are discussed in Section 2.4. In Section 2.5 a comparison of the special forms of the Bussgang algorithms is carried out. The basic idea behind the explicit HOS-based, polyspectra-based algorithms and their different classes is presented in Section 2.6. In Section 2.7, a comparison between different types of HOS-based algorithm is carried out. In Section 2.8, cyclostationary statistics-based algorithms are discussed briefly. A comparison and limitations of all the algorithms presented in this chapter, are carried out in Section 2.9. Finally, Section 2.10 summarizes the material presented in this chapter.

2.2 Blind Equalization Problem

Consider the baseband model of a digital communication system, depicted in Fig. 2.1. The model consists of the cascade of a linear communication channel and a blind equalizer.

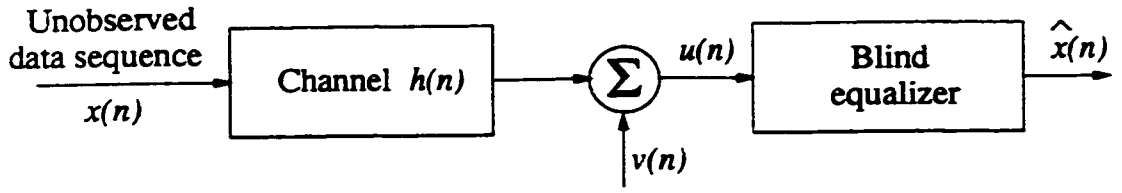

Figure 2.1: A cascade of an unknown channel and a blind equalizer.

The effects of transmit filter, transmission medium, and receiver filter are combined and is included in the channel. The channel is characterized by an impulse response $h(n)$ which is unknown. The channel is time varying, but this variation with time is generally very slow. Whether the impulse response $h(n)$ is real or complex valued in nature, is determined by the type of modulation employed. For simplicity, only real impulse response is discussed. In the case of real impulse response of the channel, the use of multilevel pulse-amplitude modulation (M-ary PAM) is employed. The sampled input-output relation of the channel may be represented by the convolution summation given by

$$u(n) = \sum_{k=-\infty}^{\infty} h(k)x(n-k), \quad n = 0, \pm 1, \pm 2, \ldots \tag{2.1}$$

where $x(n)$ is the channel input, and $u(n)$ is the resulting channel output [1]. Degradation in the performance of data transmission, e.g., over a voice-grade telephone channel, is usually dominated by the inter symbol interference produced by the channel dispersion. Thus in Eq. (2.1), the effect of receiver noise is ignored. Also its assumed that

$$\sum_{k} h^2(k) = 1 \tag{2.2}$$

Eq. (2.2) implies the use of automatic gain control (AGC) to keep the variance of the channel output $u(n)$ constant. Also, in general, the channel is noncausal which means that

$$h(n) \neq 0 \quad \text{for } n < 0 \tag{2.3}$$

The problem of blind equalization can be stated as follows: Given the received signal $u(n)$, reconstruct the original data sequence $x(n)$ applied to the channel input. Equivalently, the problem can be restated as: Design a blind equalizer, that is the inverse of the unknown channel, with the channel input being unobservable and the desired response not available.

2.3 Bussgang Algorithm for Blind Equalization of Real Baseband Channels

Bussgang algorithms are so called because the equalized sequence assumes Bussgang statistics when the algorithm converges in the mean value. To solve the problem stated in Section 2.2, a probabilistic model for the data sequence $x(n)$ is prescribed and the following assumptions are made [1].

2.3.1 Assumptions

1. The data sequence $x(n)$ is white; that is, the data symbols are independently and identically distributed (iid) random variables, with zero mean and unit variance, that is,

$$E[x(n)] = 0 \tag{2.4}$$

and

$$E[x(n)x(k)] = \begin{cases} 1, & k = n \\ 0, & k \neq n \end{cases} \tag{2.5}$$

where E is the statistical expectation operator.

2. The probability density function of the data symbol $x(n)$ is symmetric and is uniformly distributed as shown in Fig. 2.2, that is,

$$f_X(x) = \begin{cases} \frac{1}{2\sqrt{3}}, & -\sqrt{3} \leq x < \sqrt{3} \\ 0, & \text{otherwise} \end{cases} \tag{2.6}$$

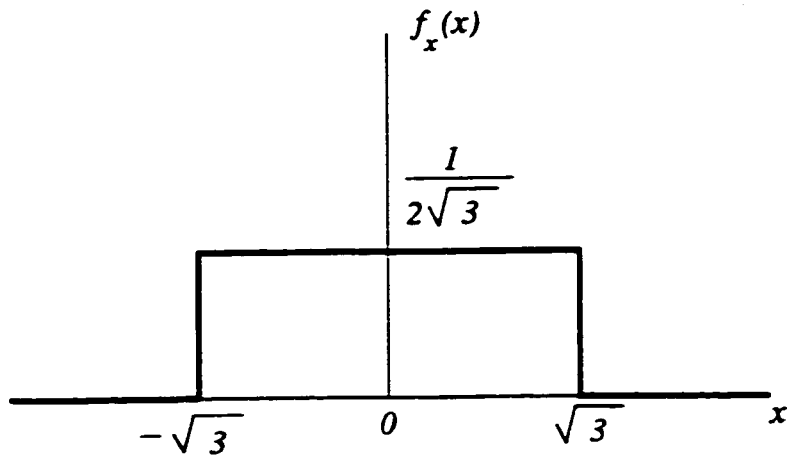

Figure 2.2: Uniform distribution.

This kind of distribution is independent of the number M of amplitude levels employed in the modulation process.

With the assumption that distribution of $x(n)$ is symmetric, as in Fig. 2.2, it can be seen that the data sequence $-x(n)$ has the same properties as $x(n)$. Hence, it is not possible to distinguish the desired inverse filter $h(n)^{-1}$ (corresponding to $x(n)$) from the opposite one $-h(n)^{-1}$ (corresponding to $-x(n)$). This sign ambiguity problem is tackled by initializing the deconvolution algorithm such that there is a single nonzero tap weight with the desired algebraic sign [5].

2.3.2 Objective Behind Iterative Deconvolution

In this section, the need for an iterative deconvolution system is discussed. For this, let us assume that w_i denotes the impulse response of the ideal inverse filter, which is related to the impulse response $h(i)$ of the channel as given by

$$\sum_i w_i h(l-i) = \delta_l \tag{2.7}$$

where δ_l is the Kronecker delta, such that

$$\delta_l = \begin{cases} 1, & l = 0 \\ 0, & l \neq 0 \end{cases} \tag{2.8}$$

An inverse filter defined in this way is ideal in nature, since it reconstructs the transmitted data sequence $x(n)$ correctly [1], e.g., by using Eq. (2.1), we can have

$$\sum_i w_i u(n-i) = \sum_i \sum_k w_i h(k) x(n-i-k) \tag{2.9}$$

Making a change of indices, $k = l - i$, and interchanging the order of summation in Eq. (2.9), we can rewrite it as

$$\sum_i w_i u(n-i) = \sum_l x(n-l) \sum_i w_i h(l-i) \tag{2.10}$$

Using Eq. (2.7) in (2.10) and then applying the definition of Eq. (2.8), we get

$$\sum_i w_i u(n-i) = \sum_l \delta_l x(n-l)$$

$$\sum_i w_i u(n-i) = x(n) \tag{2.11}$$

which is the transmitted input data sequence.

In Eq. (2.7), the impulse response $h(n)$ is unknown, therefore, Eq. (2.7) cannot be used to determine the inverse filter. Therefore, an iterative deconvolution procedure is required to compute an approximate inverse filter characterized by the impulse response $\widehat{w}_i(n)$. The index i refers to the tap weight number in the transversal filter realization of the approximate inverse filter, as shown in Fig. 2.3. The index n refers to the iteration number. Each iteration corresponds to the transmission of a data symbol. The computation is performed iteratively in such a way that the convolution of the impulse response $\widehat{w}_i(n)$ with the received signal $u(n)$ results in a complete or partial removal of the inter symbol interference [1]. Thus, at the nth iteration, we have an approximately deconvolved sequence

$$y(n) = \sum_{i=-L}^{L} \widehat{w}_i(n) u(n-i) \tag{2.12}$$

where $2L + 1$ is the truncated length of the impulse response $\widehat{w}_i(n)$ and L is a positive integer. It is customary to assume that the transversal filter or equalizer is symmetric about the midpoint $i = 0$.

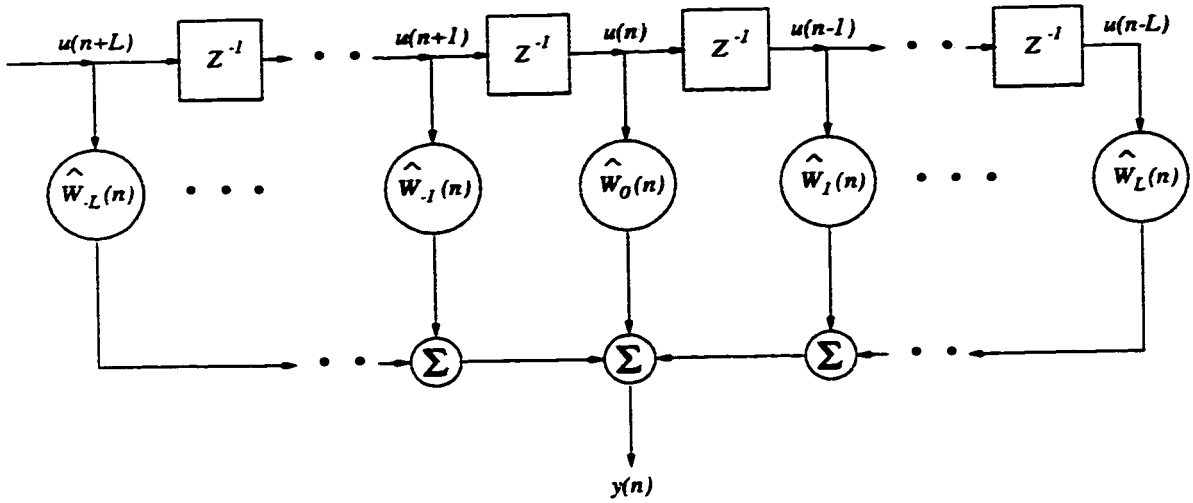

Figure 2.3: Transversal filter realization of an approximate inverse filter, assuming that the data is real.

Looking at Eqs. (2.11) and (2.12) we notice that the convolution summation on the left side of Eq. (2.11), representing an ideal inverse filter, is infinite in extent with index i ranging from $-\infty$ to ∞. This case is called a doubly infinite filter or equalizer. On the other hand, the convolution summation on the right side of Eq. (2.12) representing the approximate inverse filter is finite in extent, in that i extends from $-L$ to L . This case is called a finitely parameterized filter or equalizer. Eq. (2.12) may be rewritten as

$$y(n) = \sum_i \widehat{w}_i(n) u(n-i), \qquad \widehat{w}_i(n) = 0 \text{ for } |i| > L$$

or as

$$y(n) = \sum_i w_i u(n-i) + \sum_i [\widehat{w}_i(n) - w_i]\, u(n-i) \tag{2.13}$$

Now, let

$$c(n) = \sum_i [\widehat{w}_i(n) - w_i]\, u(n-i), \qquad \widehat{w}_i = 0 \text{ for } |i| > L \tag{2.14}$$

Then, using Eqs. (2.11) and (2.14), Eq. (2.13) can be simplified to yield

$$y(n) = x(n) + c(n) \tag{2.15}$$

where $c(n)$ is called the convolutional noise and represents the residual inter symbol interference. This inverse filter output $y(n)$ is then applied to a zero-memory nonlinear

estimator, which produces the final estimate $\hat{x}(n)$ for the data symbol $x(n)$, given by

$$\hat{x}(n) = g(y(n)) \tag{2.16}$$

where $g(.)$ is a nonlinear function operator. The estimate $\hat{x}(n)$, obtained at iteration n is generally not very reliable. Also, it is never used in an adaptive scheme to obtain a better estimate at the next iteration, $n+1$.

There are a variety of linear adaptive algorithms which can be used to adjust the weight of the transversal filter. Amongst them the least mean square (LMS) algorithm is the simplest and most effective. A block diagram of the blind equalizer using zero-memory nonlinear estimator and an LMS algorithm is shown in Fig. 2.4. For this blind equalizer, an estimation error is defined as

$$e(n) = \hat{x}(n) - y(n) \tag{2.17}$$

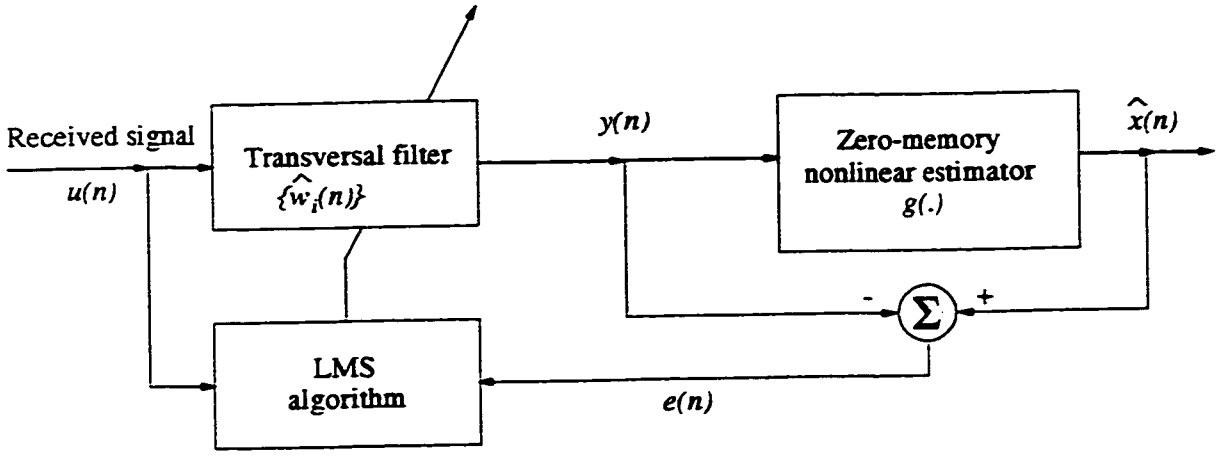

Figure 2.4: Block diagram of a blind equalizer.

The updated value of the ith tap weight at iteration $n+1$ can be calculated as

$$\hat{w}_i(n+1) = \hat{w}_i(n) + \mu u(n-i)e(n), \qquad i = 0, \pm 1, \ldots, \pm L \tag{2.18}$$

where μ is the step-size parameter. The iterative deconvolution algorithm is, therefore, generally described by Eqs. (2.12) and (2.16)-(2.18).

In the case of an LMS algorithm, the cost function is a convex (quadratic) function of the tap weights. Therefore, there is always a well defined minimum point. From Eq. (2.18), the ensemble averaged cost function corresponding to the tap weight can be defined by

$$J(n) = E[e^2(n)]$$

or

$$J(n) = E[(\widehat{x}(n) - y(n))^2] \tag{2.19}$$

Also, using Eq. (2.16), Eq. (2.19) can be rewritten as

$$J(n) = E[(g(y(n)) - y(n))^2]$$

where $y(n)$ is given by Eq. (2.12). Now, it can be observed from Eq. (2.19) that the cost function $J(n)$ is a nonconvex function of the tap weights. It can be concluded that the error performance surface of the iterative deconvolution procedure discussed in this section may have local minima, in addition to the global minima. In some cases more than one global minima may exist. This corresponds to the data sequences that are equivalent under the chosen blind deconvolution criterion (e.g, sign ambiguity). The cost function $J(n)$ becomes nonconvex because of the fact that the estimate is assumed to be the internally generated desired response. The estimate $\widehat{x}(n)$ is produced by passing the output $y(n)$ through a zero-memory nonlinearity. Also, this $y(n)$ itself is a function of the tap weights. This nonconvex form of the cost function $J(n)$ may some times mar the convergence of the iterative deconvolution algorithm. To improve this convergence, some important issues are discussed in the next section.

2.3.3 Convergence Issues for the Bussgang Algorithm

For the iterative deconvolution, described by Eqs. (2.16)-(2.18), to converge in the mean square sense, it is required that the expected value of the tap weights $\widehat{w}_i(n)$ approach some constant value as the number of iteration n approaches infinity. Therefore, the condition for convergence in the mean square sense can be described as

$$E[u(n-i)y(n)] = E[u(n-i)g(y(n))], \quad \text{for large } n \text{ and } i = 0, \pm 1, \ldots, \pm L \tag{2.20}$$

Multiplying both sides of this equation by $\widehat{w}_{i-k}$ and summing over i, we get

$$E[y(n)\sum_{i=-L}^{L}\widehat{w}_{i-k}(n)u(n-i)] = E[g(y(n))\sum_{i=-L}^{L}\widehat{w}_{i-k}(n)u(n-i)], \quad \text{for large } n \quad (2.21)$$

Also, from Eq. (2.12) we can write

$$y(n-k) = \sum_{i=-L}^{L}\widehat{w}_i(n)u(n-k-i), \quad \text{for large } n$$

$$= \sum_{i=-L+k}^{L+k}\widehat{w}_{i-k}(n)u(n-i), \quad \text{for large } n$$

Assuming that L is very large such that the transversal equalizer can achieve a perfect equalization, the expression for $y(n-k)$ can be further approximated as

$$y(n-k) \simeq \sum_{i=-L}^{L}\widehat{w}_{i-k}(n)u(n-i), \quad \text{for large } n \text{ and large } L \quad (2.22)$$

Eq. (2.22) can be used to simplify Eq. (2.21) to give

$$E[y(n)y(n-k)] \simeq E[g(y(n))y(n-k)], \quad \text{for large } n \text{ and large } L \quad (2.23)$$

A stochastic process $y(n)$ is a Bussgang process [1], if it satisfies the condition

$$E[y(n)y(n-k)] = E[y(n)g(y(n-k))] \quad (2.24)$$

where the function $g(.)$ is a zero memory nonlinearity. In other words, a Bussgang process has the property that its autocorrelation function is equal to the cross-correlation between that process and the output of a zero memory nonlinearity produced by that process, with both correlations being measured for the same lag [1].

Now, the process $y(n)$ acting as the input to the zero-memory nonlinearity (Fig. 2.4) can be approximately called as a Bussgang process, if and only if L is large. The approximation becomes better as L is made larger. This is the reason for the blind equalization algorithm being referred to as a Bussgang algorithm.

Convergence of the Bussgang algorithm is not always guaranteed, since the cost function of the Bussgang algorithm operating with a finite L is nonconvex. Therefore, it may have some false minima.

However, for the idealized case of a doubly infinite equalizer, a proof of convergence of the Bussgang algorithm can be found. The proof relies on a theorem derived in [5], which provides sufficient conditions for convergence. The main points of the proof are as follows.

Let the function $\psi(y)$ denote the dependence of the estimation error in the LMS algorithm on the transversal filter output $y(n)$. Then,

$$\psi(y) = g(y) - y \tag{2.25}$$

The Benveniste-Goursat-Ruget theorem states that convergence of the Bussgang algorithm is guaranteed if the probability distribution of the data sequence $x(n)$ is sub-Gaussian and the second derivative of $\psi(y)$ is negative in the interval (0,∞) [1]. In particular, it may be stated that :

1. A random variable x with the probability density function (for example)

$$f_X(x) = Ke^{-|x/\beta|^\nu}, \quad K = \text{constant} \tag{2.26}$$

   is sub-Gaussian when $\nu > 2$. For the limiting case of $\nu = \infty$, the probability density function given by Eq. (2.26) reduces to that of a uniformly distributed random variable. Also, by choosing $\beta = \sqrt{3}$, the second-order expectation of the data sequence $x(n)$ is equal to unity, i.e., $E[x^2] = 1$. Thus, the probabilistic model assumed in Eq. (2.6) satisfies the first part of the Benveniste-Goursat-Ruget theorem.

2. The second part of the theorem is also satisfied by the Bussgang algorithm, since we have

$$\frac{\partial^2 \psi}{\partial y^2} < 0 \quad \text{for } 0 < y < \infty \tag{2.27}$$

   This can be directly verified by examining the nonlinear estimation curves given in [1].

The Benveniste-Goursat-Ruget theorem is based on the assumption of a doubly infinite equalizer. However, this assumption does not hold true in practice, since the parameters of an equalizer are always finite.

2.3.4 Algorithm for the Decision-Directed Mode

Once the Bussgang algorithm has converged and the eye pattern is widely open, the equalizer is switched smoothly to the decision-directed mode of operation. In this case, the minimum mean squared error (MSE) control of the tap weights of the transversal filter component in the equalizer is exercised, as is done in a conventional adaptive equalizer.

The block diagram of an equalizer operating in a decision-directed mode is shown in Fig. 2.5. The only difference between this mode of operation and that of a blind equalization mode is the type of zero-memory nonlinearity used. The zero-memory nonlinear

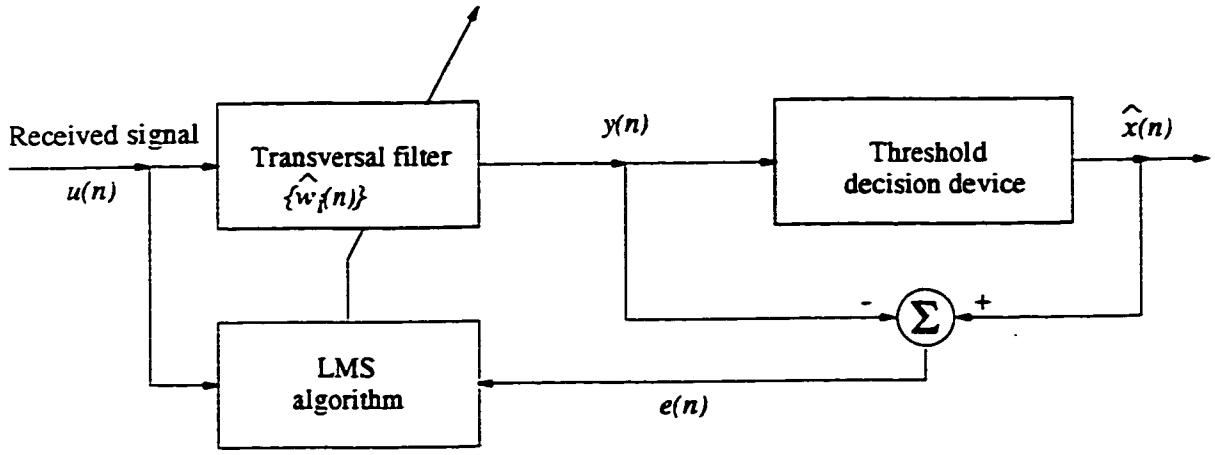

Figure 2.5: Block diagram of decision-directed mode of operation.

estimator of the blind equalizer in Fig. 2.4 is replaced by a threshold decision device. Given the observation $y(n)$, that is, the equalized signal at the transversal filter output, the threshold device makes a decision in favor of a particular value in the known alphabet of the transmitted data sequence that is closest to $y(n)$ [1]. Therefore,

$$\hat{x}(n) = dec(y(n)) \tag{2.28}$$

In the simple case of an equiprobable data sequence, the data levels and decision levels

are as follows:

$$x(n) = \begin{cases} +1, & \text{for symbol 1} \\ -1, & \text{for symbol 0} \end{cases} \tag{2.29}$$

and

$$dec((y(n)) = sgn(y(n)) \tag{2.30}$$

where $sgn(.)$ is the signum function equal to $+1$ if the argument is positive, and -1 if it is negative.

The equations for the decision-directed algorithm are the same as those of the Bussgang algorithm, except that Eq. (2.16) in replaced by Eq. (2.28).

Now, if the following conditions are met:

1. the eye pattern is open i.e., the blind equalization mode is completed.
2. the step-size parameter μ used in the LMS implementation of the decision directed algorithm is fixed.
3. the sequence of observations at the channel output, denoted by the vector $u(n)$ is ergodic in the sense that

$$\lim_{n_1 \to \infty} \frac{1}{n_1} \sum_{n=1}^{n_1} u(n)u^T(n) \;\to\; E[u(n)u^T(n)] \tag{2.31}$$

then the tap weight vector in the decision-directed algorithm converges to the optimum solution in the mean square sense. This is a powerful result, making the decision-directed algorithm an important adjunct of the Bussgang algorithm for blind equalization in digital communication [1].

Statistical properties of the convolution noise and zero-memory nonlinear estimation of the data sequences are two other very important issues in the Bussgang algorithm. As the main aim of this chapter is to review different kinds of blind equalization algorithms, these issues are not discussed here. However, these can be found in [1].

2.3.5 Bussgang Algorithm for Complex Baseband Channels

In this section the use of Bussgang algorithm discussed in previous sections for M-ary PAM system, characterized by a real baseband channel, is extended to a blind equalization algorithm for quadrature amplitude modulation (QAM) system. Quadrature amplitude modulation (QAM) systems use hybrid combination of amplitude and phase modulation.

In the case of a complex baseband channel, the transmitted data sequence $x(n)$, the channel impulse response $h(n)$, and the received signal $u(n)$ are all complex valued. Therefore,

$$x(n) = x_I(n) + jx_Q(n) \tag{2.32}$$

$$h(n) = h_I(n) + jh_Q(n) \tag{2.33}$$

and

$$u(n) = u_I(n) + ju_Q(n) \tag{2.34}$$

where the subscripts I and Q refer to to the in-phase (real) and quadrature (imaginary) components, respectively. Now, the condition for the mean estimate of the complex data $x(n)$, given the observation $y(n)$ at the transversal filter output, can be written as

$$\begin{aligned} \widehat{x}(n) &= E[x(n)|y(n)] \\ &= \widehat{x}_I(n) + j\widehat{x}_Q(n) \\ &= g(y_I(n)) + jg(y_Q(n)) \end{aligned} \tag{2.35}$$

where $g(.)$ is a zero-memory nonlinearity. From Eq. (2.35), it can be observed that the in-phase and quadrature components of the transmitted data sequence $x(n)$ can be estimated separately from the in-phase and quadrature components of the transversal filter output $y(n)$, respectively. However, the conditional mean $E[x(n)|y(n)]$ can only be expressed as in Eq. (2.35) if the in-phase and quadrature components of the data transmitted are statistically independent of the each other. A summary of Bussgang algorithm for a complex baseband channel is presented in Table 2.1.

Table 2.1: Summary of Bussgang algorithm for blind equalization of complex baseband channels.

Initialization: Set

$$\widehat{w}(0) = \begin{cases} 1, & i = 0 \\ 0, & i = \pm 1, \ldots, \pm L \end{cases}$$

Computation: $n = 1, 2, \ldots$

$$y(n) = y_I(n) + jy_Q(n)$$

$$y(n) = \sum_{i=-L}^{L} \widehat{w}_i^*(n) u(n-i)$$

$$\widehat{x}(n) = \widehat{x}_I(n) + j\widehat{x}_Q(n)$$

$$\widehat{x}(n) = g(y_I(n)) + jg(y_Q(n))$$

$$e(n) = \widehat{x}(n) - y(n)$$

$$\widehat{w}_i(n+1) = \widehat{w}_i(n) + \mu u(n-i) e^*(n)$$

2.4 Two Important Cases of the Bussgang Algorithm

In the previous section, the general form of a Bussgang algorithm was discussed. Many other blind equalization algorithms have been derived from this general algorithm. In this section, the two most important and widely used cases of Bussgang algorithm are discussed. These algorithms are known as Sato algorithm [4] and Godard algorithm [7].

2.4.1 Sato Algorithm

A pioneering work, in the field of blind equalization of M-ary PAM systems was done by Sato [4]. The idea behind the Sato algorithm is to minimize a nonconvex cost function

$$J(n) = E[(\widehat{x}(n) - y(n))^2] \tag{2.36}$$

where $y(n)$ is the transversal filter output given by Eq. (2.12), and $\widehat{x}(n)$ is an estimate of the transmitted datum $x(n)$. This estimate is obtained by a zero-memory nonlinearity described as

$$\widehat{x}(n) = Gsgn[y(n)] \tag{2.37}$$

The constant G sets the gain of the equalizer, and it is defined by

$$G = \frac{E[x^2(n)]}{E[|x(n)|]} \tag{2.38}$$

It is clear that the Sato algorithm is a special case of the Bussgang algorithm, with the nonlinear function $g(y)$ defined by

$$g(y) = G\ sgn(y) \tag{2.39}$$

where $sgn(.)$ is the signum function. It can be observed from Eq. (2.39) that the nonlinearity defined in the Sato algorithm is similar to that used in the decision-directed mode of the binary PAM Bussgang algorithm. The only difference is the data-dependent gain factor G.

The Sato algorithm initialy treats one-dimensional multilevel (M-ary PAM) signals as a binary signal by estimating the most significant bit. In the blind equalization mode of operation, the remaining bits of the signal are treated by the algorithm as additive noise. The algorithm then uses the results of this preliminary step to modify the error signal obtained from a conventional decision-directed algorithm.

The Benveniste-Goursat-Ruget theorem for convergence holds for the Sato algorithm even though the nonlinear function $\psi(.)$ is not differentiable in this case. According to this theorem, the global convergence of the Sato algorithm can be achieved provided that the probability density function of the transmitted data sequence can be approximated by a sub-Gaussian function such as the uniform distribution [5]. However, the global convergence of the Sato algorithm holds only for the limiting case of a doubly infinite equalizer [1].

2.4.2 Godard Algorithm

The Sato algorithm is very robust only for one-dimensional multilevel (M-ary PAM) signals. Godard proposed a family of constant modulus blind equalization algorithms for use in two-dimensional digital communication systems (e.g., M-ary phase shift keying) [7]. The Godard algorithm minimizes a nonconvex cost function of the form

$$J(n) = E[(|y(n)|^p - R_p)^2] \tag{2.40}$$

where p is a positive integer and R_p is a positive real constant defined by

$$R_p = \frac{E[|x(n)|^{2p}]}{E[|x(n)|^p]} \tag{2.41}$$

The Godard algorithm is designed to control the deviation of the blind equalizer output $\hat{x}(n)$ from a constant modulus. The value of p in Eq. (2.41) is chosen such that the gradient of the cost function $J(n)$ is zero when a perfect equalization (i.e., $\hat{x}(n) = x(n)$) is attained [1].

The tap weight vector of the equalizer is adapted in accordance with the stochastic gradient algorithm [7]

$$\hat{w}_i(n+1) = \hat{w}_i(n) + \mu u(n) e^*(n) \tag{2.42}$$

where μ is the step-size parameter, $u(n)$ is the received signal, and $e(n)$ is the error signal defined by

$$e(n) = y(n)\,|y(n)|^{p-2}\,(R_p - |y(n)|^p) \tag{2.43}$$

From the definition of the cost function $J(n)$ given by Eqs. (2.40) and (2.43), it can be noted that the equalizer adaptation according to the Godard algorithm does not require carrier phase recovery [1]. The algorithm, therefore, tends to converge slowly. However, it offers the advantage of decoupling the ISI equalization from the carrier phase recovery problem.

Two special cases of the Godard algorithm, when the positive integer value of $p = 1$ and $p = 2$ are substituted in Eqs. (2.40) and (2.41), can be obtained as follows:

Case 1; $p = 1$: The cost function of Eq. (2.40) for this case reduces to

$$J(n) = E[(|y(n)| - R_1)^2] \tag{2.44}$$

where

$$R_1 = \frac{E[|x(n)|^2]}{E[|x(n)|]} \tag{2.45}$$

This case becomes a slight modification of the Sato algorithm.

Case 2; $p = 2$: In this case, the cost function of Eq. (2.40) reduces to

$$J(n) = E[(|y(n)|^2 - R_2)^2] \tag{2.46}$$

where

$$R_2 = \frac{E[|x(n)|^4]}{E[|x(n)|^2]} \tag{2.47}$$

This special case is referred to as the constant modulus algorithm (CMA) [7].

2.5 Comparison of Decision-Directed Bussgang, Sato and Godard Algorithms

Table 2.2 gives a brief summary of the decision-directed Bussgang, Sato and Godard algorithms for a binary PAM system. The entries for the decision-directed Bussgang and Sato algorithms follow directly from the definition

$$\hat{x}(n) = g(y(n))$$

Also, since

$$e(n) = \hat{x}(n) - y(n)$$

and

$$g(y(n)) = y(n) + e(n), \tag{2.48}$$

Eqs. (2.43) and (2.48) can be used to show that the zero-memory nonlinear function $g(.)$ for Godard algorithm is given by

$$\frac{y(n)}{|y(n)|}(|y(n)| + R_P\,|y(n)|^{P-1} - |y(n)|^{2P-1}) \tag{2.49}$$

Table 2.2: Summary of the decision-directed Bussgang, Sato and Godard algorithms.

Algorithm	Zero-memory nonlinear function $g(.)$	Definitions
Decision-directed (Bussgang)	$sgn(.)$	
Sato	$G\ sgn(.)$	$G = \frac{E[x^2(n)]}{E[\|x(n)\|]}$
Godard	$\frac{y(n)}{\|y(n)\|}(\|y(n)\| + R_P\,\|y(n)\|^{P-1} - \|y(n)\|^{2P-1})$	$R_p = \frac{E[\|x(n)\|^{2p}]}{E[\|x(n)\|^{p}]}$

The Bussgang algorithm that incorporates the decision-directed algorithm has a practical advantage in that its implementation is only slightly more complex than that of a conventional adaptive equalizer, yet it does not require the use of a training sequence.

The Sato algorithm for blind equalization is good for one-dimensional multilevel (M-ary PAM) signals. For such signals the Sato algorithm is more robust than the decision-directed algorithm.

The Godard algorithm is considered to be the most successful among the Bussgang family of blind equalization algorithms, and is the most widely used algorithm, because of the following advantages.

- The Godard algorithm is more robust than other Bussgang algorithms with respect to carrier phase offset. This important property of the Godard algorithm is due to the fact that the cost function used for its derivation is based solely on the amplitude of the received signal.
- Under steady state conditions, the Godard algorithm attains a mean squared error that is lower than the Bussgang and Sato algorithms.

- The Godard algorithm is often able to equalize a dispersive channel such that the eye pattern is opened up when it is initialy closed for all practical purposes.

2.6 Polyspectra-Based Blind Equalization Methods

In the case of Bussgang algorithm, the higher-order statistics (HOS) of the received signal was used in an implicit sense. But in the case of polyspectra-based algorithm, the higher-order statistics of the received signal is used in an explicit sense. This class of blind equalization techniques has received a greater attention. These algorithms utilize the higher-order statistics, moments or cumulants of the data at the output of the communication channel. The higher-order statistics of a stationary stochastic process is described in terms of the cumulants and their Fourier transforms known as polyspectra. These cumulants and polyspectra may be viewed as generalizations of the autocorrelation function and power spectrum, respectively. Polyspectra provide the basis for the identification, and therefore, blind equalization of a nonminimum-phase channel because of their ability to preserve the phase information of the channel output. The basic need for a higher-order statistics-based algorithm can be understood from the following points.

1. Most of the classical adaptive equalization methods, based exclusively on second-order statistics, fail to equalize nonminimum-phase channels correctly, since the second-order statistics cannot distinguish the minimum-phase from the maximum-phase information of the channel.

2. When the input data are Gaussian-distributed and the channel is nonminimum-phase, then there is no solution to the problem.

3. In most digital communication links, the transmitted data are non-Gaussian sequences and the distorting linear channels are, in general, nonminimum-phase.

4. Higher-order statistics has the ability to preserve the true phase character of signals. That is why, in order to achieve blind equalization of nonminimum-phase channels, statistics of order greater than two is employed. In fact, all the proposed blind equalizers, indirectly through nonlinear transformations or directly, utilize higher-order statistics [10].

The HOS polyspectra-based algorithms have the capability to meet these needs, as elaborated below.

1. All digital communication signals are data sequences with common statistical properties. Therefore, equalization technique based on higher-order statistics would be independent of a particular transmitted sequence.

2. Polyspectra have the ability to identify nonminimum-phase communication channels from the output measurement without resorting to any training sequence. This is why polyspectra preserve both the nonminimum-phase as well as magnitude information.

3. All polyspectra of Gaussian processes of order greater than two are identically zero. Consequently, polyspectra technique would not be affected by additive Gaussian noise that might be present in a communication system [10].

Now, keeping the same assumptions as those made for Bussgang algorithm, it is further assumed that the FIR channel transfer function $H(z^{-1})$ can be factorized with no zeros on the unit circle as

$$H(z^{-1}) = kS(z^{-1})O(z^{-1}) \tag{2.50}$$

where $S(z^{-1})$ is a minimum-phase polynomial, $O(z^{-1})$ is a maximum-phase polynomial and k is a scaling factor. The polynomial $S(z^{-1})$ has all the zeros inside the unit circle in the z-plane and can be written as

$$S(z^{-1}) = \prod_{i=1}^{d}(1 - \xi_i^i\, z^{-1}), \quad \left|\xi_i^i\right| < 1 \tag{2.51}$$

Similarly, the second polynomial $O(z^{-1})$ has all the zeros outside the unit circle in the z-plane and can be written as

$$O(z^{-1}) = \prod_{j=1}^{s}(1 - \xi_j^o\, z), \quad \left|\xi_j^o\right| < 1 \tag{2.52}$$

With this presentation, the channel is characterized by a finite length impulse response with a nonminimum-phase transfer function. Now, consider a baseband communication link shown in Fig. 2.6, where $\{v(n)\}$ is zero-mean, Gaussian additive noise, which is generally colored and is statistically independent of the channel input sequence $\{x(n)\}$.

The objective of a blind equalizer with transfer function $M(z^{-1})$ is to recover the input sequence $\{x(n)\}$ within a constant delay d_t and a constant phase shift θ. Now, assuming

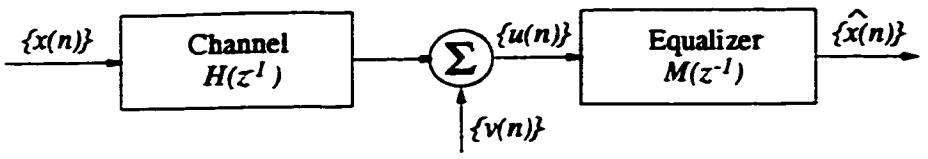

Figure 2.6: A baseband communication link.

that $\{\widehat{x}(n)\}$ is the output of the equalizer, we can write

$$\widehat{X}(z^{-1}) = X(z^{-1}).z^{-d_t}.e^{j\theta} \tag{2.53}$$

The delay is introduced by the causal channel and the equalizer impulse responses. In a QAM system, the phase shifts of $\theta = \pm 90^{\circ}, \pm 180^{\circ}$ cannot be detected until and unless a training sequence is used. Now, if we ignore the additive noise shown in Fig. 2.6, then Eq. (2.53), can be rewritten as

$$H(z^{-1}).X(z^{-1}).M(z^{-1}) = X(z^{-1}).z^{-d_t}.e^{j\theta} \tag{2.54}$$

The unknown delay d_t does not affect the recovery of the original message. Phase shift θ can also be removed by properly adjusting the carrier phase prior to or after the equalization [10]. Therefore, if we assume that d_t and θ are equal to zero, then from Eq. (2.54) we have

$$M(z^{-1}) = \frac{1}{H(z^{-1})} \tag{2.55}$$

Hence, the equalizer must first identify and approximate the inverse channel characteristics to cancel the inter symbol interference. This is known as the zero-forcing equalization criterion. In other words, we can say that, the main idea is to formulate a zero-forcing blind equalization algorithm. The basic structure for this kind of algorithm is shown in Fig. 2.7. It consists of two major operation blocks, namely, a channel estimator and a channel equalizer. Channel estimation is usually done by using a block estimation approach. However, an adaptive estimation approach of the LMS type can also be employed.

In a broad sense, the polyspectra-based algorithms can be divided in four categories. Fig. 2.8 shows the classification of polyspectra-based blind equalizers. Amongst all the four major categories, the polycepstra-based blind equalization algorithms are the most popular ones, because of their following properties.

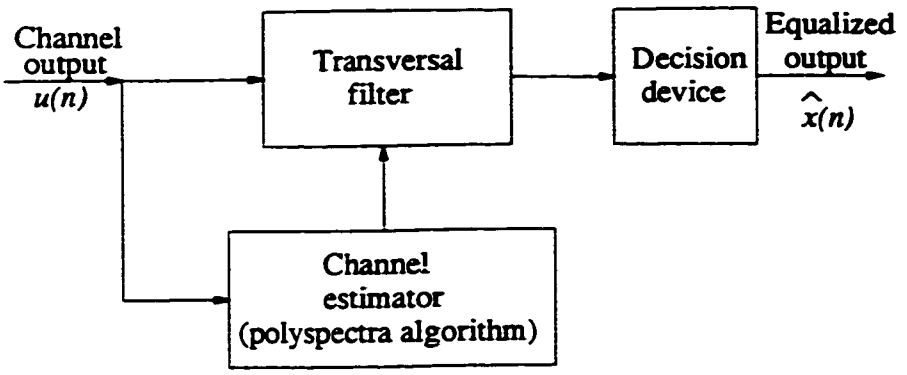

Figure 2.7: Block diagram of a polyspectra-based blind equalizer.

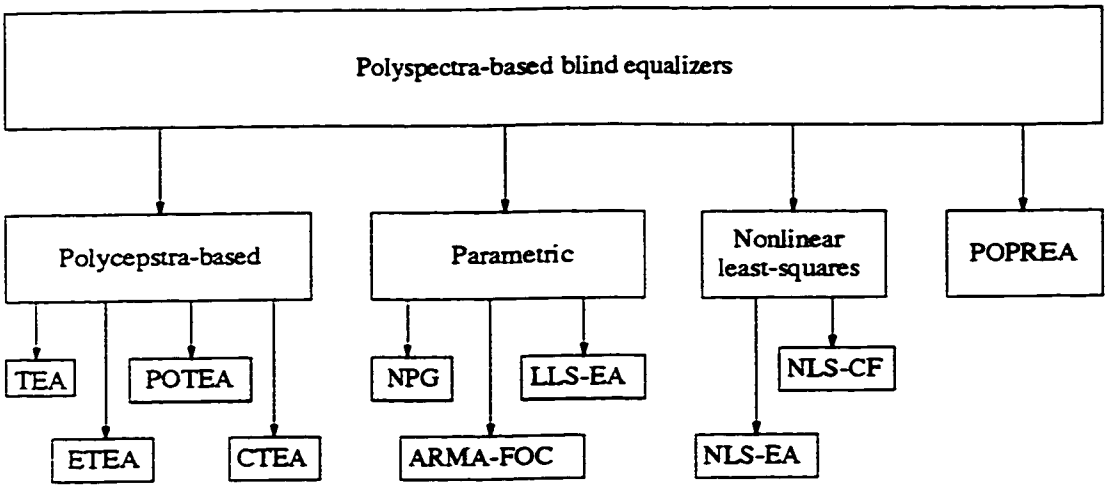

Figure 2.8: Classification of polyspectra-based equalizer.

1. Polycepstra-based blind equalization algorithm are used for both channel identification and equalization techniques which extract magnitude and phase information from the fourth-order cumulants of the channel output.

2. Either the channel impulse response or the equalizer impulse response can be obtained from the other just by changing the sign of the differential cepstrum parameters.

3. These algorithms can identify the minimum-phase and maximum-phase components of the channels separately.

4. The coefficients of the equalizer filters can be calculated indirectly by updating the cepstrum parameters of the channel response.

5. These algorithms are very robust to additive Gaussian noise.

6. They exhibit fast initial convergence.

7. Convergence to a global solution is guaranteed.

8. The only assumption made about the input data is that the input is independently and identically distributed and is non Gaussian.

9. A priori knowledge of the channel model is not required. These techniques work equally well with auto-regressive (AR), moving-average (MA), or auto-regressive-moving-average (ARMA) channels of any order.

The main disadvantage of polyspectra-based algorithms is that they have high computational complexity, which increases rapidly as the zeros of the channel approach the unit circle. More details regarding the mathematical derivation and the working of these different algorithms can be found in [1] and [10].

2.7 Comparison of HOS-Based Blind Equalizer Algorithms

The basic advantages of the implicit HOS-based blind equalization algorithms over the explicit ones are as follows:

1. The implicit HOS-based blind equalization algorithm are relatively simple to implement as compared to the explicit ones.

2. For some specific applications, e.g, line-of-sight digital radio systems, the implicit HOS-based blind equalization algorithms are capable of delivering better performance than the explicit HOS-based blind equalization algorithms.

On the other hand, the major disadvantages of the implicit HOS-based blind equalization algorithms over the explicit ones can be summarized as follows:

1. The implicit HOS-based blind equalization algorithm are sensitive to timing jitter, which is a serious problem.

2. The implicit HOS-based blind equalization algorithms can converge to a local minima and may spoil the performance of the blind equalizer. The explicit HOS-based blind equalization algorithms are free from this problem and always converge to the unique global minima, because they do not need minimization of the nonconvex cost function.

The most serious limitation of both implicit and explicit HOS-based blind equalization algorithms is their slow rate of convergence. This is because the time-average estimation of higher-order statistics requires a much larger sample size than in the case of second-order statistics. Generally, the sample size needed to estimate the n_cth-order statistics of a stochastic process, subject to prescribed values of estimation bias and variance, increases almost exponentially with the order n_c [1].

For the tricepstrum-based blind equalization method [10], which is the most popular amongst the explicit HOS-based blind equalization algorithms, the channel equalization requires at least fourth-order statistics. Similarly, for Bussgang algorithms, we use fourth-order statistics. This causes the HOS-based blind equalization algorithms exhibit a slow rate of convergence, compared to conventional adaptive filtering using a training sequence.

From the available experimental results, one can also find that the conventional adaptive filtering algorithms [1] generally require a few hundred iterations to converge as compared to the existing HOS-based blind equalization algorithm which may require several thousand iterations to converge.

2.8 Cyclostationary Statistics-Based Blind Equalization Algorithms

In a complete statistical description of a random process, for any n and any time instant $(t_1, t_2, \ldots, t_n)$, the joint probability density function $f_{X(t_1),X(t_2),\ldots,X(t_n)}(x_1, x_2, \ldots, x_n)$ always exists. This joint probability density function (pdf) in general depends on the choice of the time origin. In a very important class of random processes, the joint density function is independent of the choice of the time origin. These processes whose statistical properties are time independent, are known as stationary processes. There are different

notions of stationarity – strictly stationary process, wide-sense stationary process and cyclostationary process.

A strictly stationary process is a process in which for all n and all $(t_1, t_2, \ldots, t_n)$, $f_{X(t_1),X(t_2),\ldots,X(t_n)}(x_1, x_2, \ldots, x_n)$ depends only on the relative positions of $t_1, t_2, \ldots, t_n$, not on their actual values. In other words, a shift in the time origin does not change the statistical properties of the process. A formal definition of a strictly stationary process is given below.

Definition: A strictly stationary process is a process in which for all n, all $(t_1, t_2, \ldots, t_n)$, and all Δ

$$f_{X(t_1),X(t_2),\ldots,X(t_n)}(x_1, x_2, \ldots, x_n) = f_{X(t_1+\Delta),X(t_2+\Delta),\ldots,X(t_n+\Delta)}(x_1, x_2, \ldots, x_n) \quad (2.56)$$

The formal definition of a wide-sense stationary process is as follows.

Definition: A process $X(t)$ is wide-sense stationary (WSS), if the following conditions are satisfied:

1. $m_X(t) = E[X(t)]$ is independent of t, and
2. $R_X(t_1, t_2)$ depends only on the time difference $\tau = t_1 - t_2$, not on t_1 and t_2 individually,

where m_X is the statistical mean and R_X is the autocorrelation function of a random process.

In cyclostationary processes, the statistical properties are not time independent, but periodic in time. Mathematically, a cyclostationary process can be defined as follows.

Definition: A random process $X(t)$ with statistical mean $m_X(t)$ and autocorrelation function $R_X(t+\tau, t)$ is called cyclostationary, if both the mean and the autocorrelation are periodic in t with some period T_0, i.e., if

$$\begin{aligned} m_X(t + kT_0) &= m_X(t), \text{ and} \\ R_X(t + \tau + kT_0, t + kT_0) &= R_X(t + \tau, t) \end{aligned} \quad (2.57)$$

for all t, τ, and k. Where k is an integer.

For finding the unknown phase response of a nonminimum-phase channel, HOS-based algorithms use higher-order statistics of the channel output. In this case, the channel output is sampled at the baud rate or symbol rate. This information can also be extracted by using another characteristic of the channel output which is known as cyclostationarity. Cyclostationarity can be explained by rewriting the received signal in a digital communications system in its most general baseband form as given by

$$u(t) = \sum_{k=-\infty}^{\infty} x_k h(t - kT) + v(t) \tag{2.58}$$

where x_k is the symbol transmitted every T seconds thus giving a baud rate of $1/T$, $h(t)$ is the overall impulse response of the channel which includes the transmit and receive filters, and $v(t)$ is the channel noise. All the quantities in Eq. (2.58) are complex valued. Under the assumption that the transmitted sequence x_k and the channel noise $v(t)$ are both wide-sense stationary with zero mean, the mean value of the received signal $u(t)$ can be calculated as

$$E[u(t)] = \sum_{k=-\infty}^{\infty} E[x_k]h(t - kT) + E[v(t)]$$

or

$$E[u(t)] = m_x \sum_{k=-\infty}^{\infty} h(t - kT) + E[v(t)] \tag{2.59}$$

where m_x is the mean amplitude value of the random sequence $\{x_k\}$. We have assumed that the transmitted sequence is wide-sense stationary with zero mean, and the noise $v(t)$ has zero mean. Therefore, we have

$$E[u(t)] = 0$$

Also, it can be observed that although m_x is either zero or constant (depending upon the assumption), the term $\sum_{k=-\infty}^{\infty} h(t - kT)$ is a periodic function with period T. Hence, the mean value of $u(t)$ is periodic with period T.

The auto correlation function of $u(t)$ can be written as

$$R_u(t+\tau,t) = E[u(t)u(t+\tau)] = \sum_{k=-\infty}^{\infty}\sum_{l=-\infty}^{\infty} E(x_k x_l)h(t-kT)h(t+\tau-lT) \quad (2.60)$$

According to the assumption that the transmitted sequence $\{x_k\}$ is WSS, one can write

$$R_x(k) = E[x_k x_{k+m}] \quad (2.61)$$

Hence, Eq. (2.60) can be expressed as

$$\begin{aligned} R_u(t+\tau,t) &= \textstyle\sum_{k=-\infty}^{\infty}\sum_{l=-\infty}^{\infty} R_x(l-k)h(t-kT)h(t+\tau-lT) \\ &= \textstyle\sum_{m=-\infty}^{\infty} R_x(m)\sum_{k=-\infty}^{\infty} h(t-kT)h(t+\tau-kT-mT) \end{aligned} \quad (2.62)$$

Now, it can be observed from Eq. (2.62) that the second summation

$$\sum_{k=-\infty}^{\infty} h(t-kT)h(t+\tau-kT-mT)$$

is periodic with period T. Consequently, the autocorrelation function $R_u(t+\tau,t)$ is periodic in the variable t, i.e.,

$$R_u(t+T+\tau,t+T) = R_u(t+\tau,t) \quad (2.63)$$

Therefore, the autocorrelation function of the received signal is also periodic in the symbol duration T. Hence, we can say that the received signal $u(t)$ is cyclostationary in the wide sense [11].

The idea behind cyclostationary statistics-based algorithm is to use the temporal diversity, i.e., oversampling of the received signal. In digital communication this operation is performed to get timing and phase recovery. In the case of blind channel equalization, to perform the equalization by doing oversampling, the equalization taps are spaced closer than the reciprocal of the incoming symbol rate. This is the reason for this type of equalization technique to be also known as fractionally-spaced equalization technique. There are many techniques available under this category. Most of these are inspired by statistical array digital signal processing. Amongst these, the subspace decomposition method [1] is the most popular one.

2.8.1 Subspace Decomposition Method

In the subspace decomposition method, the channel is modeled as an FIR filter, and for each sampling period T, several measurements are made. To make these measurements, three kinds of techniques can be used:

1. Oversampling of the received signal
2. Use of multiple sensors
3. Combination of techniques 1 and 2

In the second case which uses multiple sensors, we have more than one received signal. These sensors are then used to approximate the channel. This technique uses statistical array signal processing. The first technique can be explained as follows.

Let the received signal $u(t)$ be oversampled by making

$$t = \frac{iT}{L} \tag{2.64}$$

where L is a positive integer. Substituting this value of t from Eq. (2.64) in Eq. (2.58), we have

$$u\left(\frac{iT}{L}\right) = \sum_{k=-\infty}^{\infty} x_k h\left(\frac{iT}{L} - kT\right) + v\left(\frac{iT}{L}\right) \tag{2.65}$$

Now, let

$$i = nL + l, \qquad l = 0, 1, \ldots, L-1 \tag{2.66}$$

Substituting this value of i in Eq. (2.65) yields

$$u\left(nT + \frac{lT}{L}\right) = \sum_{k=-\infty}^{\infty} x_k h\left((n-k)T + \frac{lT}{L}\right) + v\left(nT + \frac{lT}{L}\right) \tag{2.67}$$

Letting

$$\begin{aligned} h_n^{(l)} &= h\left(nT + \tfrac{lT}{L}\right) \\ u_n^{(l)} &= u\left(nT + \tfrac{lT}{L}\right) \\ v_n^{(l)} &= v\left(nT + \tfrac{lT}{L}\right) \end{aligned} \tag{2.68}$$

Eq. (2.67) can be further rewritten as

$$u_n^{(l)} = \sum_{k=-\infty}^{\infty} x_k h_{n-k}^{(l)} + v_n^{(l)}, \qquad l = 0, 1, \ldots, L-1 \tag{2.69}$$

Now, since the channel is assumed to be a causal FIR filter, we have

$$h_k^{(l)} = 0, \quad \text{for } k < 0 \text{ or } k > n_c \text{ for all } l \tag{2.70}$$

where n_c is the order of the filter. It is further assumed that at any time n, the processing involves the use of a transmitted signal vector with $(n_c + n_1)$ symbols as given by

$$\mathbf{x}_n = [x_n, x_{n-1}, \ldots, x_{n-n_c-n_1+1}]^T \tag{2.71}$$

where T represents the transpose of the matrix. Now at the receiving end, instead of n_1 samples, we have $n_1 L$ samples for each block, meaning that the received signal has been oversampled by a factor L. These samples can now be grouped in two different ways to give two different matrix representations for the oversampled channel. These matrix representations are known as:

1. Sylvester matrix representation.
2. Single input multiple output (SIMO) model.

The basic representation of an oversampled channel as a single input multiple output model is shown in Fig. 2.9. It can be seen that it has L virtual channels fed from a common input. Each virtual channel or subchannel has the same time support and its own noise contribution. More details can be found in [1] and [11].

2.9 Limitations of the HOS-Based and Cyclostationary Statistics-Based Blind Equalization Algorithms

In a broad sense, blind equalizers can be divided into three categories. These are implicit higher-order statistics-based blind equalizers, explicit higher-order statistics-based blind equalizers, and cyclostationary statistics-based blind equalizers. All of these blind equalizers have certain advantages and disadvantages.

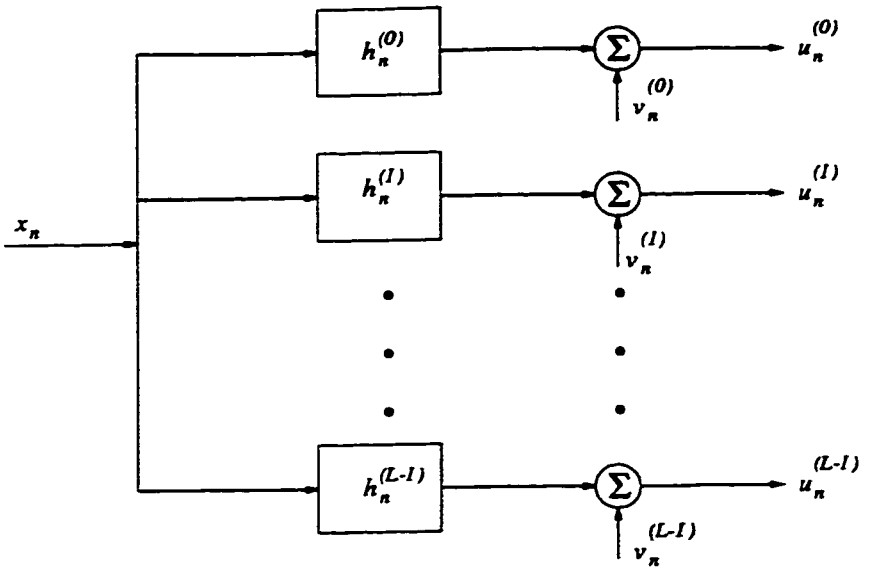

Figure 2.9: An oversampled channel for single input multiple output model.

Implicit higher-order blind equalizers are the least complex from the implementation point of view. But they have a tendency to converge to local minima. This problem is not there with other kinds of blind equalizers.

Explicit higher-order statistics-based blind equalizers have the advantage of always converging to a global minima. But they use a minimum of fourth-order cumulants to estimate the channel leading to a complex implementation.

Cyclostationary statistics-based blind equalizers use only the second-order statistics, and therefore, are much faster than implicit and explicit higher-order statistics-based blind equalizers. But for an efficient operation they require a precise knowledge of the order of the channel, which is not a problem with the higher-order statistics-based blind equalizers.

In cases where channels are characterized by a single input single output (SISO) FIR filter, we require infinite impulse response (IIR) equalizers for achieving a perfect equalization. Bussgang algorithms generally use FIR equalizers for approximating these IIR equalizers. Now, if the IIR equalizer has roots close to the unit circle, we require an extremely long FIR equalizer to approximate the IIR equalizer [12].

Polyspectra-based algorithms use higher-order statistics, which gives rise to higher complexity and much larger size of the FIR filter. This complexity further increases as the zeros of the channel approach the unit circle.

Perfect equalization (zero-forcing) can also be achieved by oversampling the channel output at a rate higher than the baud rate. In this case, as discussed earlier, the channel is modeled as a single input multiple output. Now, if this oversampled channel has repeated zeros, then this technique also fails to achieve the required inverse of the channel with an FIR filter. Further, for channels having their zeros close to the unit circle, this scheme requires a much higher order FIR filter to approximate the inverse of the channel.

It can be seen from the above discussion that Bussgang, polyspectra and cyclostationarity based algorithms suffer from a common problem: when the zeros of the channel approach the unit circle, the equalization becomes more difficult and complex.

2.10 Summary

In this chapter, the underlying theory behind blind equalization techniques has been discussed and some widely used blind equalization structures are presented. The blind equalization algorithms have been grouped into two categories. The first category consists of higher-order statistics-based algorithms, which has been further subdivided into two categories, namely, implicit higher-order statistics-based algorithms and explicit higher-order statistics-based algorithms. The second one consists of cyclostationary statistics-based algorithms.

It has been shown that the decision-directed Bussgang, Godard and Sato algorithms use higher-order statistics in an implicit sense and perform the blind equalization by subjecting the received signal to an iterative deconvolution process. In these algorithms the channel estimation is obtained by minimizing a nonconvex cost function, but the algorithms have the potential of converging to a local minimum. However, the algorithms have a low computational complexity when the zeros of the channel are not very close to the unit circle.

The polyspectra-based algorithms use higher-order statistics in an explicit sense. It has been shown that these algorithms exploit the fourth or higher order cumulants of the received signal to extract the phase information about the channel. In these algorithms, the channel estimation is obtained by identifying the minimum-phase and maximum-phase parts of the channel transfer function without involving the cost function, but the computational complexity is rather high. However, the problem of a false convergence does not exist here.

The common limitations of these higher-order statistics-based algorithms have been discussed and it has been shown that these algorithms have slow rate of convergence and the computational complexity increases substantially as the zeros of the channel approach the unit circle of the z-plane.

Finally, it has been noted that the problem of slow rate of convergence can be overcome by using cyclostationary statistics-based algorithms. But for an efficient operation, they require a precise knowledge of the order of the channel. Also, if the zeros of the channel are repeated, then this technique fails to achieve the required inverse of the channel.

Chapter 3

A New Blind Equalization Scheme

3.1 Introduction

One aspect that is common in implicit HOS, explicit HOS, and cyclostationary statistics based algorithms is that they generally employ finite impulse response (FIR) filters for blind equalization. Bussgang algorithms, when applied to FIR filter-based blind equalizer structures, perform poorly when one or more maximum-phase zero of the channel is close to the unit circle. For the polyspectra-based algorithms, the computational complexity is very high and it increases rapidly as the zeros of the channel approach the unit circle. In the case of cyclostationary statistics-based algorithms, the channel is modeled as a single input multiple output (SIMO) system. If the zeros of this oversampled channel are repeated, this scheme also fails to achieve the required inverse with a FIR filter, because of the reasons explained in Chapter 2.

The above problem can be solved by using a blind equalization structure that is based on an IIR filter and an all-pass filter [16]-[18]. This equalizer models the inverse of the nonminimum-phase channel completely, and is called a sufficient-order equalizer. Even though this blind equalization structure performs better than the other structures discussed in Chapter 2, it makes use of a fourth-order norm. This results in a much higher order all-pass filter and the computational complexity is extremely high for channels whose maximum-phase zeros are close to the unit circle.

The high computational complexity can be reduced by using a block-based time reverser scheme [12]. This structure uses two infinite impulse response (IIR) filters, an

FIR filter, and two block-based time reversers. The computational complexity for this blind equalization structure is lower than that of the sufficient-order equalizers presented in [16]-[18], but it is still quite high. Also, the adaptive IIR filter algorithm may not converge, if the denominator polynomial of the IIR filter does not satisfy the strictly positive real (SPR) condition (see Section 3.3) [14].

In this chapter, we look for simpler and less complex solutions to the blind equalization problem and propose new algorithms for the adaptation of the IIR predictor and the adaptive FIR filter of the structure employed in the equalization scheme. In Section 3.2, the basic components of a sufficient-order equalizer are presented, the assumptions necessary for the design of this class of blind equalizers are mentioned, and a sufficient-order blind equalization structure presented in [12] is briefly discussed. In Section 3.3, the limitations of the sufficient-order equalizer presented in [12] are discussed. A new algorithm for the block-based sufficient-order blind equalizer is proposed in Section 3.4. In Section 3.5, a comparison is made between the proposed block-based sufficient-order blind equalization algorithm and the one presented in [12]. Finally, Section 3.6 gives a brief summary of the work described in this chapter.

3.2 Sufficient-Order Equalizer

The basic block diagram of a baseband communication system is shown in Fig. 3.1 [1]. The system is subjected to inter symbol interference (ISI) and an additive white Gaussian noise (AWGN). The channel model includes the effect of the physical channel together with the spectral shaping caused by the transmit and receive filters. In this figure, $x(n)$ is

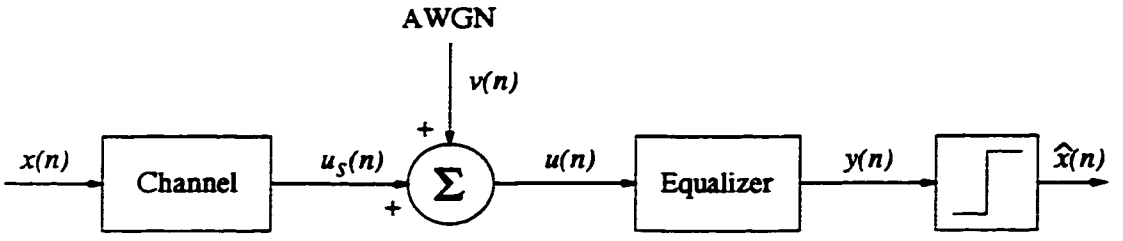

Figure 3.1: Baseband communication system with the channel and an equalizer.

the input data sequence applied to the channel, $u_s(n)$ is the output of the channel, $v(n)$

is the additive white Gaussian noise, which is added to the output $u_s(n)$ of the channel, $u(n)$ is the received signal at the input of the equalizer and $\hat{x}(n)$ is the desired output.

The channel is modeled as an FIR system. Therefore, the sampled input-output relationship of the channel can be expressed by the convolution summation given by

$$u_s(n) = \sum_{i=0}^{n_c} h(i)x(n-i) \tag{3.1}$$

where $h(n),\ 0 \leq n \leq n_c$ are the impulse response coefficients of the channel and n_c is the order of the channel.

The input to the equalizer can be expressed as

$$u(n) = u_s(n) + v(n) \tag{3.2}$$

The additive white Gaussian noise $v(n)$ is statistically independent of the input signal $x(n)$. The objective of the blind equalization is to recover the input sequence $\{x(n)\}$ or, equivalently, to find the impulse response of the channel $h(n),\ 0 \leq n \leq n_c$, by processing only $\{u(n)\}$.

For the purpose of analysis, the following assumptions are made for the sufficient-order blind equalizers [12].

1. The input data sequence $\{x(n)\}$ is independently and identically distributed (iid), and is non-Gaussian with a zero mean. For example, $x(n)$ could be a bipolar sequence with equiprobable symbols $\{-1, +1\}$.

2. The additive noise is modeled as a zero-mean Gaussian and is statistically independent of $\{x(n)\}$.

3. The FIR system (channel) is assumed to be strictly minimum, strictly maximum, or mixed phase. Therefore, the polynomial

$$H(z^{-1}) = \sum_{i=0}^{n_c} h(i)z^{-i} \tag{3.3}$$

has zeros inside and/or outside the unit circle, but none on the unit circle. The

transfer function $H(z^{-1})$ can be written in terms of the product of the minimum and the maximum phase factors of the channel as follows:

$$H(z^{-1}) = \prod_{i=1}^{d}(1 - \xi_i^i z^{-1}) \prod_{j=1}^{s}\left[\left(\xi_j^o\right)^{-1} - z^{-1}\right] \tag{3.4}$$

where $\left|\xi_i^i\right| < 1$ for $i = 1, \ldots, d$ corresponds to the minimum-phase zeros, $\left|\xi_j^o\right| > 1$ for $j = 1, \ldots, s$ corresponds to the maximum-phase zeros, and $n_c = d + s$.

4. In a digital communication channel, the interference is dominated by the inter symbol interference rather then the additive white Gaussian noise. Therefore, for the simplicity of the analysis, the effect of AWGN is not considered.

5. The channel is assumed to be constant at least during each block length [12].

An equalizer which models the inverse of a maximum-phase channel completely is called a sufficient-order equalizer [16]-[18]. A sufficient-order blind equalization technique based on an IIR predictor and an all-pass filter is shown in Fig. 3.2 [16]-[18].

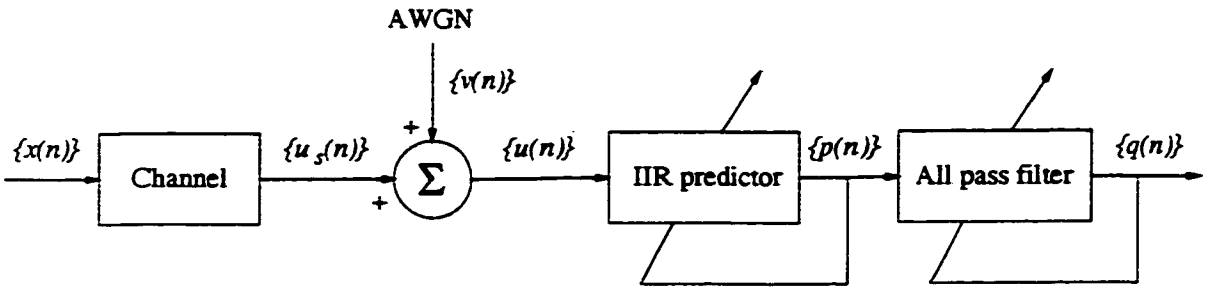

Figure 3.2: Blind equalization structure based on an IIR filter and an all-pass filter.

The IIR predictor is an adaptive IIR filter and is called a predictor. The IIR predictor coefficients are adapted to minimize the mean square of its output $\{p(n)\}$ as given by

$$J = E\{p^2(n)\} \tag{3.5}$$

The order of the channel can be estimated from the autocorrelation values of the channel output. This can be done by choosing the largest length that corresponds to the significant

nonzero autocorrelation value [12]. The blind equalization scheme shown in Fig. 3.2, first searches for a global minimum for the cost function $E\{p^2(n)\}$. As the cost function $E\{p^2(n)\}$ reaches a global minima, the transfer function of the IIR predictor represents the inverse of the spectrally equivalent minimum-phase (SEMP) model of the channel and can be represented as [16]

$$I(z^{-1}) = \frac{1}{R(z^{-1})} = \frac{1}{\prod_{i=1}^{d}(1-\xi_i^i z^{-1})\ \prod_{j=1}^{s}\left[1-\left(\xi_j^o z\right)^{-1}\right]} \tag{3.6}$$

where $R(z^{-1})$ represents the z-domain impulse response of a standard spectrally equivalent minimum-phase channel [12]. Now, using Eqs. (3.4) and (3.6), the transfer function of the cascade of the channel and the IIR predictor can be written as

$$P(z^{-1}) = \frac{H(z^{-1})}{R(z^{-1})} = \frac{\prod_{j=1}^{s}\left[\left(\xi_j^o\right)^{-1} - z^{-1}\right]}{\prod_{j=1}^{s}\left[1-\left(\xi_j^o z\right)^{-1}\right]} \tag{3.7}$$

Eq. (3.7) represents an all-pass z-domain transfer function.

The output of the IIR predictor $\{p(n)\}$ is an auto-regressive-moving-average (ARMA) sequence of the flat magnitude spectrum with a distorted phase because the sequence $\{p(n)\}$ is second-order white. In order to remove this phase distortion another all-pass filter is required [12]. This all pass filter is adapted to minimize the function

$$J1 = E\{q^4(n)\} \tag{3.8}$$

It can be observed from Eq. (3.8), that now a fourth-order norm is required as the correlation is absent from the output of the IIR predictor. It again requires a much higher order all-pass filter for the channels whose maximum-phase zeros are close to the unit circle.

3.2.1 The IIR-IIR-FIR Blind Equalization Structure

The high computational complexity of the sufficient-order equalizer presented in [16]-[18] and discussed above can be reduced by using a block-based time reverser scheme presented in [12]. This blind equalization structure makes use of an adaptive IIR predictor, an IIR filter and an adaptive FIR filter together with two block-based time reverser as

depicted in Fig. 3.3. The operation of equalization is based on a theorem established by Lambotharan and Chambers [12]. According to this theorem, if we let $\{p(n)\}$ and $\{\overline{x}(n)\}$

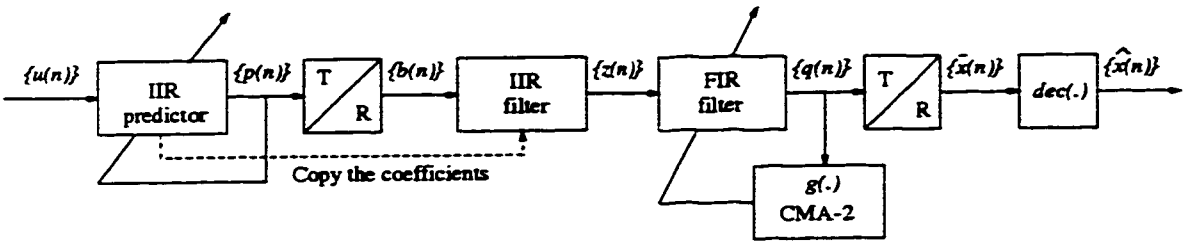

Figure 3.3: Blind equalizer structure based on two filters, an FIR filter and two block-based time reversers.

to be the input and output of an all-pass filter $P(z^{-1})$, then time reversed sequence of $\{\overline{x}(n)\}$ can be reconstructed exactly by sending the time reversed sequence of $\{p(n)\}$ through an all-pass filter whose transfer function is $P(z^{-1})$.

The use of block-based time reversers in the structure brings the following advantages.

1. The scheme has a reduced computational complexity [12].
2. It is well suited for stability monitoring.
3. The order of all-pass filter, to reconstruct the transmitted sequence perfectly, is equal to the number of maximum-phase zeros of the channel.

Now, let the z-domain transfer function of the channel be

$$H(z^{-1}) = \prod_{i=1}^{d}(1-\xi_i^l z^{-1}) \prod_{j=1}^{s}\left[\left(\xi_j^o\right)^{-1} - z^{-1}\right] \tag{3.9}$$

where $\left|\xi_i^l\right| < 1$ for $i = 1,\ldots,d$ and $\left|\xi_j^o\right| > 1$ for $j = 1,\ldots,s$, and let the z-domain transfer function of the IIR predictor be

$$I(z^{-1}) = \frac{1}{\prod_{i=1}^{d}(1-\xi_i^l z^{-1}) \prod_{j=1}^{s}\left[1-(\xi_j^o z)^{-1}\right]} \tag{3.10}$$

then the cascade of the channel and the predictor is an all-pass filter with the transfer

function given by

$$P(z^{-1}) = \frac{H(z^{-1})}{R(z^{-1})} = \frac{\prod_{j=1}^{s}\left[\left(\xi_j^o\right)^{-1} - z^{-1}\right]}{\prod_{j=1}^{s}\left[1 - \left(\xi_j^o z\right)^{-1}\right]} \tag{3.11}$$

Now, according to the Lambotharan and Chambers [12], the transfer function of the combined IIR and FIR filters required to reconstruct the transmitted sequence is

$$F(z^{-1})I'(z^{-1}) = \frac{\prod_{j=1}^{s}\left[\left(\xi_j^o\right)^{-1} - z^{-1}\right]}{\prod_{j=1}^{s}\left[1 - \left(\xi_j^o z\right)^{-1}\right]} \tag{3.12}$$

where $I'(z^{-1})$ and $F(z^{-1})$ are, respectively, the z-domain transfer functions of the IIR filter and the adaptive FIR filter. Multiplying and dividing Eq. (3.12) by the minimum-phase part of the channel, Eq. (3.12) can be rewritten as

$$F(z^{-1})I'(z^{-1}) = \frac{\prod_{i=1}^{d}(1 - \xi_i^l z^{-1})\ \prod_{j=1}^{s}\left[\left(\xi_j^o\right)^{-1} - z^{-1}\right]}{\prod_{i=1}^{d}(1 - \xi_i^l z^{-1})\ \prod_{j=1}^{s}\left[1 - \left(\xi_j^o z\right)^{-1}\right]} \tag{3.13}$$

Using Eqs. (3.9) and (3.10) in Eq. (3.13), we have

$$F(z^{-1})I'(z^{-1}) = H(z^{-1})I(z^{-1}) \tag{3.14}$$

Eq. (3.14) is the condition for perfectly reconstructing the transmitted sequence. Now, if the transfer function of the IIR predictor is chosen to be equal to the transfer function of the IIR filter, i.e.,

$$I(z^{-1}) = I'(z^{-1}) \tag{3.15}$$

then the Eq. (3.14) simplifies to

$$F(z^{-1}) = H(z^{-1}) \tag{3.16}$$

Eq. (3.16) shows that the coefficients of the FIR filter given by $F(z^{-1})$ required to reconstruct the transmitted sequence are the same as those for the channel.

The operation of the blind equalization structure shown in Fig. 3.3 can be explained

using the result given in Eq. (3.16). The IIR predictor is an adaptive filter and it adapts itself to minimize the cost function of $E\{p^2(n)\}$. At the optimum, the transfer function of the predictor is the inverse of the spectrally equivalent minimum-phase of the channel. The output of the IIR predictor is collected in a block and time reversed. The output of the time reverser is sent to another IIR filter whose coefficients are copied from the IIR predictor.

The sequence $\{z(n)\}$ obtained at the output of the second IIR filter is sent to an FIR adaptive filter. The output of the FIR adaptive filter is collected in a block and the block is again time reversed to reconstruct the transmitted sequence in the right order.

Number of data outputs stored in a block can be consistent with the transmission system, e.g., in a packet transmission system each block can be equal to the length of each packet.

3.2.2 Adaptation of the IIR Predictor

A simplified stochastic-gradient method has been used in [12] for the adaptation of the IIR filter for the scheme shown in Fig. 3.3. According to this algorithm

$$\mathbf{r}_{n+1} = \mathbf{r}_n + \mu p(n)\mathbf{p}_n \tag{3.17}$$

where μ is the adaptation gain, $\mathbf{r}$ is the IIR predictor weight vector, and $\mathbf{p}$ is an IIR feedback vector. The adaptation gain μ is chosen small enough to maintain the stability. The IIR predictor weight vector $\mathbf{r}$ is expressed as

$$\mathbf{r}_n^T = [r_n(1)\ \ r_n(2)\ \cdots\ r_n(n_r)] \tag{3.18}$$

where $r_n(i)$'s represent the coefficients of the IIR predictor. The IIR predictor feedback vector $\mathbf{p}$ is expressed as

$$\mathbf{p}_n^T = [p(n-1)\ \ p(n-2)\ \cdots\ p(n-n_r)] \tag{3.19}$$

In the Eqs. (3.17) and (3.18), $[.]^T$ represents the transpose of the associated column vector and n_r the length of the IIR predictor [12].

3.2.3 Adaptation of the FIR Filter

A normalized constant modulus adaptive CMA-2 algorithm [7] has been used in the scheme of Fig. 3.3 for the adaptive FIR filter. The length of the adaptive FIR filter is first chosen as $2n_c + 1$, where n_c is the order of the channel and the center tap weight is initialized to unity [12] to avoid the sign ambiguity. The adaptation of the FIR filter is carried out as follows:

$$\mathbf{w}(n+1) = \mathbf{w}(n) + \mu * \frac{[|q(n)|^2 - R]q(n)\mathbf{z}}{\rho + \mathbf{z}^T\mathbf{z}} \tag{3.20}$$

where the tap weight vector given by

$$\mathbf{w}^T(n) = [w_0(n)\ w_1(n)\ \cdots\ w_{2n_c+1}(n)] \tag{3.21}$$

represents the coefficients of the FIR filter, $\mathbf{z}$ is the input weight vector of the FIR filter expressed as

$$\mathbf{z}^T(n) = [z(n-1)\ z(n-2)\ \cdots\ z(n-2n_c-1)], \tag{3.22}$$

R_p is a positive real constant defined as

$$R_p = \frac{E\{|x(n)|^4\}}{E\{|x(n)|^2\}}, \tag{3.23}$$

and ρ is $E\{|z(n)|^3\}$ which is estimated at each sample as

$$\widehat{\rho}_{n+1} = \gamma\widehat{\rho}_n + (1-\gamma)|z(n)|^3 \tag{3.24}$$

The constant $\gamma \in (0,1)$ is the adaptation constant usually approximately equal to unity [12].

The IIR predictor is an adaptive IIR filter, and the second IIR filter copies the coefficients of the adaptive IIR predictor. Therefore, the input to the FIR filter is statistically nonstationary. Thus, the power of the output of the IIR filter or the input to the FIR filter changes with time. After a small number of iterations, n_c coefficients of the filter remain around zero with a negligible amplitude, and therefore, may be switched off in the adaptation [12]. This provides a direct-form of the channel-order selection.

The estimate of the channel is obtained by multiplying the FIR filter-parameter vector by a gain G as follows:

$$\mathbf{h} = [h(0)\ h(1)\ \cdots\ h(n_c)] = \mathbf{w}G \tag{3.25}$$

The gain G is given by

$$G = \sqrt{\frac{\sigma^2}{\mathbf{w}^T\mathbf{w}}} \tag{3.26}$$

where σ^2 is the output power of the IIR predictor estimated as follows:

$$\hat{\sigma}^2_{n+1} = \gamma\hat{\sigma}^2_n + (1-\gamma)p^2(n) \tag{3.27}$$

3.3 Limitations of the IIR-IIR-FIR Blind Equalization Structure of [12]

The main purpose of the blind equalization scheme presented in [12] and discussed above was to reduce the computational complexity for the communication channels having deep spectral nulls. From the above discussions, it can be seen that the complexity of the blind equalization structure depicted in Fig. 3.3 depends mainly on the adaptation algorithms of the IIR predictor and the FIR filter. This structure, in general, reduces the computational complexity of the blind equalization as compared to the other conventional schemes discussed in Chapter 2, but more specifically when one or more zeros of the channel approach the unit circle. However, the scheme is still computationally intensive because of the normalized constant modulus adaptive CMA-2 algorithm employed for the adaptation of the FIR filter.

The blind equalization of communication channels without deep spectral nulls can be achieved efficiently by the use of decision-directed Bussgang algorithm or Sato algorithm discussed in Chapter 2. The complexity of these algorithms are much less than that of the normalized constant modulus adaptive CMA-2 algorithm. Thus, for the case when the channel is not a deep spectral null channel, the use of the normalized constant modulus adaptive CMA-2 algorithm makes the entire blind equalization scheme unnecessarily computationally complex.

The adaptation of the IIR predictor in [12] is done using a simplified stochastic-gradient algorithm presented in [14]. The major disadvantage of this algorithm is that it cannot converge to the minimum of the mean square output error surface unless the denominator polynomial of the IIR predictor satisfies a strictly positive real condition[1]. If this condition is not satisfied, the algorithm may converge to an arbitrary point on the mean square output error surface and the overall performance may not be acceptable.

The noise present at the channel output passes through the IIR predictor and then through the all-pass filter formed by the cascade of the IIR filter and the adaptive FIR filter. If the noise present at the channel output is high and the noise amplification by the IIR predictor is not in an acceptable range, then the positions of the IIR filter and the adaptive FIR filter after the time reverser are swapped in order to keep the noise level within an acceptable range [12]. This makes the blind equalization process more complex.

The blind equalization structure presented in [12], makes use of adaptive IIR and adaptive FIR filter algorithms which are not similar to the well known least mean square (LMS) norms. Most of the hardware available is based on the least mean square adaptive algorithms. Therefore, additional hardware is required for the implementation of the blind equalization structure that uses adaptive IIR predictor and FIR filter algorithms [12].

3.4 Proposed Blind Equalization Scheme

The disadvantages of the adaptive IIR filter algorithm that it may not converge if the denominator polynomial of the transfer function of the IIR predictor does not satisfy a strictly positive real condition and the high computational complexity of the adaptive FIR filter algorithm are the major source of concerns of the equalization scheme presented in [12]. We will now address these concerns by replacing the existing adaptive IIR predictor algorithm of [12] by a gradient-based adaptation algorithm and adaptive FIR filter algorithm by a simpler and less complex adaptive algorithm.

[1] In [14], it has been shown that in order to guarantee convergence of their algorithm, it is necessary that the following strictly positive real condition (SPR) be satisfied:

$$Re[I(z^{-1})] - \frac{1}{2} > 0, \quad \text{for all } |z| = 1$$

where $Re[I(z^{-1})]$ denotes the real part of the IIR predictor transfer function.

We now propose a new blind equalization structure as shown in Fig. 3.4. Using the assumptions made in Section 3.2, we next propose and discuss the adaptation schemes for the IIR predictor and the adaptive FIR filter.

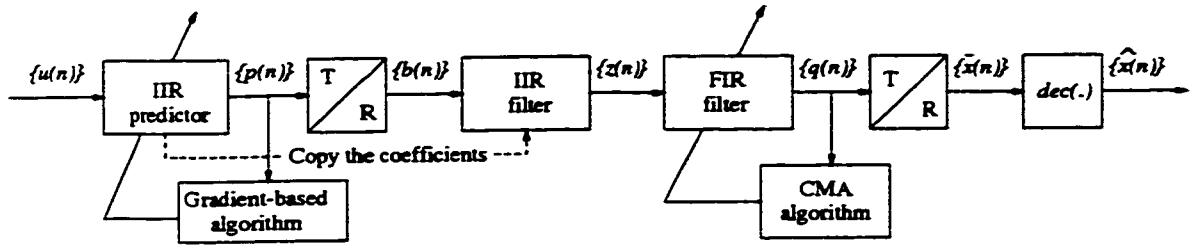

Figure 3.4: The proposed blind equalization structure.

3.4.1 Adaptive IIR Predictor

Fundamentally, there have been two approaches to adaptive IIR filtering that correspond to two different formulations for the prediction error [15]. These are known as the equation error and output error methods. In the equation error approach, the feedback coefficients of an IIR filter are updated in an all-zero nonrecursive form, which are then copied by the second IIR filter implemented in an all-pole form. This formulation can lead to unbiased estimates of the IIR filter coefficients. On the other hand, the output error formulation updates the feedback coefficients directly in a pole-zero recursive form, and therefore, does not generate biased estimates [14].

The IIR predictor used in the scheme of Fig. 3.3 has been based on a simplified stochastic-gradient method and it belongs to the later class of the adaptive IIR filtering. We now propose a gradient-based adaptation algorithm which also belongs to the later class and is based on Gauss-Newton algorithm for the adaptation of the IIR predictor. Contrary to the scheme of [14], this algorithm does not require the denominator polynomial of the IIR predictor to follow the strictly positive real condition defined in Section 3.3. It only requires that the order of the IIR predictor must be greater than or equal to that of the channel[2] . The general structure of the IIR predictor is depicted in Fig. 3.5.

[2]The other condition of convergence is that

$$Re[I(e^{-j\omega})] > 0, \quad \text{for all } \omega \quad -\pi < \omega < \pi$$

which is always satisfied for the predictor transfer function $I(z^{-1})$ of the type given in Eq. (3.6).

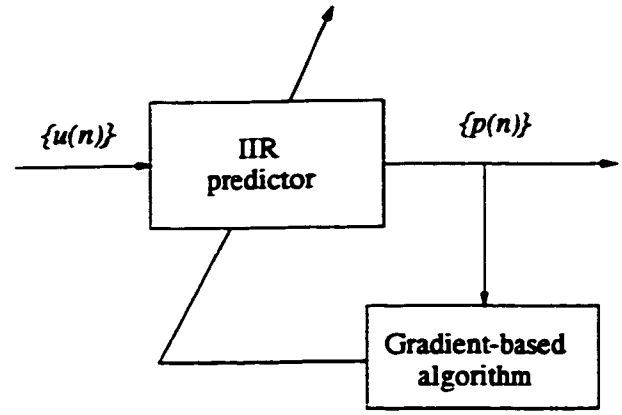

Figure 3.5: Basic block diagram of an adaptive IIR predictor.

The IIR predictor coefficients are adapted to minimize the mean square of its output $\{p(n)\}$ as given by

$$J = E\{p^2(n)\} \tag{3.28}$$

where $p(n)$ is the observed output of the adaptive IIR predictor. The objective of the adaptive IIR predictor is to reduce a function of the output given by

$$J(n) = f(p(n)) \tag{3.29}$$

Considering that the adaptive IIR predictor is realized using the direct form structure shown in Fig. 3.6, i.e., it is an all-pole filter, it meets the requirements discussed in Section 3.2. The predictor's output signal information vector in this case can be represented as

$$\mathbf{s}(n) = [p(n-1)\ p(n-2)\ \cdots\ p(n-n_r)]^T \tag{3.30}$$

where n_r is the length of the adaptive IIR predictor denominator and $[.]^T$ denotes the transpose of the associated column matrix. The direct form adaptive predictor can be characterized in the time-domain by the following difference equation

$$p(n) = u(n) - \sum_{j=1}^{n_r} a_j(n)p(n-j) \tag{3.31}$$

This difference equation can also be rewritten in a vector form, which is more suitable

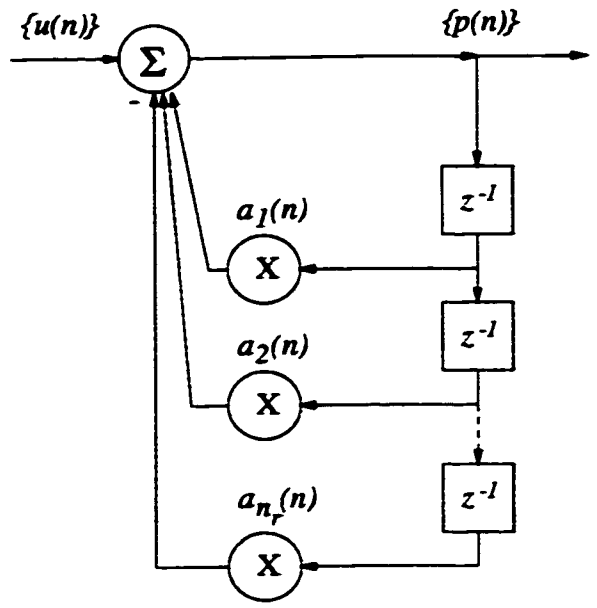

Figure 3.6: Adaptive IIR predictor with direct form realization.

for the algorithm description and implementation as

$$p(n) = \mathbf{a}^T(n)\mathbf{s}(n) \tag{3.32}$$

where $\mathbf{a}(n)$ is the adaptive IIR predictor coefficient vector given by

$$\mathbf{a}(n) = [a_1(n)\ a_2(n)\ \cdots\ a_{n_r}(n)]^T \tag{3.33}$$

Now, consider the output mean square function defined as

$$J = E\{p^2(n)\} \tag{3.34}$$

In the Gauss-Newton algorithm, the minimization of the objective function J is obtained by performing searches in the Newton direction [15] using the estimates of the inverse Hessian matrix and the gradient vector. This gradient vector is calculated as follows:

$$\frac{\partial J}{\partial \mathbf{a}(n)} = E[2p(n)\Psi(n)] \tag{3.35}$$

where the vector $\Psi(n)$ is given by

$$\Psi(n) = \frac{\partial p(n)}{\partial \mathbf{a}(n)} \tag{3.36}$$

which can be approximated by

$$\Psi(n) \approx [p(n-1)\ p(n-2)\ \cdots\ p(n-n_r)]^T = \mathbf{s}(n) \tag{3.37}$$

The Hessian matrix is then given by

$$\frac{\partial^2 J}{\partial \mathbf{a}^2(n)} = 2E\left[\Psi(n)\Psi^T(n) + \frac{\partial^2 p(n)}{\partial \mathbf{a}^2(n)} p(n)\right] \tag{3.38}$$

The expected value of the second term of the bracketed expression of Eq. (3.38) is approximately zero, since in close neighborhood of the solution, the output $p(n)$ is almost a white noise [15], independent of the term

$$\frac{\partial^2 p(n)}{\partial \mathbf{a}^2(n)}$$

The determination of the gradient vector and the Hessian matrix requires the calculation of statistical expectations. In order to derive a recursive algorithm, estimates of the gradient vector and Hessian matrix have to be used. For the gradient vector, the most commonly used estimation is given by

$$\frac{\partial \widehat{J}}{\partial \mathbf{a}(n)} = 2p(n)\Psi(n) \tag{3.39}$$

where $\widehat{J}$ is an estimate of J given by Eq. (3.34).

The Hessian estimate can be generated by employing a weighted summation as follows:

$$\widehat{\mathbf{R}}(n+1) = \alpha\Psi(n)\Psi^T(n) + \alpha\sum_{i=0}^{n-1}(1-\alpha)^{n-i}\Psi(i)\Psi^T(i) \tag{3.40}$$

where α is a small factor chosen in the range $(0,\ 0.1)$ [15]. Eq. (3.40) can be rewritten as

$$\widehat{\mathbf{R}}(n+1) = \alpha\Psi(n)\Psi^T(n) + (1-\alpha)\widehat{\mathbf{R}}(n) \tag{3.41}$$

Taking expectation of the quantities on both sides of the Eq. (3.41) and letting $n \to \infty$,

we have

$$E[\widehat{\mathbf{R}}(n+1)] = \alpha \sum_{i=0}^{n} (1-\alpha)^{n-i} E[\Psi(i)\Psi^T(i)] \tag{3.42}$$

The expected value given by Eq. (3.42) can be approximated as

$$E[\widehat{\mathbf{R}}(n+1)] \approx E[\Psi(n)\Psi^T(n)] \tag{3.43}$$

By applying the approximation discussed, the Gauss-Newton algorithm for IIR adaptive filtering for the proposed blind equalization scheme can be written as

$$\Psi(n) = \frac{\partial p(n)}{\partial \mathbf{a}(n)} \tag{3.44}$$

$$\widehat{\mathbf{R}}^{-1}(n+1) = \frac{1}{1-\alpha}\left[\widehat{\mathbf{R}}^{-1}(n) - \frac{\widehat{\mathbf{R}}^{-1}(n)\Psi(n)\Psi^T(n)\widehat{\mathbf{R}}^{-1}(n)}{\frac{1-\alpha}{\alpha} + \Psi^T(n)\widehat{\mathbf{R}}^{-1}(n)\Psi(n)}\right] \tag{3.45}$$

$$\mathbf{a}(n+1) = \mathbf{a}(n) + \mu\widehat{\mathbf{R}}^{-1}(n+1)\Psi(n)p(n) \tag{3.46}$$

where μ is the convergence factor [15].

If in the Gauss-Newton algorithm discussed above, the Hessian matrix is replaced by an identity matrix, the resulting algorithm becomes a gradient-based algorithm [45]. Eq. (3.46) in this case becomes

$$\mathbf{a}(n+1) = \mathbf{a}(n) + \mu\Psi(n)p(n) \tag{3.47}$$

The computational complexity of this algorithm is much less than that of the Gauss-Newton algorithm.

The gradient-based algorithm for the proposed blind equalization scheme can be summarized as follows:

$$\Psi(n) = [p(n-1)\ p(n-2)\ \cdots\ p(n-n_r)]^T \tag{3.48}$$

$$\mathbf{a}(n+1) = \mathbf{a}(n) + \mu\Psi(n)p(n) \tag{3.49}$$

where $\mathbf{a}(n)$ is the weight vector of the adaptive IIR predictor given by

$$\mathbf{a}(n) = [a_1(n)\ a_2(n)\ \cdots\ a_{n_r}(n)]^T \tag{3.50}$$

The advantages of using the gradient-based algorithm are as follows:

1. This algorithm does not require the denominator polynomial of the IIR filter to follow the strictly positive real condition of [14].
2. The proposed algorithm converges provided that the order of the IIR predictor is greater than or equal to that of the channel.
3. It has a reduced computational complexity.
4. Unstable poles have the tendency to migrate back into the stable region, so the algorithm generally has a self-stabilizing feature.
5. Easy to monitor stability.

3.4.2 Adaptive FIR Filter

The computational complexity of the blind equalization structure presented in [12] can be decreased by using a less complex FIR filter adaptation algorithm. As in [12], the new algorithm proposed for the adaptation of the FIR filter is also a constant modulus adaptive CMA algorithm but it has a much less computational complexity. The basic block diagram of an adaptive FIR filter with constant modulus adaptive algorithm is depicted in Fig. 3.7. The input to the FIR adaptive filter is the output $z(n)$ of second IIR filter and the output is $q(n)$. The filter output $q(n)$ may be written as

$$q(n) = \mathbf{z}^T(n)\mathbf{w}(n) \tag{3.51}$$

where $\mathbf{z}(n)$ is the input data vector in the filter delay line, given by

$$\mathbf{z}(n) = [z(n)\ z(n-1)\ \cdots\ z(n-N+1)]^T \tag{3.52}$$

and $\mathbf{w}(n)$ is the tap weight vector, represented by

$$\mathbf{w}(n) = [w_0(n)\ w_1(n)\ \cdots\ w_{N-1}(n)]^T \tag{3.53}$$

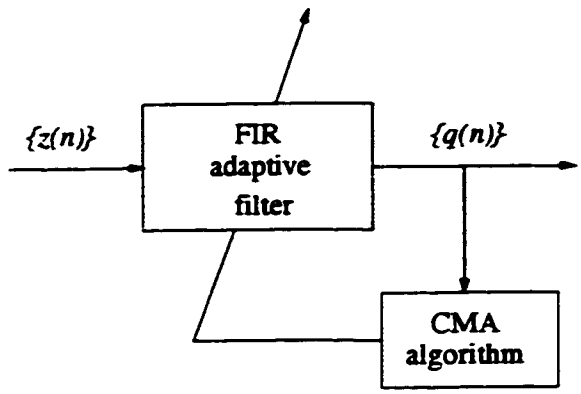

Figure 3.7: Basic block diagram of an adaptive FIR filter with CMA algorithm.

The tap weights are adjusted at each sampling instant. In Eqs. (3.51), (3.52) and (3.53), N represents the length of the FIR adaptive filter and is chosen as

$$N = 2n_c + 1 \tag{3.54}$$

where n_c is the order of the channel. The most straightforward realization for the adaptive FIR filter is through the direct-form realization as illustrated in Fig. 3.8.

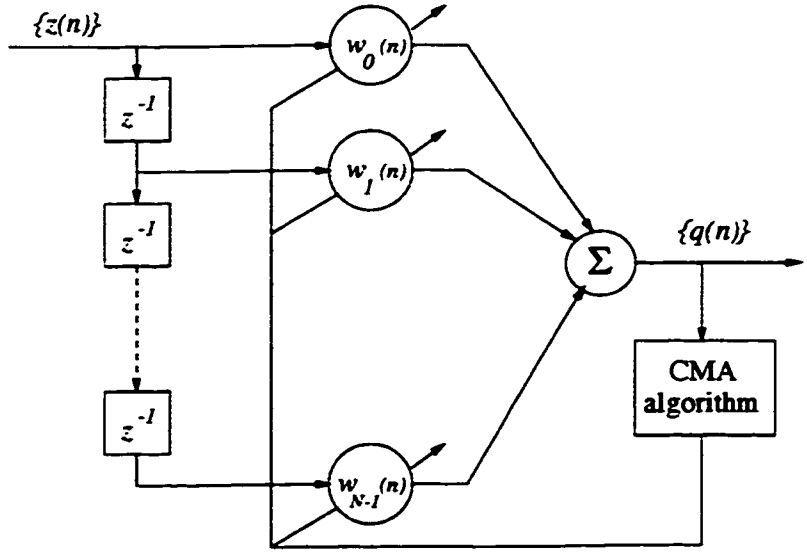

Figure 3.8: Direct form realization of the adaptive FIR filter.

The objective of the adaptive filtering is to make $q(n)$ to have a constant instantaneous modulus as an average. This can be done by choosing the tap weight vector $\mathbf{w}$ in such a

way as to minimize a positive definite measure of the signal modulus variation, given by

$$J = \frac{1}{4}E\{[|q(n)|^2 - 1]^2\} \tag{3.55}$$

It can be seen from this equation that J is just a positive measure of the average amount that the filter output $q(n)$ deviates from the unity modulus condition [8]. The tap weight vector $\mathbf{w}$ is adjusted in such a way that J attains a minimum value and in the process $q(n)$ becomes as close to a unit length as possible. Knowing the performance function and the type of the filter structure, there are many possible approaches for updating the tap weight vector $\mathbf{w}$ [15]. Simple gradient search algorithms are generally easy to implement on hardware and are computationally less complex. Therefore, a simple gradient search algorithm is used to minimize J. In the proposed algorithm the tap weight vector $\mathbf{w}$ is updated as follows:

$$\mathbf{w}(n+1) = \mathbf{w}(n) - \mu\nabla_w J \tag{3.56}$$

where $\mathbf{w}(n)$ is the set of coefficients used to generate output $q(n)$ as given by Eq. (3.51), the parameter μ is a positive step-size that regulates the convergence rate, and ∇_w is the gradient operator with respect to the elements of the tap weight vector $\mathbf{w}$. In Eq. (3.56), the gradient of J with respect to the tap weight vector $\mathbf{w}$ can be written as

$$\nabla_w J = \frac{1}{2}E\{[|q(n)|^2 - 1]\nabla_w[\mathbf{w}^H\mathbf{z}^*\mathbf{z}^T\mathbf{w}]\} \tag{3.57}$$

where $\mathbf{w}^H$ is the Hermitian transposition of $\mathbf{w}$ (i.e., transposition of $\mathbf{w}$ followed by complex conjugation or vice versa). Eq. (3.57) can also be written as

$$\nabla_w J = \frac{1}{2}E\{[|q(n)|^2 - 1]\mathbf{z}^*(n).\mathbf{z}^T(n)\mathbf{w}\} \tag{3.58}$$

Using Eq. (3.51) in Eq. (3.58) yields

$$\nabla_w J = \frac{1}{2}E\{[|q(n)|^2 - 1]q(n)\mathbf{z}^*(n)\} \tag{3.59}$$

The adaptive algorithm can now be obtained by replacing the true gradient given by Eq. (3.59) with an instantaneous gradient estimate given by

$$\widehat{\nabla}_w J = [|q(n)|^2 - 1]q(n)\mathbf{z}^*(n) \tag{3.60}$$

In Eq. (3.56), replacing $\nabla_w J$ with , $\widehat{\nabla}_w J$ we have

$$\mathbf{w}(n+1) = \mathbf{w}(n) - \mu\{[|q(n)|^2 - 1]q(n)\mathbf{z}^*(n)\} \tag{3.61}$$

For a real baseband PAM system, the data sequence is real, i.e., it does not have any imaginary part. Therefore, for a real baseband PAM system, Eq. (3.61) can be written as

$$\mathbf{w}(n+1) = \mathbf{w}(n) - \mu\{[|q(n)|^2 - 1]q(n)\mathbf{z}(n)\} \tag{3.62}$$

Eq. (3.62) gives the desired adaptive algorithm for the adaptation of the FIR filter.

Once the algorithm converges, it can be seen that n_c tap weights fluctuate around zero with a negligible amplitude. Then, the final estimate of the channel is obtained by multiplying the non-zero FIR filter-parameter vector by a gain G as follows:

$$\mathbf{h} = [h(0)\ h(1)\ \cdots\ h(n_c)] = \mathbf{w}G \tag{3.63}$$

where G is the gain given by

$$G = \sqrt{\frac{\sigma^2}{\mathbf{w}^T\mathbf{w}}} \tag{3.64}$$

with σ^2 being the output power of the IIR predictor estimated as

$$\widehat{\sigma}^2_{n+1} = \gamma\widehat{\sigma}^2_n + (1-\gamma)p^2(n) \tag{3.65}$$

The constant γ is the adaptation parameter in the range $(0, 1)$.

The following two advantages of the proposed constant modulus adaptive algorithm, based on gradient search algorithm can be readily noted.

1. The true gradient used in Eq. (3.56) has been replaced by an instantaneous gradient estimate. This instantaneous estimate can be averaged and used periodically to update $\mathbf{w}$. This leads to a hardware simplification.

2. This algorithm can be used for the complex baseband PAM systems.

3.5 Comparison of the Proposed Blind Equalization Scheme with the Scheme of [12]

In this section we compare the merits of the blind equalization scheme proposed in Section 3.4 with that of the one presented in [12].

3.5.1 Computational Complexity

The sufficient-order equalizer presented in [16]-[18] uses an IIR filter predictor and an all-pass filter. This structure models the inverse of the maximum-phase channel effectively, but as discussed in Section 3.2, it uses a fourth-order norm $J2 = E\{q^4(n)\}$ which, in turn, requires a much higher order all-pass filter for the channels whose maximum-phase zeros are close to the unit circle. The overall computational complexity for this structure is comparable to the blind equalization techniques that make use of FIR filters discussed in Chapter 2.

The blind equalizer structure presented in [12] is based on two IIR filters, an FIR filter and two block-based time reverser. This structure reduces the computational complexity of the blind equalization schemes of [16]-[18] when one or more zeros of the channel is close to the unit circle, but the use of a normalized constant modulus adaptive CMA-2 algorithm for the adaptation of the FIR filter still makes it computationally demanding. We now analyze the proposed scheme and the one presented in [12] for the adaptations of IIR predictor and FIR filter algorithms for their computational complexities.

Computational complexity of IIR predictor

We first evaluate the number of multiplications and additions required by the IIR predictor proposed in [12]. For convenience, rewrite Eq. (3.17) as follows:

$$\mathbf{r}_{n+1} = \mathbf{r}_n + \mu p(n)\mathbf{p}_n \tag{3.66}$$

For the calculation of $\mu p(n)\mathbf{p}_n$, we require $n_r + 1$ multiplications, where n_r represents the length of the IIR predictor. Therefore, for the updatation of the IIR predictor weight vector at each sample instant, a total of $n_r + 1$ multiplications and a total of n_r additions are required.

The computational complexity of the proposed IIR predictor can be calculated by using Eq. (3.49) which is rewritten here for convenience:

$$\mathbf{a}(n+1) = \mathbf{a}(n) + \mu\Psi(n)p(n) \tag{3.67}$$

For the calculation of $\mu\Psi(n)p(n)$, n_r+1 multiplications are required. Therefore, for each sample instant, we require a total of n_r+1 multiplications and a total of n_r additions.

The total number of multiplications and the total number of additions for the IIR predictor presented in [12] and those for the proposed one are summarized in Table 3.1.

Table 3.1: The number of multiplications and additions required for the proposed IIR predictor and for the one presented in [12].

	Algorithm presented in [12]	Proposed algorithm
Multiplications	n_{r+1}	n_{r+1}
Additions	n_r	n_r

Computational complexity of adaptive FIR filter

The computational complexity of the adaptive FIR filter algorithm presented in [12] can be calculated by using Eqs. (3.20) and (3.24) which are written here as follows:

$$\mathbf{w}(n+1) = \mathbf{w}(n) + \mu * \frac{[|q(n)|^2 - R_p]q(n)\mathbf{z}}{\rho + \mathbf{z}^T\mathbf{z}} \tag{3.68}$$

$$\widehat{\rho}_{n+1} = \gamma\widehat{\rho}_n + (1-\gamma)|z(n)|^3 \tag{3.69}$$

For each sample, ρ is updated requiring 5 multiplications and 2 additions. The calculation of $\mathbf{z}^T\mathbf{z}$ requires N multiplications and $(N-1)$ additions, where N is the length of the adaptive FIR filter. Therefore, for the evaluation of $\rho + \mathbf{z}^T\mathbf{z}$, $(N+5)$ multiplications and $(N+2)$ additions are required. For calculating R_p (see Eq. (3.23)), 9 multiplications per sample are needed. Now for each sample, $\mu * [|q(n)|^2 - R_p]q(n)\mathbf{z}$ requires $(N+13)$ multiplications and 1 addition. Therefore, the total number of multiplications required for one sample are $(2N+19)$ and the total number of additions required for each sample are $(2N+3)$.

The computational complexity for the proposed adaptive FIR algorithm can be evaluated using Eq. (3.62) which is again rewritten here for convenience:

$$\mathbf{w}(n+1) = \mathbf{w}(n) - \mu\{[|q(n)|^2 - 1]q(n)\mathbf{z}(n)\} \tag{3.70}$$

For each sample, the calculation of $\mu\{[|q(n)|^2 - 1]q(n)\mathbf{z}(n)\}$ requires $(N+4)$ multiplications and 1 addition. Thus, for the complete adaptive FIR algorithm, $(N+4)$ multiplications and $(N+1)$ additions are necessary.

The computational complexity of the proposed adaptive FIR filter algorithm and the one presented in [12] is summarized in Table 3.2.

Table 3.2: Number of multiplications and additions for the proposed algorithm and the one presented in [12] for the adaptation of FIR filter.

	Algorithm presented in [12]	Proposed algorithm
Multiplications	$2N+19$	$N+4$
Additions	$2N+3$	$N+1$

From Tables 3.1 and 3.2, it can be seen that the computational complexity of the proposed IIR predictor algorithm is same as that of the one presented in [12]. However, the total number of multiplications and additions required for the adaptation of the proposed adaptive FIR filter algorithm are substantially less than the one proposed in [12].

Total computational complexity

For calculating the computational complexity of the entire blind equalization scheme, we also need to calculate the number of multiplications and additions required for calculating the outputs of the IIR predictor, second IIR filter and the adaptive FIR filter. For each sample, the calculation of the output $\{p(n)\}$ of the IIR predictor requires n_r multiplications and $n_r - 1$ additions. As the second IIR filter copies the coefficients of the IIR predictor, the calculation of the output $\{z(n)\}$ of the second IIR filter also requires n_r multiplications and $n_r - 1$ additions. For the calculation of $\{q(n)\}$, the output of adaptive FIR filter, N multiplications and $N-1$ additions are required.

We know that the order of the IIR predictor is equal to or greater than the order of the channel n_c. Since the cascade of the channel and the IIR predictor should behave as an

all-pass filter, we choose the length of the IIR predictor $n_r = n_c + 1$. The length of the adaptive FIR filter is $2n_c + 1$. Therefore, the total computational complexity of the blind equalization in terms of n_c can be summarized as given in Table 3.3.

Table 3.3: Number of multiplications and additions for the proposed algorithm and the one presented in [12] for the entire blind equalization operation.

	Existing algorithm	Proposed algorithm	% reduction for $n_c = 3$
Multiplications	$9n_c + 26$	$7n_c + 10$	41.50
Additions	$9n_c + 6$	$7n_c + 3$	27.27

From Table 3.3, it can be observed that for a communication channel modeled by an FIR filter of length 3, e.g., a linear telephone channel, the proposed algorithm requires 41.50% less multiplications and 27.27% less additions than those required in [12]. For the adaptation of the IIR predictor in [12], a check of the strictly positive real condition is required at each sample instant, which further increases the computational complexity of the scheme presented in [12]. The computational complexity for this testing has not been included in the above calculations. Also, the final channel estimate is obtained by multiplying the adaptive FIR filter coefficients by a gain factor G. This final estimation is to check the validity of the proposed technique and it does not add to the computational complexity. Therefore, the number of operations in calculating G and for finding the final channel estimate is not included in the above calculation of the computational complexity of the two blind equalizers. However, from the above discussion, we can say that the computational complexity of the proposed blind equalization algorithm is substantially less than that of the one given in [12].

3.5.2 Comments on Hardware Implementation

In adaptive filtering, the least mean square (LMS) algorithms [15] are the most commonly used algorithm. For the hardware implementation of these algorithms many DSP chips are commercially available [32]. The proposed blind equalization algorithm does not require any extra hardware for the implementation of the proposed adaptive IIR and FIR filters. The proposed adaptive algorithm for the IIR predictor is a gradient-based algorithm, derived from the basic least mean square algorithm. The proposed adaptive FIR filter is also similar to the least mean square algorithm. This can be shown as follows.

If a scalar term $\widehat{e}(n)$ is defined as

$$\widehat{e}(n) = \{|q(n)|^2 - 1\}q(n) \tag{3.71}$$

then the updating algorithm of Eq. (3.62) can be written as

$$\mathbf{w}(n+1) = \mathbf{w}(n) - \mu\widehat{e}(n)\mathbf{z}(n) \tag{3.72}$$

In the above equation, if the term $\widehat{e}(n)$ defined by Eq. (3.71) is replaced by

$$e(n) = d(n) - q(n) \tag{3.73}$$

where $d(n)$ is some externally applied reference signal, then it can be seen that the proposed constant modulus adaptive algorithm is similar to the well known least mean square (LMS) adaptive algorithm. Therefore, the hardware configuration used for the LMS algorithm can be used directly for the proposed constant modulus adaptive algorithm, if $\widehat{e}(n)$ given by Eq. (3.71) is employed instead of $e(n)$.

Thus, the proposed blind equalization structure is better suited for hardware implementation than the one presented in [12].

3.5.3 Stability Monitoring of the Adaptive IIR Filter

The stability monitoring of the adaptive IIR filter is generally difficult [15], since it requires either factorization of the high-order denominator polynomial in each iteration or the use of a sophisticated stability test. The adaptive IIR algorithm presented in [12], has a tendency to converge to a local minimum of the mean square output error surface, if the denominator polynomial of the IIR predictor does not satisfy the strictly positive real condition. Unlike this algorithm, a stability monitoring is not needed for the proposed adaptive IIR predictor. If the order of the denominator polynomial is greater than or equal to the order of the channel, then the proposed adaptive IIR filter converges to the global minimum [19]. The denominator of the adaptive IIR predictor need not follow a strictly positive real condition.

3.5.4 Noise Consideration

In the case of a high channel output noise, the blind equalization structure presented in [12] fails to provide a solution with the existing scheme. The positions of the adaptive FIR filter and IIR filter between the two time reversers have to be interchanged to keep the output noise within an acceptable range. On the other hand, the proposed blind equalization algorithm does not require any such an exchange. The proposed blind equalization algorithm works efficiently with the higher channel output noise. However, to increase the convergence rate of the blind equalizer, a signum function in the feedback loop of the IIR predictor can be employed.

3.6 Summary

In this chapter, sufficient-order blind equalization schemes for modeling the inverse of the maximum-phase channels have been discussed and a new algorithm for the blind equalization of communication channels has been proposed.

First, a blind equalization technique based on an IIR predictor and an all-pass filter [16]-[18] is discussed. In this technique the channel estimation is obtained by minimizing a fourth-order norm. The technique has drawbacks in that the algorithm may converge to a local minimum and it has a very high computational complexity. The high computational complexity of this scheme was reduced in the scheme presented in [12] by using a block-based time reverser between the IIR predictor and the all-pass filter. Thus, this blind equalization structure is based on an IIR predictor, an IIR filter, an adaptive FIR filter, and two block-based time reversers. The scheme makes use of a simplified stochastic-gradient algorithm for the adaptation of the adaptive IIR predictor and a normalized version of the constant modulus adaptive CMA-2 algorithm for the adaptation of the adaptive FIR filter. This blind equalization structure reduces the computational complexity of the blind equalization for the nonminimum-phase channels to a certain extent and makes the blind equalization scheme less susceptible to converge to a local minima. However, for the blind equalizer to converge to the global minimum, it has drawback of requiring the denominator polynomial of the transfer function of the adaptive IIR predictor to satisfy the strictly positive real condition. Also, a hardware implementation of this blind equalization algorithm cannot be readily obtained.

In this chapter, a new sufficient-order blind equalization technique that uses the same architecture as the one presented in [12] but different and more efficient adaptation methods for the IIR predictor and adaptive FIR filter has been proposed. Unlike the scheme presented in [12], the proposed algorithm for the adaptation of the IIR predictor does not require strictly positive real condition for the convergence of the algorithm to the global minimum. The computational complexity of the proposed scheme has been carried out and compared with that presented in [12]. It has been shown that the new scheme has a substantially lower computational complexity. It has also been shown that the proposed algorithms for the adaptation of IIR predictor and adaptive FIR filter have close proximity to the well known least mean square adaptive algorithm, thereby making the proposed blind equalization algorithm better suited for the hardware implementation.

Chapter 4

Experimental Results for Minimum-Phase Communication Channels

4.1 Introduction

In the previous chapter we have proposed a new scheme for the blind equalization that is based on a structure with an IIR predictor, an IIR filter, an adaptive FIR filter and two block-based time reversers, as shown in Fig. 4.1. We now check the validity of the model proposed in the presence of additive white Gaussian noise. As discussed in Chapter 3, the adaptation of the IIR predictor is carried out by using the algorithm

$$\mathbf{a}(n+1) = \mathbf{a}(n) + \mu\Psi(n)p(n) \tag{4.1}$$

where $p(n)$ is the output of the IIR predictor, $\mathbf{a}(n)$ is predictor's tap weight vector defined as

$$\mathbf{a}(n) = [a_1(n)\ a_2(n)\ \cdots\ a_{n_r}(n)]^T \tag{4.2}$$

and

$$\Psi(n) = [p(n-1)\ p(n-2)\ \cdots\ p(n-n_r)]^T \tag{4.3}$$

On the other hand, the adaptation of the adaptive FIR filter is carried out by employing the algorithm

$$\mathbf{w}(n+1) = \mathbf{w}(n) - \mu\{[|q(n)|^2 - 1]q(n)\mathbf{z}(n)\} \tag{4.4}$$

where $q(n)$ is the output of the adaptive FIR filter, $\mathbf{z}(n)$ is the input data vector in the filter delay line, given by

$$\mathbf{z}(n) = [z(n)\ z(n-1)\ \cdots\ z(n-N+1)]^T \tag{4.5}$$

and $\mathbf{w}(n)$ is the filter's tap weight vector represented by

$$\mathbf{w}(n) = [w_0(n)\ w_1(n)\ \cdots\ w_{N-1}(n)]^T \tag{4.6}$$

In Eq. (4.2), n_r represents the length of the adaptive IIR predictor and for the stability reasons, it is always taken as greater than or equal to the length of the channel. In Eq.

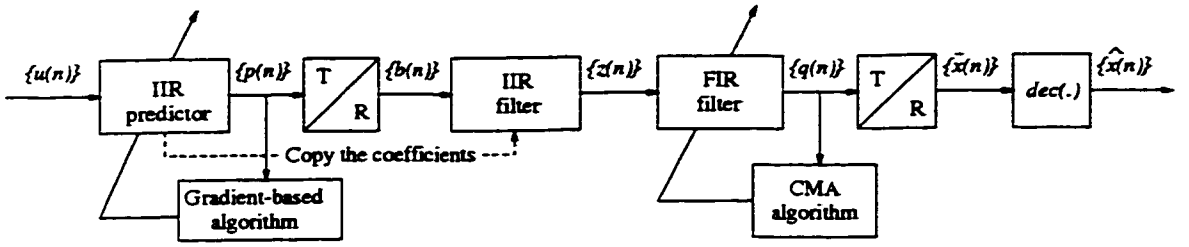

Figure 4.1: The proposed blind equalization structure.

(4.6), N is the length of the adaptive FIR filter and is given by

$$N = 2n_c + 1 \tag{4.7}$$

where n_c is the order of the channel. The channel estimate is obtained by multiplying the FIR filter-parameter vector by a gain G as

$$\mathbf{h} = [h(0)\ h(1)\ \cdots\ h(n_c)] = \mathbf{w}G \tag{4.8}$$

where

$$G = \sqrt{\frac{\sigma^2}{\mathbf{w}^T\mathbf{w}}} \tag{4.9}$$

In this expression, σ^2 is the output power of the IIR predictor and is estimated as

$$\widehat{\sigma}^2_{n+1} = \gamma\widehat{\sigma}^2_n + (1-\gamma)p^2(n) \tag{4.10}$$

where γ is the adaptation constant and it is assumed to have a value of 0.99 for all the simulations.

In Section 4.2, the experimental results for minimum-phase channels are presented and discussed. This section is divided into two subsections. In the first subsection, the effect of the inter symbol interference is studied, the experimental results are presented and discussed in detail, and a comparison is drawn with the simulation results of the blind equalization scheme proposed in [12]. In the second subsection, the effect of the additive white Gaussian noise is studied by presenting the experimental results of the symbol error rate on the performance of the proposed blind equalizer. Finally, Section 4.3 summarizes the simulation results obtained in this chapter for the proposed blind equalization scheme as applied to minimum-phase communication channels.

4.2 Experimental Results for Minimum-Phase Communication Channels

A minimum-phase filter derives its name from the fact that, for a specified magnitude response, it has the minimum phase response possible for all values of z on the unit circle [1]. The channel is assumed to be an FIR filter with the transfer function of $H(z^{-1})$. For this channel to be a minimum-phase communication channel, its zeros must lie within the unit circle of the z-plane.

The transfer function of a minimum-phase channel can be written as

$$H(z^{-1}) = \prod_{i=1}^{n_c}(1 - \xi_i^l z^{-1}) \tag{4.11}$$

where $\left|\xi_i^l\right| < 1$ for $i = 1, \ldots, n_c$. To check the suitability of the proposed blind equalization algorithm for minimum-phase communication channels, simulations have been carried out. As discussed in Chapters 2 and 3, the transmitted data sequence $\{x(n)\}$ should be independently and identically distributed (iid) and it should also be non-Gaussian with zero mean. Therefore, an input data sequence of bipolar symbols with equal probability, namely, $\{-1, +1\}$ is considered for all the simulations. The additive noise $v(n)$ is modeled as a zero-mean Gaussian and it is statistically independent of the input data

sequence $\{x(n)\}$. The two block-based time reversers reverse the output sequences of the IIR predictor and the adaptive FIR filter, respectively. The number of samples stored and time reversed is chosen to be consistent with the size of the packet, in the case of packet switching. For the purpose of simulations, a packet size of 200 samples has been considered. The coefficients of both the IIR predictor and the adaptive FIR filter are estimated from 20 Monte Carlo [20] trials.

The simulation study has been divided into two sections. In the first section we study the effect of the inter symbol interference on the proposed bind equalizer. In the second section simulations have been carried out to study the effect of additive white Gaussian noise on the performance of the proposed blind equalizer.

4.2.1 Effect of Inter Symbol Interference on the Performance of the Proposed Blind Equalizer

To study the effect of the inter symbol interference on the performance of the proposed blind equalizer, six channels have been considered starting from the case where the zeros of the channel are well inside the unit circle to the case when the zeros are very close to the unit circle.

In the first experiment, the channel is modeled as a first-order FIR filter with the transfer function

$$H(z^{-1}) = 1.0 + 0.1z^{-1} \tag{4.12}$$

According to the proposed blind equalization algorithm, the adaptive IIR predictor should have its length greater than or equal to the length of the channel. Accordingly, the length of the IIR predictor has been taken as equal to the length of the channel. Also, according to Eq. (4.7), the number of coefficients used for the adaptation of the adaptive FIR filter has been chosen as three. The simulation results for the adaptation of the IIR predictor and the adaptive FIR filter are depicted in Fig. 4.2.

The simulation has been carried out for 2000 samples. It can be seen from Fig. 4.2(a) and (b) that the first coefficient of the IIR predictor converges to the value 0.1 and the second one fluctuates around zero. For the adaptation of the FIR filter, three coefficients were used. From Fig. 4.2(c)-(e), it can be noticed that the first coefficient of the FIR filter

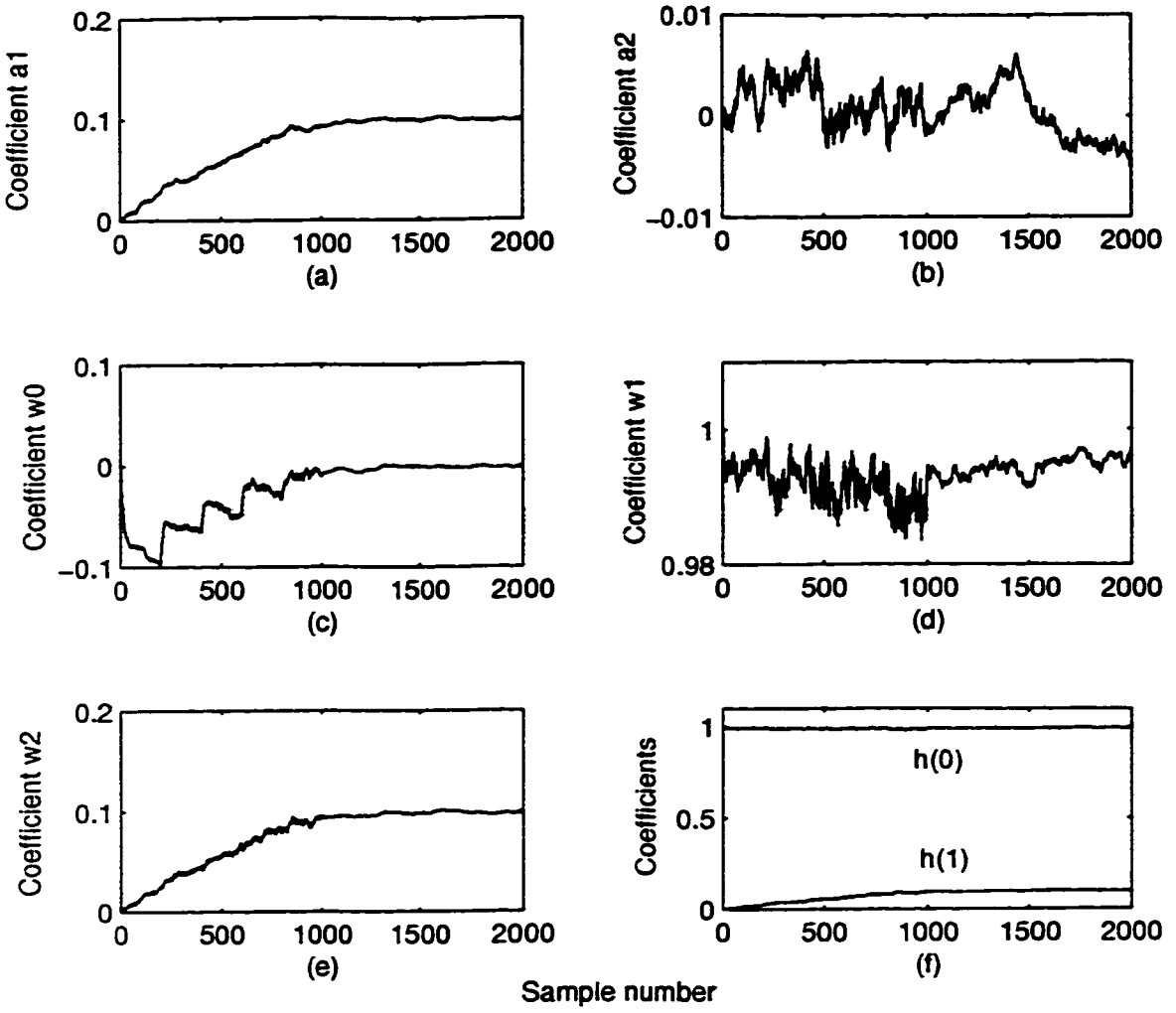

Figure 4.2: Equalizer coefficients for the channel with $H(z^{-1}) = 1.0 + 0.1z^{-1}$. (a) First coefficient of the IIR predictor. (b) Second coefficient of the IIR predictor. (c) First coefficient of the adaptive FIR filter. (d) Second coefficient of the adaptive FIR filter. (e) Third coefficient of the adaptive FIR filter. (f) Final channel estimate.

converges to zero, the second one fluctuates around one and the third converges to 0.1. The final channel estimate is obtained by multiplying the non-zero FIR filter coefficients by the gain G. From the simulation, the value of the gain G is obtained as equal to 1 for the first experiment. It can be observed from Fig. 4.2(f) that the proposed blind equalizer successfully estimates the unknown channel.

To study the effect of an increased inter symbol interference, in the second experiment, the channel is modeled as a first-order FIR filter with the transfer function

$$H(z^{-1}) = 1.0 + 0.5z^{-1} \tag{4.13}$$

It can be seen from Fig. 4.3(a) and (b) that the first coefficient of the IIR predictor converges to a value of 0.5 and the second one remains around 0. From Fig. 4.3(c)-(e), it

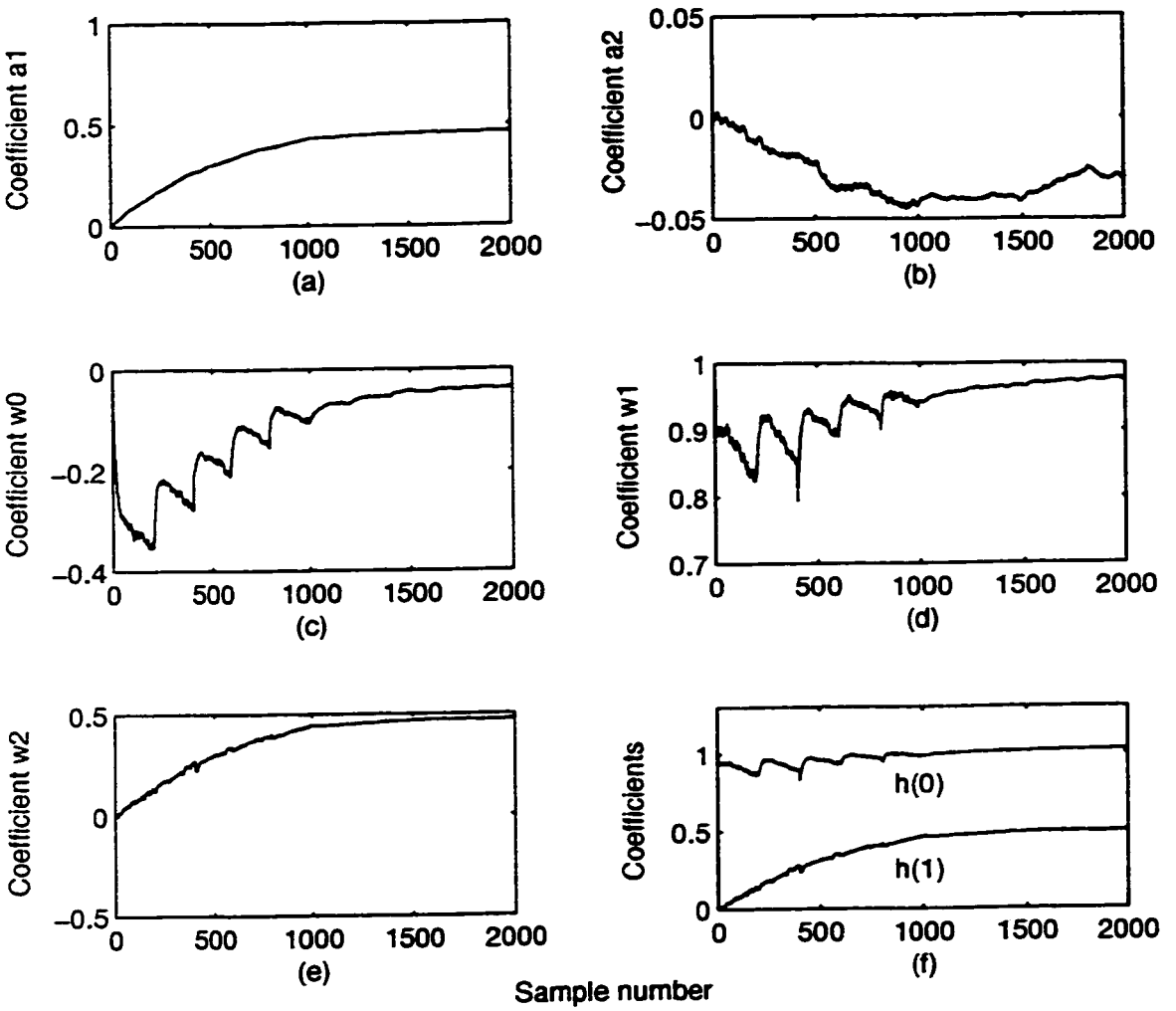

Figure 4.3: Equalizer coefficients for the channel with $H(z^{-1}) = 1.0 + 0.5z^{-1}$. (a) First coefficient of the IIR predictor. (b) Second coefficient of the IIR predictor. (c) First coefficient of the adaptive FIR filter. (d) Second coefficient of the adaptive FIR filter. (e) Third coefficient of the adaptive FIR filter. (f) Final channel estimate.

can be noticed that the first coefficient of the FIR filter converges to almost 0, the second one converges to 0.98 and the third converges to 0.49. In this experiment, the value of the gain $G = 1.0475$. The final channel estimate is shown in Fig. 4.3(f). Even though the inter symbol interference is more than in the case of the previous experiment, it is seen from Fig. 4.3 that the adaptation rate for the equalizer coefficients is not affected.

In the third experiment, the zeros of the channel are moved further close to the unit circle, by taking its transfer function as

$$H(z^{-1}) = 1.0 + 0.7z^{-1} \tag{4.14}$$

and thus increasing the inter symbol interference of the channel even further.

The adaptation coefficients of the IIR predictor and the adaptive FIR filter are depicted in Fig. 4.4. From the Fig. 4.4(a), it is clear that the first coefficient of the IIR predictor converges to a value of 0.7. The second coefficient converges to a value -0.07 as shown in Fig. 4.4(b). The first coefficient of the adaptive FIR filter is convergent towards 0 (Fig. 4.4(c)), second one towards 0.95 (Fig. 4.4(d)), and after 1200 samples the third coefficient attains a value of 0.66 (Fig. 4.4(e)). The value of the gain is obtained as 1.055 for this experiment. The final estimate of the channel is depicted in Fig. 4.4(f). From the plots of the IIR predictor and adaptive FIR filter it can be seen that the adaptation rate of the coefficients is still not affected by an increase in the inter symbol interference.

To study the effect of even higher inter symbol interference on the adaptation of the IIR predictor and adaptive FIR filter, a more noisy channel is taken for the fourth experiment. The channel is modeled as a first-order FIR filter with the transfer function

$$H(z^{-1}) = 1.0 + 0.8z^{-1} \tag{4.15}$$

The adaptation of the IIR predictor and the adaptive FIR filter is shown in Fig. 4.5. It can be seen from the plots of this figure that even though the amount of inter symbol interference has increased significantly, still there is not much effect on the convergence of the coefficients of the IIR predictor and adaptive FIR filter. The value of the gain obtained for this experiment is $G = 1.0694$. The final estimate of the channel is shown in Fig. 4.5(f).

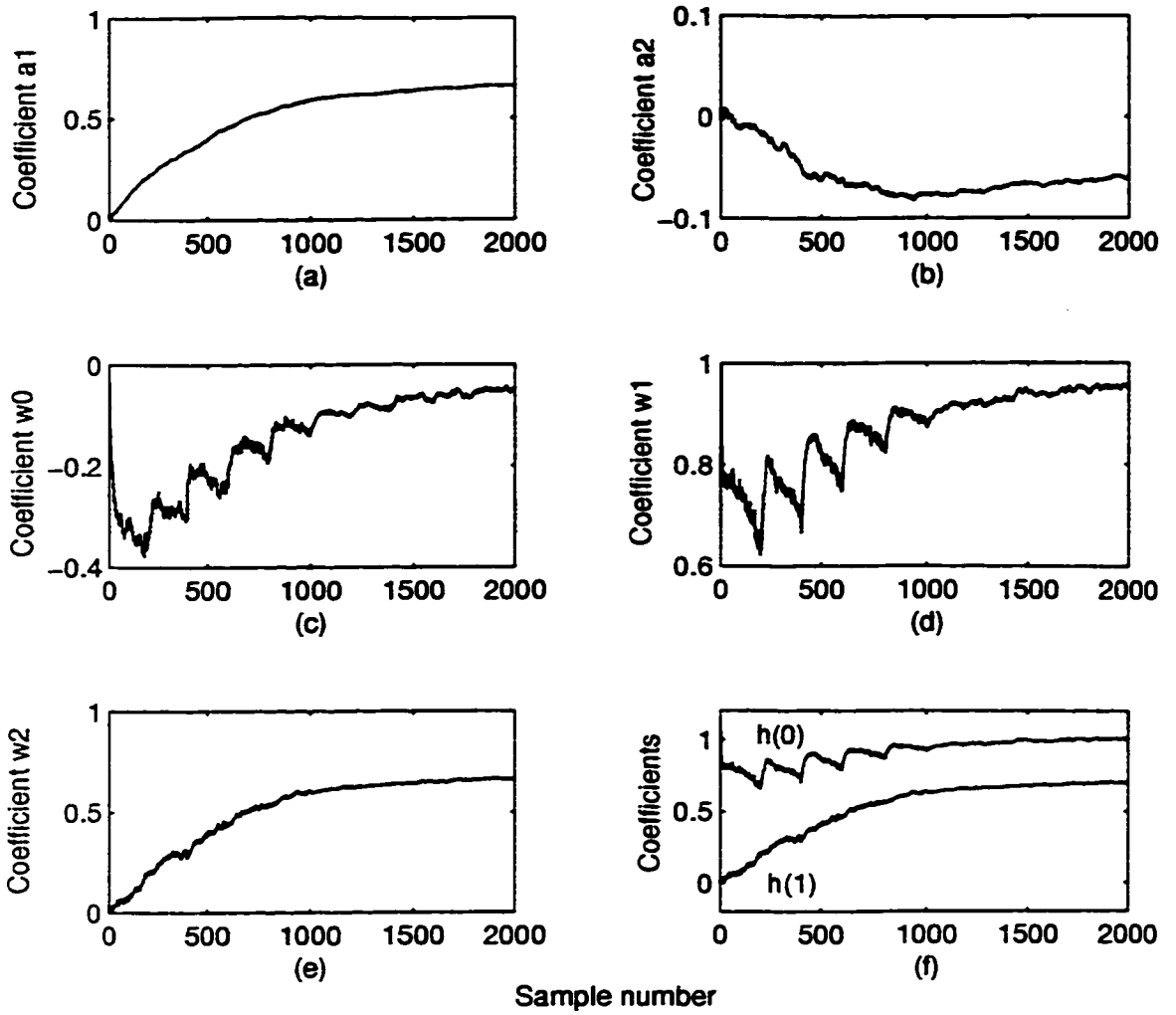

Figure 4.4: Equalizer coefficients for the channel with $H(z^{-1}) = 1.0 + 0.7z^{-1}$. (a) First coefficient of the IIR predictor. (b) Second coefficient of the IIR predictor. (c) First coefficient of the adaptive FIR filter. (d) Second coefficient of the adaptive FIR filter. (e) Third coefficient of the adaptive FIR filter. (f) Final channel estimate.

In the fifth experiment the channel is modeled as a first-order FIR filter with the z-domain transfer function given by

$$H(z^{-1}) = 1.0 + 0.9z^{-1} \tag{4.16}$$

This channel has its zero close to the unit circle, and therefore, causes a much higher inter symbol interference than in the case of the previous four channels.

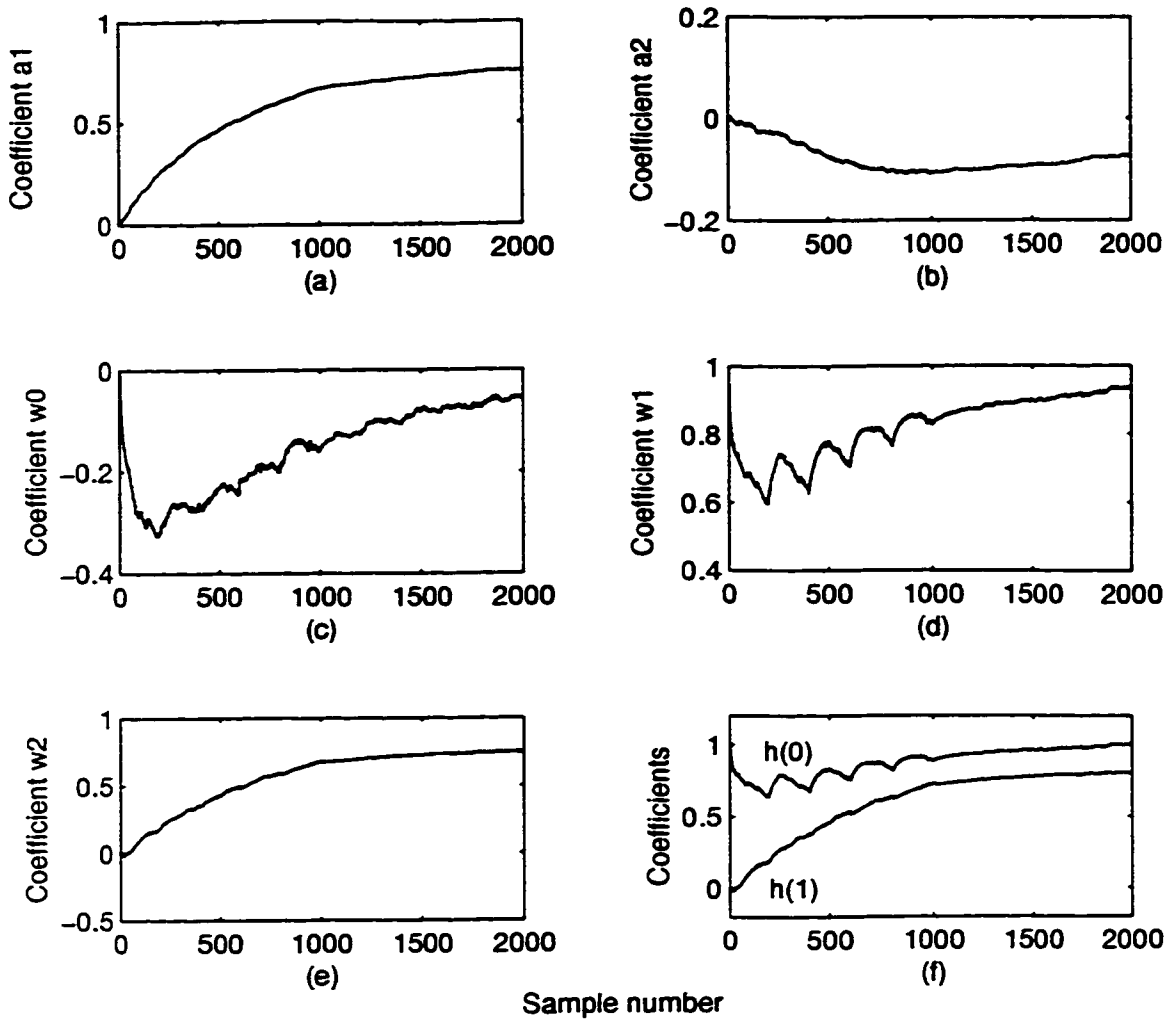

Figure 4.5: Equalizer coefficients for the channel with $H(z^{-1}) = 1.0 + 0.8z^{-1}$. (a) First coefficient of the IIR predictor. (b) Second coefficient of the IIR predictor. (c) First coefficient of the adaptive FIR filter. (d) Second coefficient of the adaptive FIR filter. (e) Third coefficient of the adaptive FIR filter. (f) Final channel estimate.

The adaptation of the IIR predictor and adaptive FIR filter is shown in Fig. 4.6. From the plots of Fig. 4.6(a) and (b), it can be noticed that the adaptation of IIR predictor coefficients is not much affected even in the presence of a high inter symbol interference. On the other hand, the effect of the inter symbol interference is visible on the adaptation of the adaptive FIR filter coefficients. From Fig. 4.6(c)-(e), it can be seen that the adaptation of the adaptive FIR filter coefficients has somewhat slowed down with the effect that higher inter symbol interference is more visible on the second coefficient of the adaptive

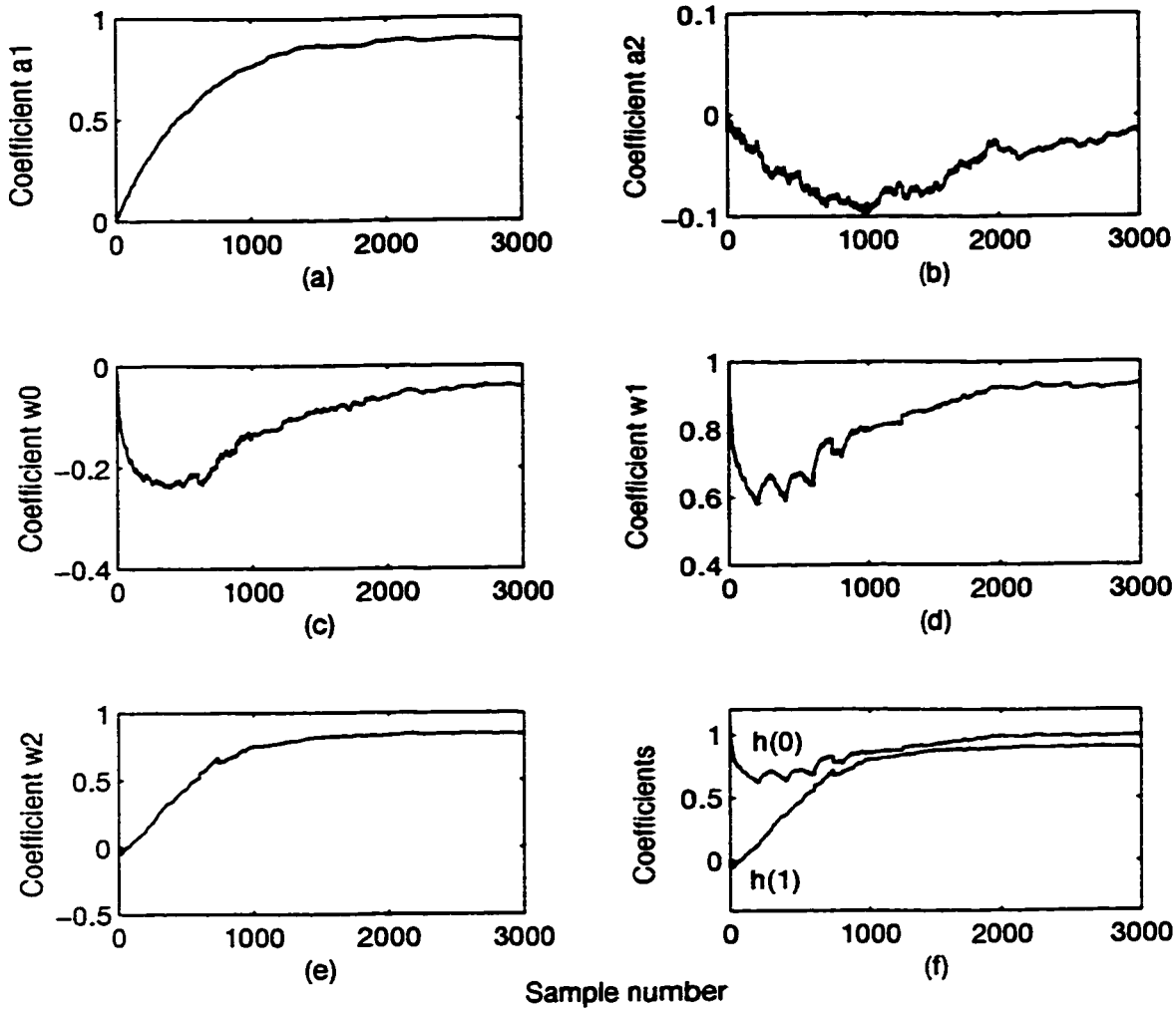

Figure 4.6: Equalizer coefficients for the channel with $H(z^{-1}) = 1.0 + 0.9z^{-1}$. (a) First coefficient of the IIR predictor. (b) Second coefficient of the IIR predictor. (c) First coefficient of the adaptive FIR filter. (d) Second coefficient of the adaptive FIR filter. (e) Third coefficient of the adaptive FIR filter. (f) Final channel estimate.

FIR filter (Fig. 4.6(d)). The value of the gain obtained for this experiment is $G = 1.072$. From the plot of Fig. 4.6(f), it can be observed that the blind equalizer still estimates the unknown channel correctly.

In the sixth and the final experiment, the zero of the channel is moved to a very close vicinity of the unit circle by characterizing the channel with the transfer function given by

$$H(z^{-1}) = 1.0 + 0.999z^{-1} \tag{4.17}$$

This channel causes a very high inter symbol interference. The adaptation of the IIR predictor and adaptive FIR filter is shown in Fig. 4.7. From Fig. 4.7(a) it can be seen that

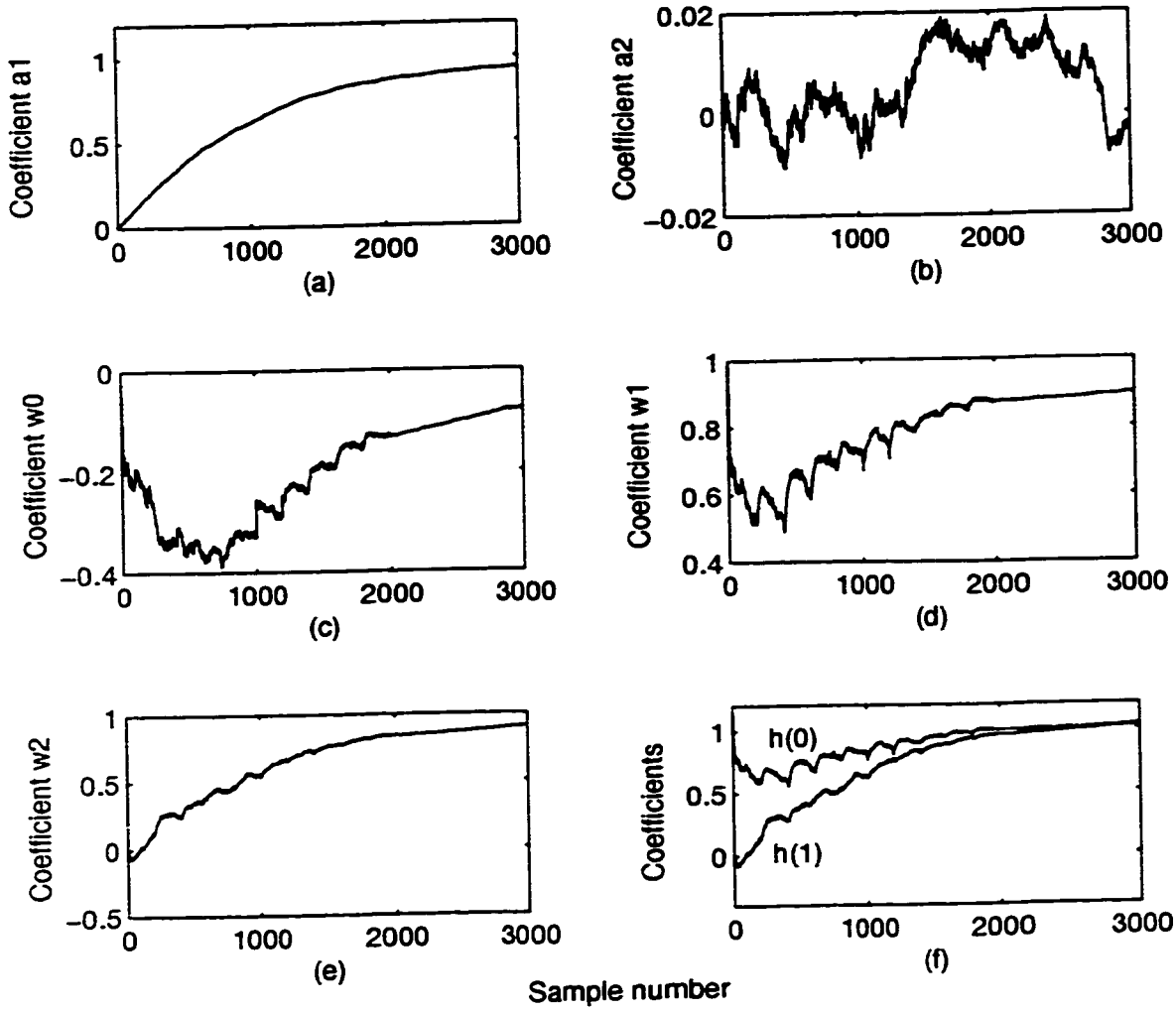

Figure 4.7: Equalizer coefficients for the channel with $H(z^{-1}) = 1.0 + 0.999z^{-1}$. (a) First coefficient of the IIR predictor. (b) Second coefficient of the IIR predictor. (c) First coefficient of the adaptive FIR filter. (d) Second coefficient of the adaptive FIR filter. (e) Third coefficient of the adaptive FIR filter. (f) Final channel estimate.

the adaptation of the first coefficient of the IIR predictor has slowed down. The second coefficient of the IIR predictor fluctuates around 0 as shown in Fig. 4.7(b). The first coefficient of the adaptive FIR filter, as shown in Fig. 4.7(c), initialy goes to a value of -0.39 before finally being convergent towards -0.07. The second and the third coefficients of the adaptive FIR filter are depicted in Fig. 4.7(d) and (e). It can be noticed form these plots that the convergence rate of these coefficients is considerably reduced as compared

to the coefficients of channels with lower inter symbol interference. However, the proposed blind equalizer is still able to estimate the channel correctly and efficiently. The value of the gain obtained for this experiment is 1.136.

To see the performance of the proposed blind equalizer on the transmitted data sequence, the data sequence $\{u(n)\}$ received at the input of the blind equalizer and the output $\overline{x}(n)$ of the second time reverser are plotted in Fig. 4.8. For our discussion, the

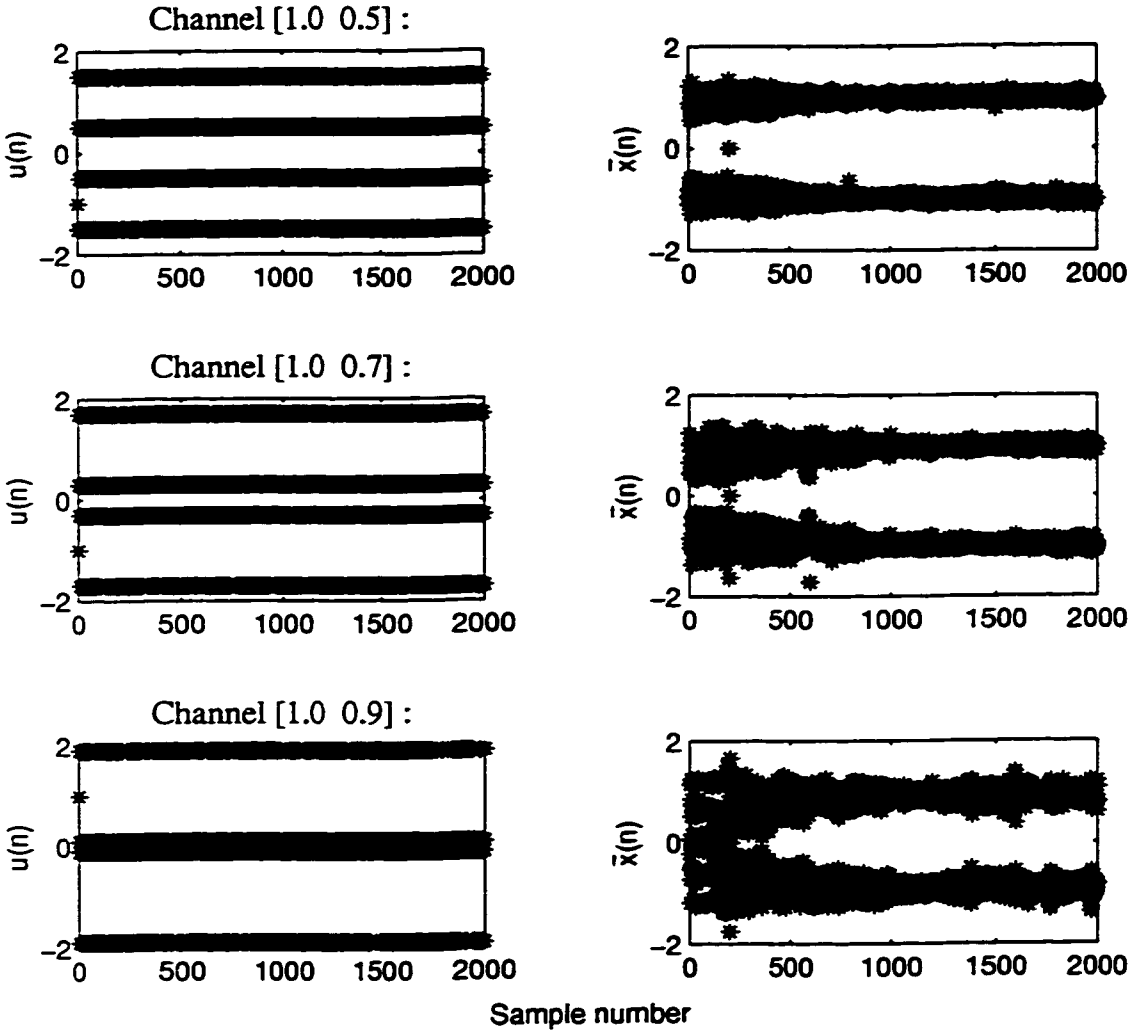

Figure 4.8: The data sequences $u(n)$ and $\overline{x}(n)$ at the input of the blind equalizer and at the output of the second time reverser, respectively, for various minimum-phase channels.

data sequences $u(n)$ and $\overline{x}(n)$ are plotted only for the channels with the transfer functions $H(z^{-1}) = 1.0 + 0.5z^{-1}$, $H(z^{-1}) = 1.0 + 0.7z^{-1}$, and $H(z^{-1}) = 1.0 + 0.9z^{-1}$.

From Fig. 4.8, it can be seen that in the case of the channel with its transfer function $H(z^{-1}) = 1.0 + 0.5z^{-1}$, the effect of inter symbol interference is very small. It can be noticed that the output of the second time reverser in this case is very well defined for all the data samples. Therefore, probability of error in the final detected data sequence is very small. From the plot of the channel $H(z^{-1}) = 1.0 + 0.7z^{-1}$, it can be seen that the data sequence received at the input of the blind equalizer is more noisy. Therefore, in the beginning of the blind equalization, there is more clouding of the output data sequence. For the channel $H(z^{-1}) = 1.0 + 0.9z^{-1}$, the presence of the inter symbol interference is more visible. From the plot of the data sequence received at the output of the second time reverser, it is clear that the blind equalizer now needs more number of samples, before it can estimate the channel correctly. This may lead to some errors in the detected data sequence.

The values of the blind estimate of the channel at the sample instants 1000 and 2000 along with their standard deviations for all the six experiments are presented in Table 4.1. For comparison, the results obtained by the blind equalization scheme proposed in [12] are also presented in Table 4.2.

Table 4.1: Blind estimate of first-order minimum-phase channels at the sample instants 1000 and 2000 using the proposed blind equalization scheme.

Channel	Channel estimate $\{h(0)\ h(1)\}$			
	$n = 1000$		$n = 2000$	
	Mean	Std. deviation	Mean	Std. deviation
{1.0 0.1}	{0.9959 0.0950}	{0.0005 0.0009}	{0.9970 0.0989}	{0.0004 0.0006}
{1.0 0.5}	{0.9878 0.4671}	{0.0004 0.0008}	{1.0215 0.5001}	{0.0002 0.0005}
{1.0 0.7}	{0.9256 0.6427}	{0.0008 0.0009}	{0.9996 0.7002}	{0.0009 0.0002}
{1.0 0.8}	{0.8882 0.7286}	{0.0009 0.0009}	{0.9979 0.8010}	{0.0011 0.0003}
{1.0 0.9}	{0.8557 0.8090}	{0.0014 0.0007}	{0.9909 0.8966}	{0.0003 0.0002}
{1.0 0.999}	{0.8268 0.6363}	{0.0007 0.0014}	{0.9920 0.9577}	{0.0004 0.0003}

Table 4.2: Blind estimate of first-order minimum-phase channels at the sample instants 1000 and 2000 using the blind equalization scheme of [12].

Channel	Channel estimate $\{h(0)\ h(1)\}$			
	$n = 1000$		$n = 2000$	
	Mean	Std. deviation	Mean	Std. deviation
{1.0 0.1}	{1.0011 0.1129}	{0.0045 0.0271}	{0.9995 0.1011}	{0.0010 0.0263}
{1.0 0.5}	{0.9756 0.4836}	{0.0188 0.0263}	{0.9993 0.4965}	{0.0035 0.0247}
{1.0 0.9}	{0.8337 0.6437}	{0.0500 0.3268}	{0.9996 0.8921}	{0.0064 0.0256}

From Table 4.1, it can be noticed that the proposed blind equalizer estimates the channel correctly. Also, by comparing the results of Table 4.2 with those given in Table 4.1, it can be seen that the proposed scheme provides the standard deviations of the channel estimates that are very much smaller than that of the ones presented in [12]. Thus, the proposed scheme yields a very consistent performance.

From the above discussion, it is clear that even in the presence of very high inter symbol interference, the proposed blind equalizer estimates the minimum-phase channels correctly and it gives more consistent results than that obtained by using the scheme of [12].

4.2.2 Effect of Additive White Gaussian Noise on the Performance of the Proposed Blind Equalizer

The performance of a blind equalizer is also measured in terms of symbol error rate, also known as bit error rate (BER) for the binary data. For calculating the symbol error rate, a sequence of data is transmitted at a specific signal-to-noise power ratio, where the signal power is the total power of the received data sequence and the noise power is the total power of the additive white Gaussian noise added at the input of the receiver. After the blind equalization and detection of the transmitted data sequence, a calculation is performed to determine the number of erroneous samples in the final output data sequence of the blind equalizer. At a given signal-to-noise ratio, the symbol error rate is defined as the number of errors divided by the total number of data symbols transmitted. The symbol error rate for various values of the signal-to-noise ratio can be calculated by changing the power level of the additive white Gaussian noise.

To study the performance of the proposed blind equalizer for various levels of additive white Gaussian noise, simulations have been carried out. All the six channels used in the previous section are tested under the presence of different values of signal-to-noise ratio. For all the channels, an equally probable binary data sequence of 20000 samples is taken for this experiment. The simulations are carried out in the range of 10 dB to 20 dB for 10 different values of the signal-to-noise ratio, to conform with the the practically encountered situations. The symbol error rate corresponding to different values of the signal-to-noise ratio for all the six channels are depicted in Fig. 4.9.

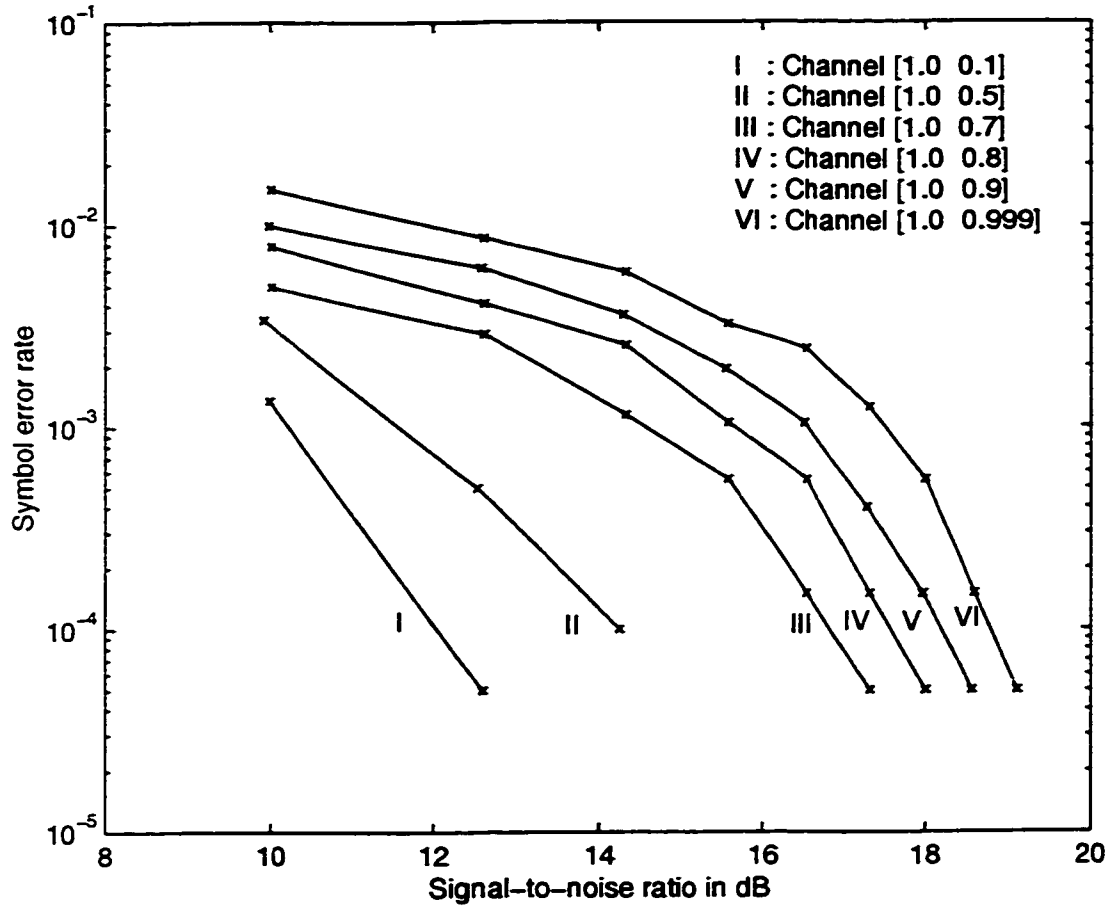

Figure 4.9: Symbol error rate for various minimum-phase communication channels.

It can be observed from Fig. 4.9 that the symbol error rate performance deteriorates as the amount of inter symbol interference increases and that the symbol error rate

decreases with the increasing level of the signal-to-noise ratio. It can also be seen that for the channels with very small inter symbol interference, the symbol error rate becomes negligible at a smaller value of signal-to-noise level as compared to the ones with higher inter symbol interference.

From the above discussion, we can say that even in the presence of a high input noise, i.e., very low signal-to-noise ratio and a high inter symbol interference, the symbol error rate obtained with the proposed blind equalization scheme is within an acceptable range. Therefore, it can be concluded that even in the presence of high input noise, the proposed blind equalization scheme works efficiently as compared to the one presented in [12], where the swapping of the IIR filter with the adaptive FIR filter is required for such a situation.

4.3 Summary

In this chapter, two different types of experiments have been carried out to check the performance of the proposed blind equalization scheme for minimum-phase communication channels.

In the first set of experiments, the effect of the inter symbol interference on the performance of the proposed blind equalizer has been studied. The communication channel is assumed to be a first-order FIR filter. Six different channels, starting from the one with a negligible inter symbol interference to the one with a very intense inter symbol interference have been considered. From the experimental results, it has been seen that even though in the presence of high inter symbol interference the convergence rate of the IIR predictor and adaptive FIR filter coefficients somewhat slows down, the proposed blind equalizer still estimates the unknown channel correctly. A comparison of the proposed blind equalization scheme with the one given in [12] has been carried out and it has been noted that the proposed scheme gives more consistent performance.

In the second set of experiments, the performance of the proposed blind equalization scheme is studied under different values of signal-to-noise ratio. Again for various types of minimum-phase channels, symbol error rate has been obtained as a function of the signal-to-noise ratio. The experimental results have demonstrated that with the increased

levels of signal-to-noise ratio, the symbol error rate performance becomes progressively better. It has also been shown that with an increase in inter symbol interference, the symbol error rate performance becomes poorer. However, its still within an acceptable range. It is also seen that even in the presence of high input noise, the proposed blind equalization scheme works efficiently without requiring the swapping of the IIR filter with the adaptive FIR filter that is necessary in the scheme of [12].

Chapter 5

Experimental Results for Nonminimum-Phase Communication Channels

5.1 Introduction

In the previous chapter, we have shown through experimental results that the proposed blind equalization scheme gives results as desired for minimum-phase communication channels. As discussed in Chapter 2, the existing blind equalization algorithms when applied to FIR-based equalizer structures perform poorly as one or more maximum-phase zeros of the channel get closer to the unit circle. This limitation is due to the difficulty of modeling the inverse of the maximum-phase component of the channel with the finite length of FIR filters. To show the performance of the proposed blind equalization scheme for such channels, in this chapter, we present experimental results for nonminimum-phase channels. The experimental results for maximum-phase and mixed-phase channels are presented and discussed in detail. Experimental results are also presented to study the performance of the proposed scheme for the communication channels having deep spectral nulls. For convenience, the block diagram of the proposed blind equalization scheme is again presented in Fig. 5.1. The algorithms used for the adaptation of the IIR predictor and adaptive FIR filter have already been presented in Chapter 3.

In Section 5.2 and Section 5.3, the experimental results for maximum-phase and

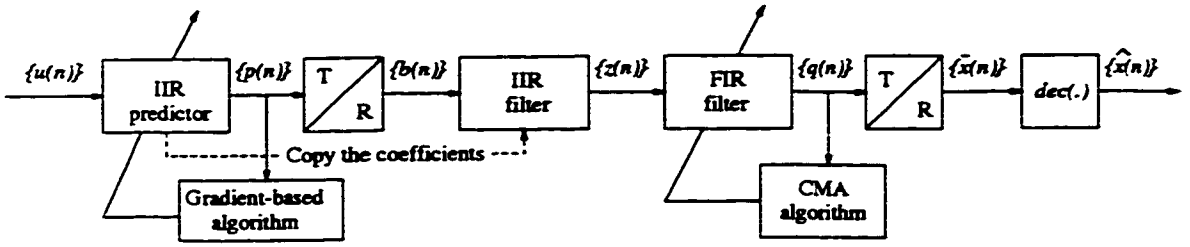

Figure 5.1: The proposed blind equalization structure.

mixed-phase channels, respectively, are presented and discussed. Each of these sections is divided into two subsections. In the first one, the effect of the inter symbol interference is studied and the experimental results are presented and discussed in detail. A comparison is drawn with the simulation results of the blind equalization scheme proposed in [12]. In the second subsection, the effect of the additive white Gaussian noise is studied by presenting the experimental results of the symbol error rate, on the performance of the proposed blind equalizer. In Section 5.4, the simulation results for a communication channel having deep spectral nulls are presented and discussed. Finally, in Section 5.5, the simulation results obtained in this chapter for the proposed blind equalization scheme as applied to nonminimum-phase communication channels are summarized.

5.2 Experimental Results for Maximum-Phase Communication Channels

A filter which has all its zeros located outside the unit circle, is known as a maximum-phase filter. A maximum-phase filter, for a specified magnitude response, gives the maximum possible phase response for all values of z on the unit circle [11]. In this section, the communication channel is modeled as a maximum-phase FIR filter with the transfer function $H(z^{-1})$. Thus, the zeros of $H(z^{-1})$ may lie anywhere outside the unit circle in the z-plane, but not within the unit circle.

The transfer function of a maximum-phase channel can be written as

$$H(z^{-1}) = \prod_{j=1}^{n_c} \left[\left(\xi_j^o\right)^{-1} - z^{-1} \right] \tag{5.1}$$

where $\left|\xi_j^o\right| > 1$ for $j = 1, \ldots, n_c$. To study the performance of the proposed blind equalization algorithm for maximum-phase communication channels, a number of experiments have been carried out. A transmitted data sequence $\{x(n)\}$ of bipolar symbols with equal probability, namely, $\{-1, +1\}$ is considered for all the simulations. This sequence is independently and identically distributed (iid) and it is also non-Gaussian with zero mean. The additive noise $v(n)$ is statistically independent of the input data sequence $\{x(n)\}$ and is modeled as a zero-mean Gaussian. A packet size of 200 samples has been considered for the block-based time reversers. The coefficients of both the IIR predictor and the adaptive FIR filter are estimated from 20 Monte Carlo [20] trials. The length of the IIR predictor has been taken as equal to the length of the channel. However, the length of the adaptive FIR filter, according to the proposed algorithm, is taken as $N = 2n_c + 1$, where n_c is the order of the channel.

Two different types of experiments are carried out to study the performance of the proposed blind equalization scheme. In the first type of experiments, the effect of the presence of inter symbol interference is studied and in the second one, the performance of the proposed blind equalization scheme is studied under the effect of different levels of additive white Gaussian noise.

5.2.1 Effect of Inter Symbol Interference on the Performance of the Proposed Blind Equalizer

In this subsection, the performance of the proposed blind equalization scheme, under the presence of different amounts of inter symbol interference, is studied. The level of the inter symbol interference is changed by moving the positions of the zeros of the maximum-phase channel. Eleven different channels are used for the experiments, starting from the one having its zeros far away from the unit circle to the one having its zeros in the close vicinity of the unit circle. To show the performance of the proposed blind equalization scheme, the updatation coefficients for 5 of these channels are shown. However, the results of the blind estimation of all the channels are presented in a table.

In the first case, the channel is modeled as a first-order maximum-phase FIR filter with the transfer function

$$H(z^{-1}) = 0.3 + z^{-1} \tag{5.2}$$

The simulations have been carried out for 2000 samples. The value of the adaptation constant μ for the IIR predictor and adaptive FIR filter has been taken as 0.002 and 0.02 for the first 1000 samples and 0.001 and 0.01 for the remaining samples, respectively. The adaptation coefficients of the IIR predictor and adaptive FIR filter, along with the final channel estimate are shown in Fig. 5.2.

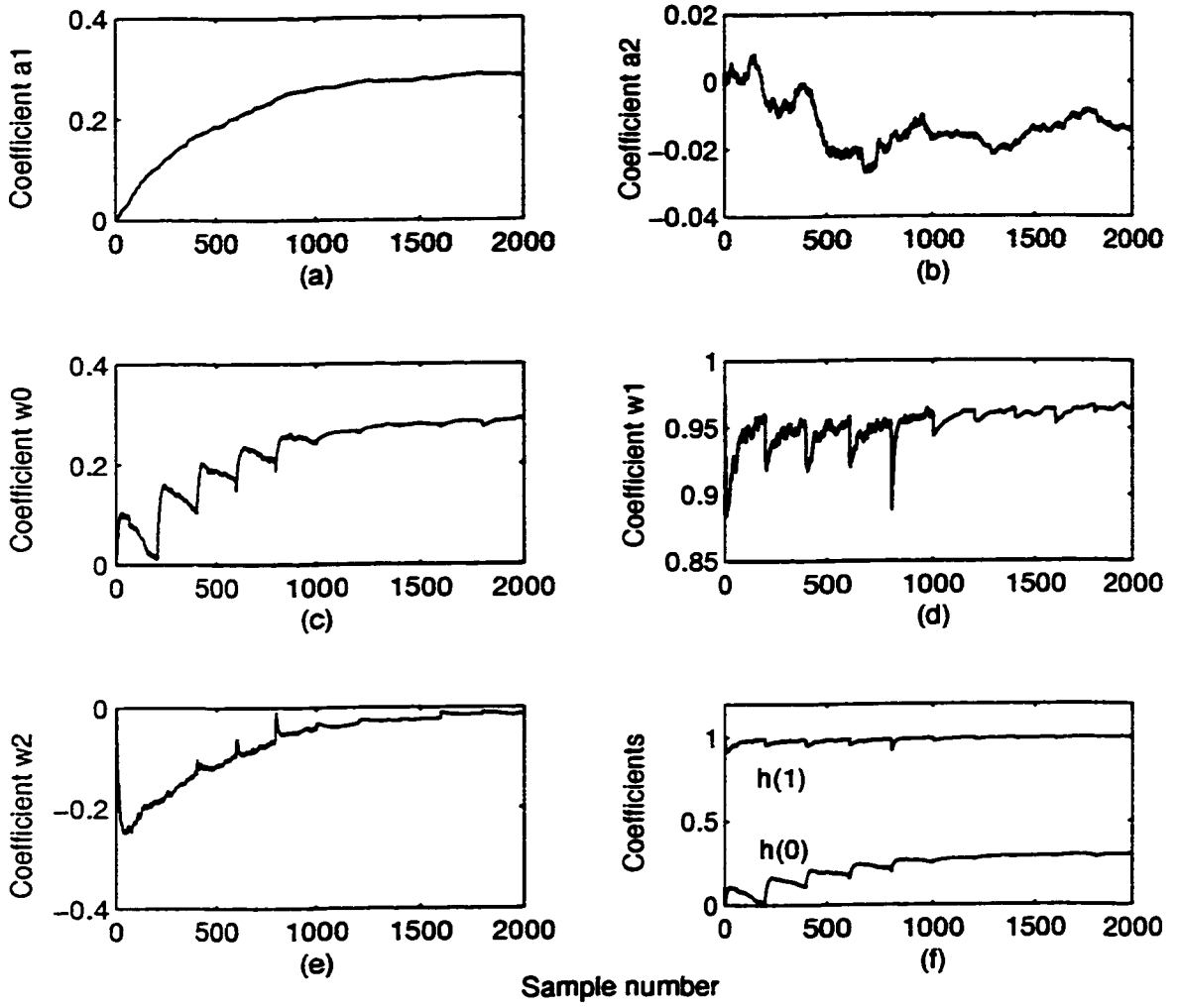

Figure 5.2: Equalizer coefficients for the channel with $H(z^{-1}) = 0.3 + z^{-1}$. (a) First coefficient of the IIR predictor. (b) Second coefficient of the IIR predictor. (c) First coefficient of the adaptive FIR filter. (d) Second coefficient of the adaptive FIR filter. (e) Third coefficient of the adaptive FIR filter. (f) Final channel estimate.

From the plots of Fig. 5.2, it can be seen that the first IIR predictor coefficient converges to a value of 0.2840; however, the second one is fluctuating around -0.01. The first coefficient of the adaptive FIR filter converges to a value of 0.2894, second one to

0.9667, and the third one to -0.01. From these plots, it can be noticed that the adaptation of all the coefficients is faster in the initial 1000 samples and it slows down thereafter. This is because of the fact that the value of the adaptation constant μ is kept higher in the beginning of the simulations and after1000 samples it is reduced to a lower value. The final channel estimate of the unknown channel is depicted in Fig. 5.2(f). From this plot, it can be seen that the proposed blind equalization scheme estimates the unknown channel completely. The value of the gain obtained for this experiment is 1.0355.

In the previous experiment the channel had its root on the negative real axis of the z-plane. To check the validity of the proposed blind equalization scheme for the maximum-phase channel having its roots on the positive axis of the z-plane, in the second experiment the channel is modeled as a first-order FIR filter with its transfer function given by

$$H(z^{-1}) = -0.5 + z^{-1} \tag{5.3}$$

The adaptation of the IIR predictor and adaptive FIR filter coefficients for this experiment is shown in Fig. 5.3. From the plots of Fig. 5.3(a) and (b), it can be seen that the first IIR predictor coefficient converges to a value of 0.50, however, the second one is converging towards -0.03. From Fig. 5.3(c)-(e), it can be noticed that the first and second coefficients of the adaptive FIR filter are converging towards the desired channel estimate and the third one is converging towards a value of 0. The final channel estimate of the unknown channel is depicted in Fig. 5.3(f). From this plot, it can be seen that the proposed blind equalization scheme estimates the unknown channel completely. The value of the gain obtained for this experiment is 1.0426.

To study the effect of higher inter symbol interference on the adaptation of the IIR predictor and adaptive FIR filter, in the third experiment, the channel is modeled as a first-order FIR filter with the z-domain transfer function given by

$$H(z^{-1}) = 0.7 + z^{-1} \tag{5.4}$$

The adaptation of the IIR predictor and the adaptive FIR filter coefficients for this channel is shown in Fig. 5.4. The final estimate of the channel is shown in Fig. 5.4(f). It can be seen from the plots of Fig. 5.4, that even though the amount of inter symbol interference has increased significantly, still the convergence of the coefficients of the IIR predictor

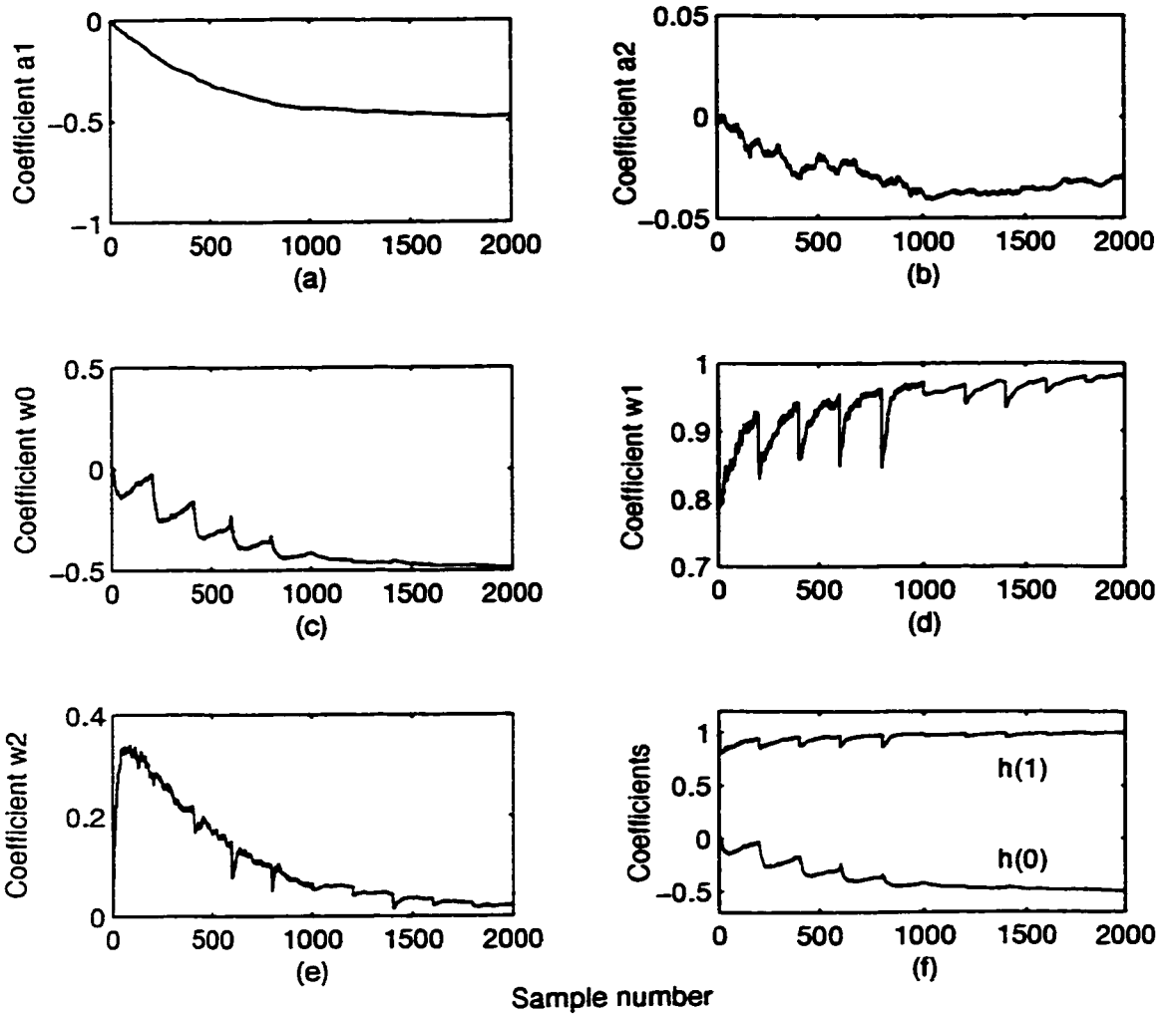

Figure 5.3: Equalizer coefficients for the channel with $H(z^{-1}) = -0.5 + z^{-1}$. (a) First coefficient of the IIR predictor. (b) Second coefficient of the IIR predictor. (c) First coefficient of the adaptive FIR filter. (d) Second coefficient of the adaptive FIR filter. (e) Third coefficient of the adaptive FIR filter. (f) Final channel estimate.

and adaptive FIR filter is not affected. The value of the gain obtained for this experiment is 1.0556.

In the fourth experiment the channel is modeled as a first-order FIR filter with its transfer function given by

$$H(z^{-1}) = 0.9 + z^{-1} \tag{5.5}$$

The amount of the inter symbol interference caused by this channel is much larger than

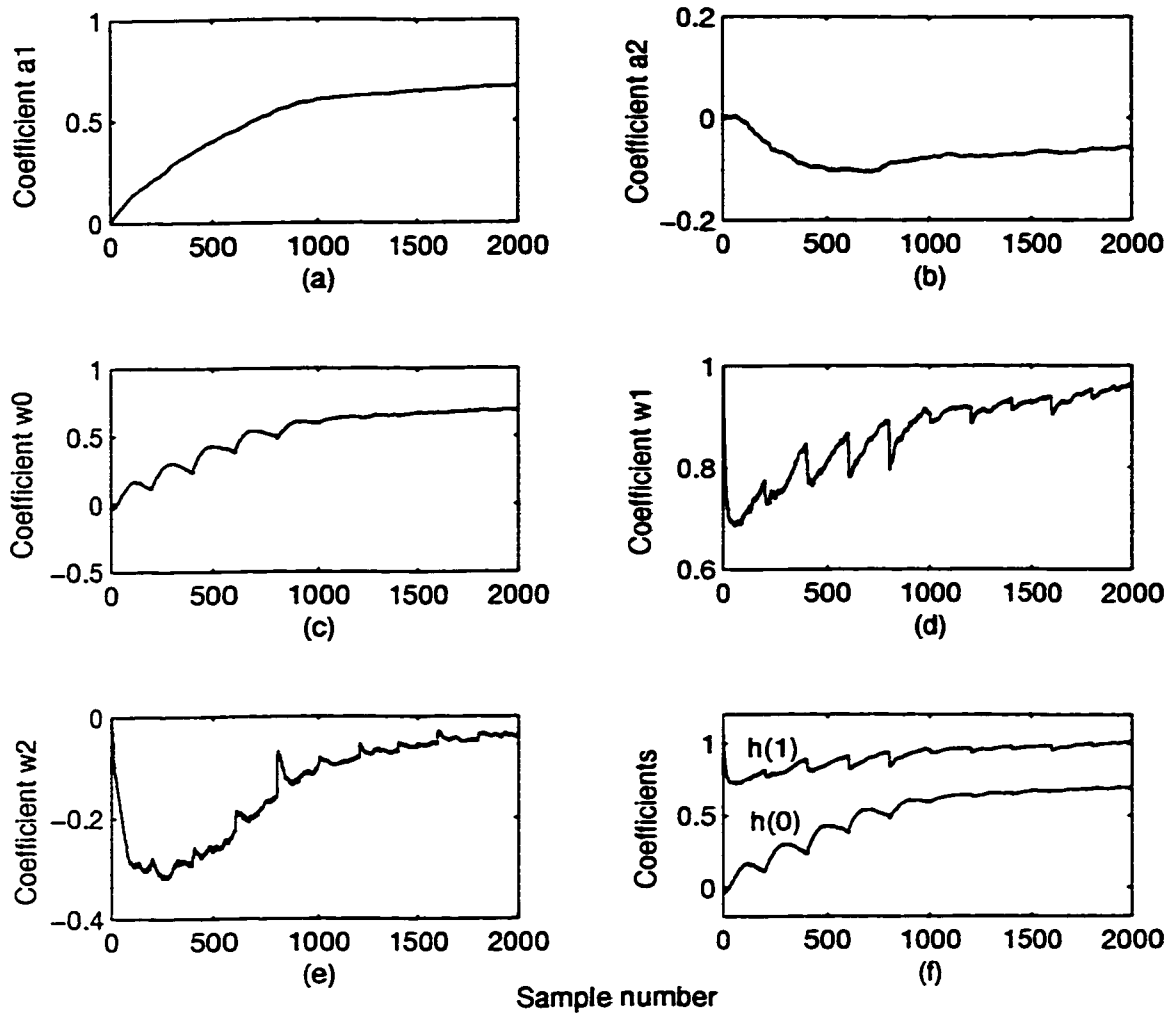

Figure 5.4: Equalizer coefficients for the channel with $H(z^{-1}) = 0.7 + z^{-1}$. (a) First coefficient of the IIR predictor. (b) Second coefficient of the IIR predictor. (c) First coefficient of the adaptive FIR filter. (d) Second coefficient of the adaptive FIR filter. (e) Third coefficient of the adaptive FIR filter. (f) Final channel estimate.

the previous three experiments. The adaptation of the IIR predictor and the adaptive FIR filter in this experiment is depicted in Fig. 5.5. From the plots of Fig. 5.5(a) and (b), it can be noticed that the adaptation of the IIR predictor is not much affected by the increase in inter symbol interference. However, the effect of the higher amount of inter symbol interference is visible on the adaptation of the adaptive FIR filter, in that it has somewhat slowed down the convergence of the coefficients. The value of the gain obtained for this experiment is 1.1585. Even though the simulation in this experiment have been carried

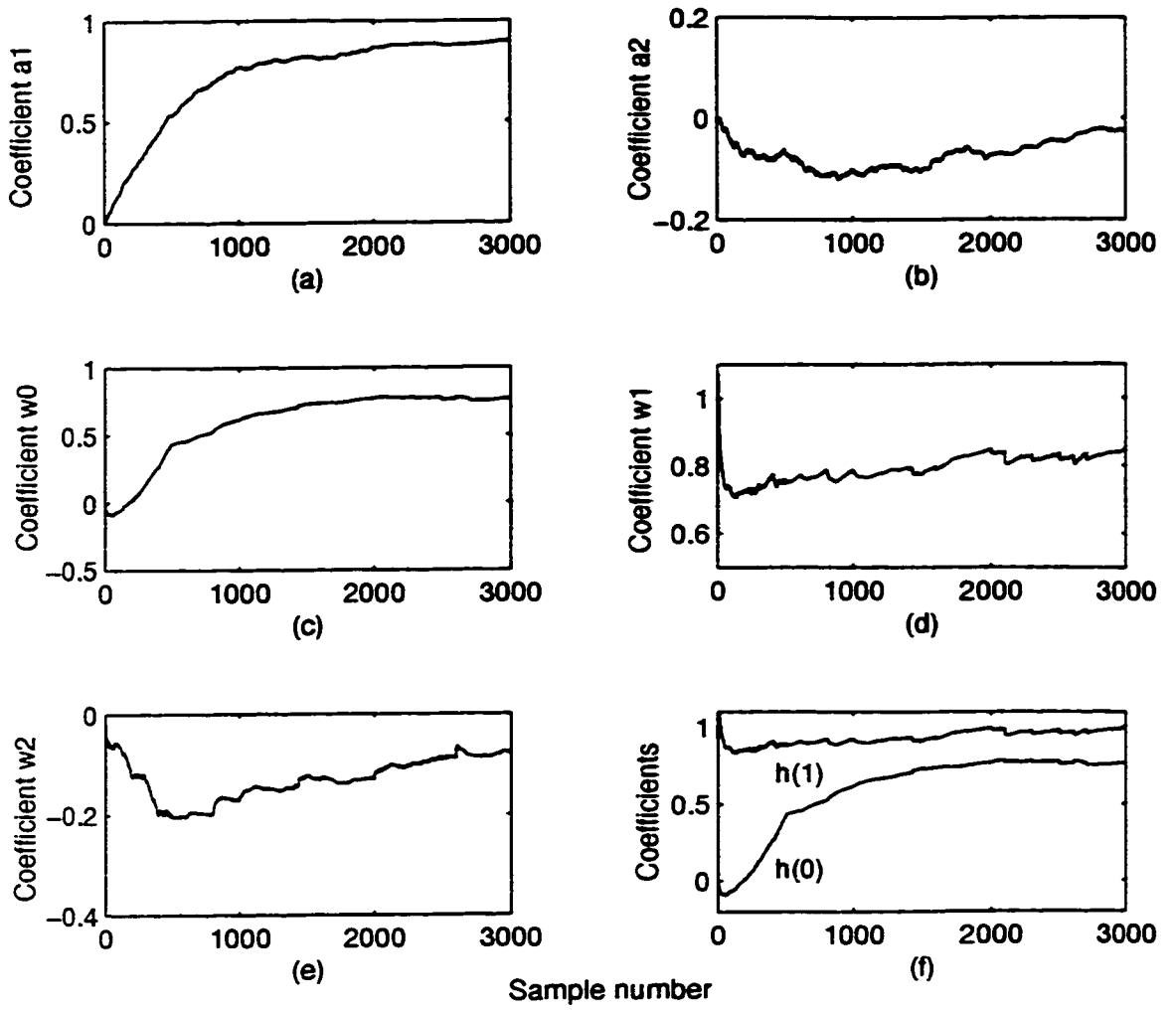

Figure 5.5: Equalizer coefficients for the channel with $H(z^{-1}) = 0.9 + z^{-1}$. (a) First coefficient of the IIR predictor. (b) Second coefficient of the IIR predictor. (c) First coefficient of the adaptive FIR filter. (d) Second coefficient of the adaptive FIR filter. (e) Third coefficient of the adaptive FIR filter. (f) Final channel estimate.

out for 3000 samples, the proposed blind equalizer estimates the channel correctly within the first 2000 samples, as shown in Fig. 5.5(f).

In the fifth experiment, the performance of the proposed blind equalization scheme is studied in the presence of an extremely high inter symbol interference. This is done by moving the zero of the channel almost on the unit circle. The channel is modeled as a

first-order FIR filter with its transfer function given by

$$H(z^{-1}) = 0.999 + z^{-1} \tag{5.6}$$

The adaptation of the IIR predictor and the adaptive FIR filter coefficients along with the final channel estimate is depicted in Fig. 5.6. It can be observed from the plots

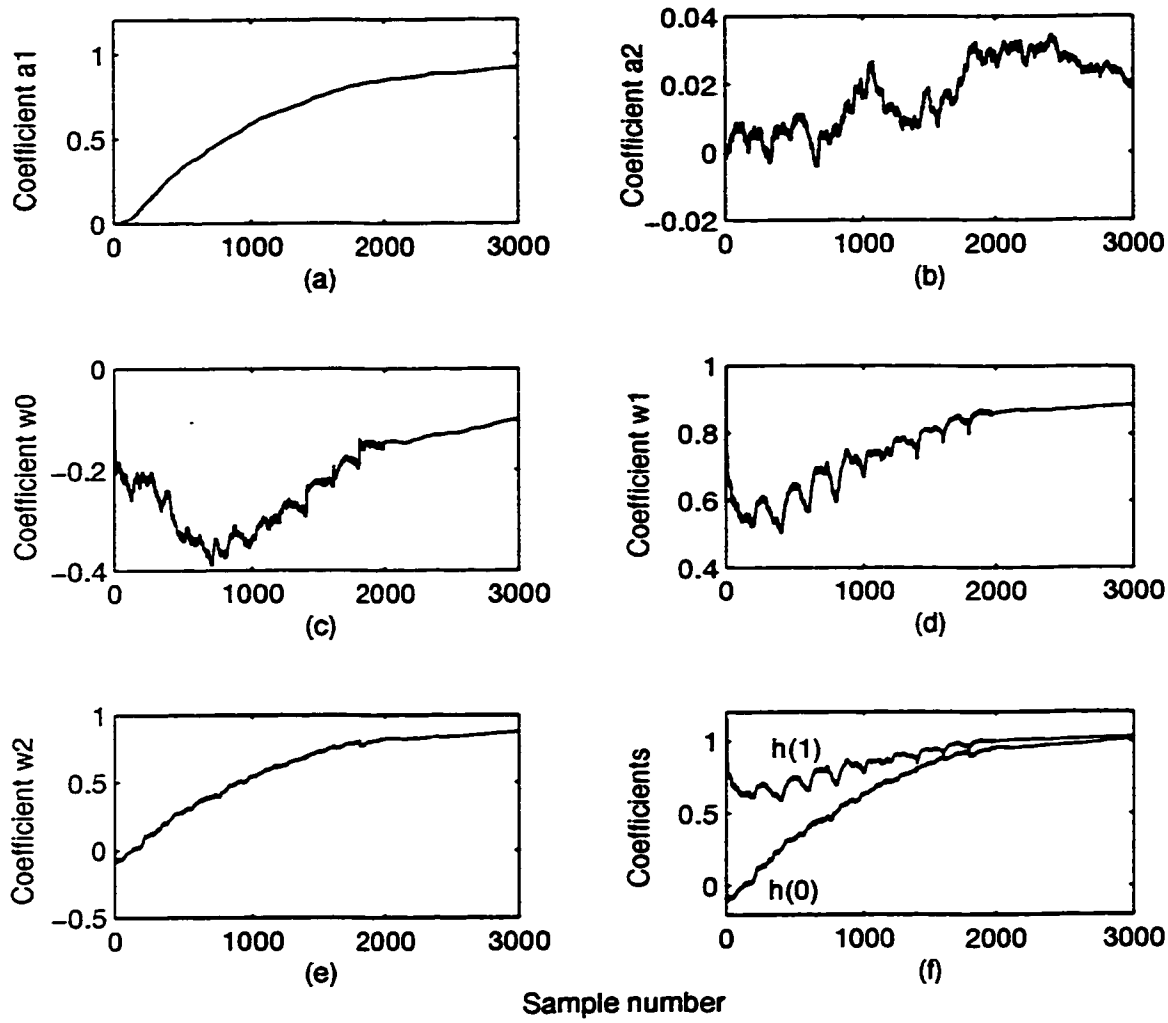

Figure 5.6: Equalizer coefficients for the channel with $H(z^{-1}) = 0.999 + z^{-1}$. (a) First coefficient of the IIR predictor. (b) Second coefficient of the IIR predictor. (c) First coefficient of the adaptive FIR filter. (d) Second coefficient of the adaptive FIR filter. (e) Third coefficient of the adaptive FIR filter. (f) Final channel estimate.

of Fig. 5.6(a) and (b) that the adaptation of the IIR predictor has slowed down a bit more as compared to the previous case. From the plots of Fig. 5.6(c)-(e), it can be noticed that even though for the convergence of the adaptive FIR filter coefficients it now takes more samples, it still estimates the unknown channel completely. The value of the gain obtained for this experiment is 1.1773. It can also be noted that in the previous experiments, the first and the second coefficients of the adaptive FIR filter were giving the channel estimate, but in the present case the second and the third coefficients give the final channel estimate. This is because of the fact the zero of the channel is almost on the unit circle and its not much different from the minimum-phase channel with its transfer function $H(z^{-1}) = 1 + 0.999z^{-1}$(Chapter 4, Fig. 4.7), where the second and the third coefficients of the adaptive FIR filter also gave the final channel estimate.

For all the five experiments discussed above, the data sequence $u(n)$ received at the input of the blind equalizer and the output of the second time reverser $\overline{x}(n)$ are plotted in Fig. 5.7 and Fig. 5.8.

From the plots of the data sequence $u(n)$ received at the input of the blind equalizer (Fig. 5.7) , it can be seen that as the inter symbol interference increases to a modestly high value, some values of the data sequence move towards a zero value. From the plots of the data sequence $\overline{x}(n)$ obtained at the output of the second time reverser, it can be seen that in the beginning of the the data sequence, the amount of crowding of the samples increases as the inter symbol interference increases. As a result, the blind equalizer takes a longer time to estimate the channel.

The presence of a much severe inter symbol interference can be noticed from the plots of Fig. 5.8. It can be noticed from the plots of the data sequence $u(n)$ that some values of the data sequence, which were close to the zero in the previous cases, are now coinciding with the zero. From the plots of data sequence $\overline{x}(n)$, it can be observed that the initial clouding of the data samples continues for a longer period of time. As a result the blind equalizer requires a longer time, before it can estimate the channel correctly.

The blind estimations for all the 11 channels, including those already discussed, for the study of the performance of the proposed blind equalization scheme for maximum-phase channels are presented in Table 5.1. The values of the channels are estimated

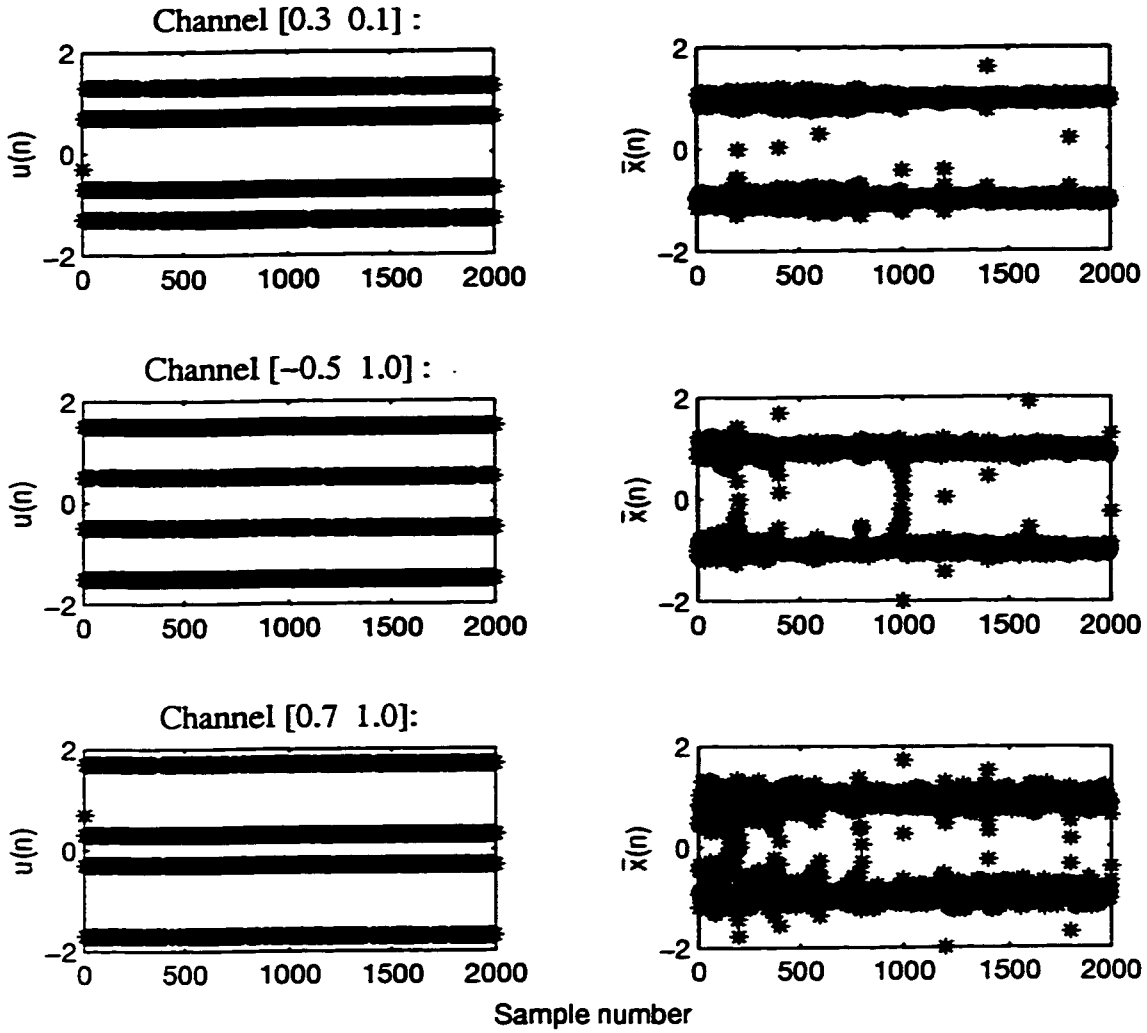

Figure 5.7: The data sequences $u(n)$ and $\bar{x}(n)$ at the input of the blind equalizer and at the output of the second time reverser, respectively, for various minimum-phase channels.

at the 1000th and 2000th sample instants and their standard deviations from the mean are calculated. The results obtained by using the blind equalization scheme of [12] are presented in Table 5.2. A comparison of the results in the two tables shows that even though both the schemes estimate the unknown channels correctly up to two decimal places, yet the proposed scheme is better in giving more consistent results than the scheme of [12], in terms of their standard deviations.

From the above discussion, we can conclude that as the amount of inter symbol

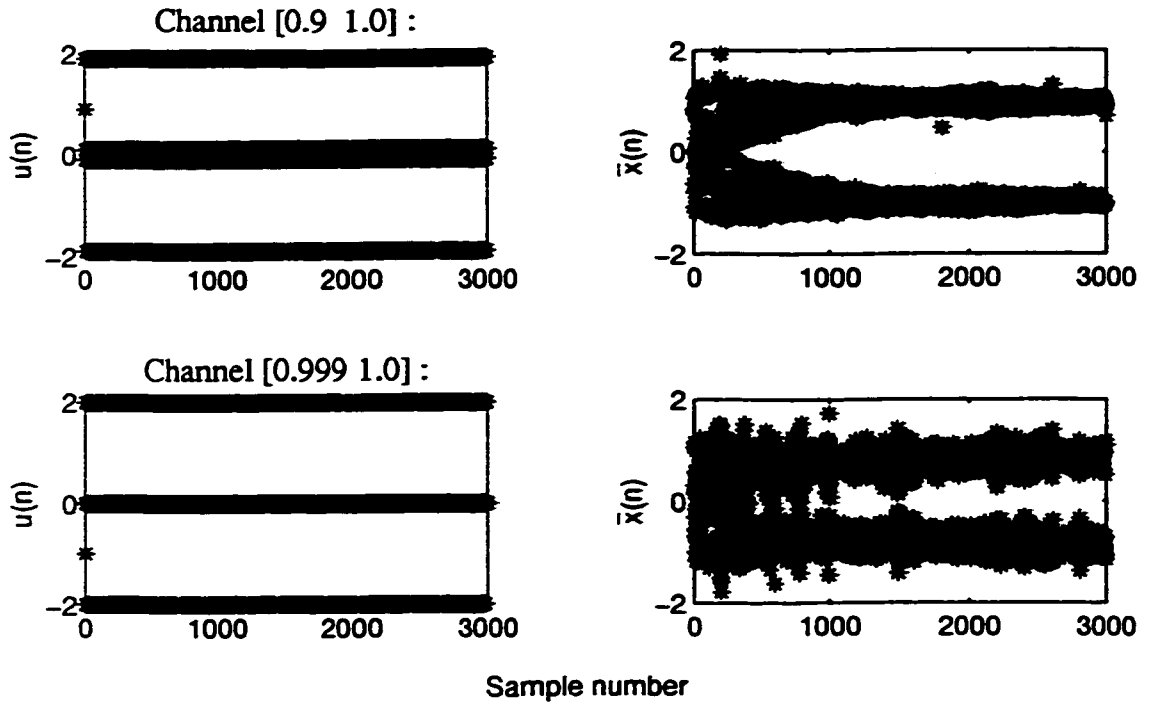

Figure 5.8: The data sequences $u(n)$ and $\bar{x}(n)$ at the input of the blind equalizer and at the output of the second time reverser, respectively, for channels $H(z^{-1}) = 0.9 + z^{-1}$ and $H(z^{-1}) = 0.999 + z^{-1}$.

interference increases, for the proposed blind equalizer it takes longer to converge. We can also conclude from the comparison of the results obtained by using the proposed scheme and the one presented in [12], that the former scheme provides more consistent results.

5.2.2 Effect of Additive White Gaussian Noise on the Performance of the Proposed Blind Equalizer

In this subsection, experimental results are presented to study the performance of the proposed blind equalization scheme for maximum-phase communication channels under the presence of different levels of additive white Gaussian noise. The simulations are carried out for all the 11 channels considered in the previous subsection. However, the plots of the symbol error rate are shown only for the 5 channels discussed in Section 5.2.1, and for the channel with the transfer function $H(z^{-1}) = 0.95 + z^{-1}$.

Table 5.1: Blind estimate of first-order maximum-phase channels at the sample instants 1000 and 2000 using the proposed blind equalization scheme.

Channel	Channel estimate $\{h(0)\ h(1)\}$			
	$n = 1000$		$n = 2000$	
	Mean	Std. deviation	Mean	Std. deviation
{0.1 1.0}	{0.0832 0.9990}	{0.0010 0.0001}	{0.1004 0.9972}	{0.0005 0.0001}
{0.3 1.0}	{0.2527 0.9942}	{0.0011 0.0001}	{0.2997 1.0011}	{0.0006 0.0001}
{−0.3 1.0}	{−0.2992 0.9934}	{0.0019 0.0003}	{−0.3001 1.0021}	{0.0005 0.0006}
{0.5 1.0}	{0.4661 0.9834}	{0.0007 0.0012}	{0.5000 0.9998}	{0.0001 0.0006}
{−0.5 1.0}	{−0.4229 0.9932}	{0.0009 0.0001}	{−0.4999 1.0045}	{0.0006 0.0004}
{0.7 1.0}	{0.5947 0.9532}	{0.0004 0.0011}	{0.6937 1.0070}	{0.0006 0.0002}
{−0.7 1.0}	{−0.6007 0.9550}	{0.0006 0.0019}	{−0.6932 0.9991}	{0.0003 0.0006}
{0.9 1.0}	{0.7269 0.9267}	{0.0006 0.0001}	{0.9049 0.9985}	{0.0003 0.0002}
{0.95 1.0}	{0.6155 0.9090}	{0.0018 0.0001}	{0.9335 0.9940}	{0.0002 0.0001}
{0.98 1.0}	{0.6052 0.7736}	{0.0027 0.0002}	{0.9796 1.0016}	{0.0003 0.0005}
{0.999 1.0}	{0.6273 0.7768}	{0.0009 0.0009}	{0.9879 0.9990}	{0.0003 0.0009}

Table 5.2: Blind estimate of first-order maximum-phase channels at the sample instants 1000 and 2000 using the blind equalization scheme of [12].

Channel	Channel estimate $\{h(0)\ h(1)\}$			
	$n = 1000$		$n = 2000$	
	Mean	Std. deviation	Mean	Std. deviation
{0.1 1.0}	{0.1060 1.0009}	{0.0310 0.0043}	{0.1060 0.9990}	{0.0242 0.0029}
{0.3 1.0}	{0.2833 0.9983}	{0.0332 0.0141}	{0.3020 0.9984}	{0.0233 0.0082}
{−0.3 1.0}	{−0.2492 0.9942}	{0.0332 0.0141}	{−0.2864 1.0028}	{0.0262 0.0076}
{0.5 1.0}	{0.4592 0.9912}	{0.0361 0.0224}	{0.5002 0.9974}	{0.0216 0.0130}
{−0.5 1.0}	{−0.4268 0.9820}	{0.0374 0.0265}	{−0.4848 1.0047}	{0.0234 0.0118}
{0.7 1.0}	{0.6232 0.9729}	{0.0424 0.0361}	{0.6983 0.9965}	{0.0204 0.0167}
{−0.7 1.0}	{−0.5920 0.9729}	{0.0412 0.0316}	{−0.6852 1.0053}	{0.0178 0.0149}
{0.9 1.0}	{0.7612 0.9188}	{0.0412 0.0332}	{0.8927 0.9989}	{0.0244 0.0217}
{0.95 1.0}	{0.7971 0.8951}	{0.0400 0.0316}	{0.9409 1.0002}	{0.0191 0.0222}
{0.98 1.0}	{0.8256 0.8813}	{0.0387 0.0316}	{0.9699 1.0009}	{0.0315 0.0256}

An equally probable binary data sequence of 20000 samples is taken for this experiment. The symbol error rate is plotted for 10 different values of the signal-to-noise ratio.

To conform with the practically encountered situations, the range of the signal-to-noise ratio is taken as 10 dB to 20 dB. The symbol error rate for different values of signal-to-noise ratio for the 6 channels considered are shown in Fig. 5.9. From this plot, it can be seen that the symbol error rate decreases with the increasing signal-to-noise ratio. It can also be noticed that as the inter symbol interference increases, the symbol error rate increases, and it takes higher value of signal-to-noise ratio to reach a negligible value of symbol error rate.

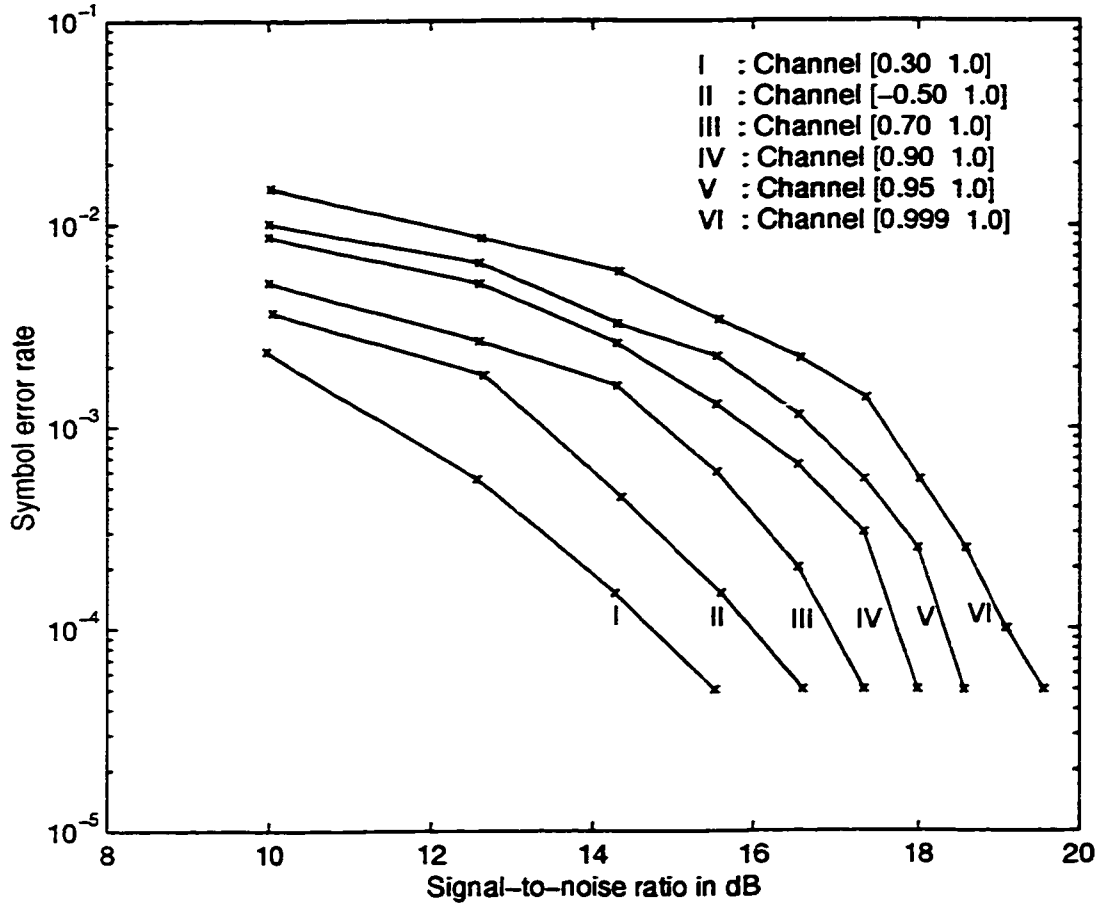

Figure 5.9: Symbol error rate for various maximum-phase communication channels.

The symbol error rate for a channel with the transfer function $H(z^{-1}) = 0.95 + z^{-1}$, obtained by using the scheme of [12] is shown in Fig. 5.10. For comparison, the symbol error rate for this channel, obtained by employing the proposed blind equalization scheme is also redrawn. The simulations are carried out for a data sequence of 15000 samples. From these plots it can be seen that the proposed blind equalization scheme gives lower

symbol error rate for all the values of signal-to-noise ratio. It can also be noticed that the proposed scheme achieves a negligible value of symbol error rate at a lower signal-to-noise ratio as compared to the scheme of [12].

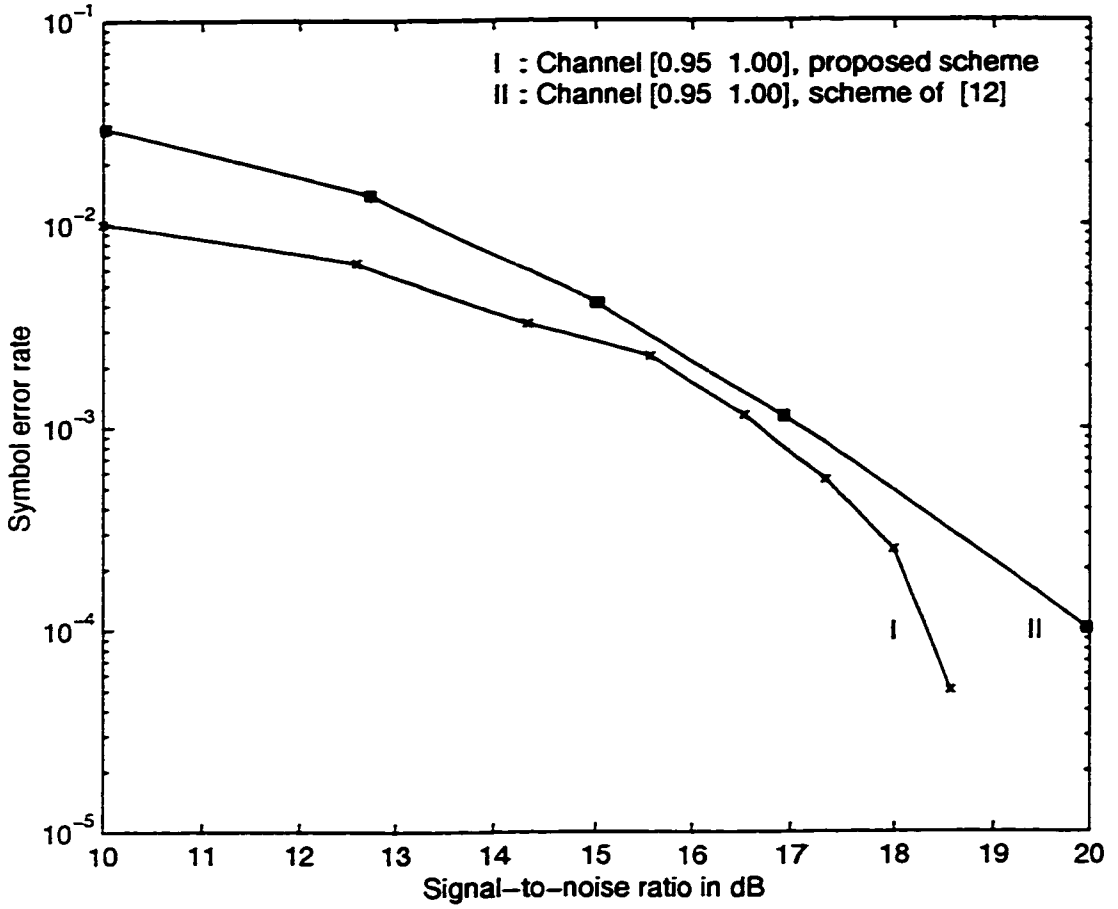

Figure 5.10: Symbol error rate comparison of the proposed scheme with the one presented in [12] for the channel $H(z^{-1}) = 0.95 + z^{-1}$.

From the above discussion, we conclude that the proposed blind equalization scheme works efficiently for the maximum-phase communication channels even for the low values of signal-to-noise ratio. It can also be concluded that the proposed blind equalization scheme is better than the one introduced in [12], in terms of symbol error rate.

5.3 Experimental Results for Mixed-Phase Communication Channels

A nonminimum-phase FIR filter with some of the zeros inside and the others outside the unit circle is called a mixed-phase FIR filter [11]. Therefore, a mixed-phase filter can be taken as cascade of a minimum-phase and a maximum-phase filter. The mixed-phase communication channel is modeled as a mixed-phase FIR filter with its transfer function given by

$$H(z^{-1}) = \prod_{i=1}^{d}(1 - \xi_i^i z^{-1}) \prod_{j=1}^{s}\left[\left(\xi_j^o\right)^{-1} - z^{-1}\right] \tag{5.7}$$

where $\left|\xi_i^i\right| < 1$ for $i = 1, \ldots, d$ corresponds to the minimum-phase zeros, $\left|\xi_j^o\right| > 1$ for $j = 1, \ldots, s$ corresponds to the maximum-phase zeros, and $n_c = d + s$. To study the performance of the proposed blind equalization scheme for mixed-phase communication channels, a number of experiments are carried out. A binary data sequence of 2000 samples is transmitted. The length of the IIR predictor has been taken as equal to the length of the channel and the length of the adaptive FIR filter is taken as $N = 2n_c + 1$, where n_c is the order of the channel. The middle coefficient of the adaptive FIR filter is initialized to unity. The weights of the adaptive FIR filter are multiplied by the gain factor G to obtain the channel estimate. The adaptation constant μ for both the IIR predictor and adaptive FIR filter are set to 0.002 for the first 1000 samples, and thereafter to 0.001. The block length is taken as 200. The coefficients of the IIR predictor and the adaptive FIR filter are estimated from 20 Monte Carlo [20] trials.

As for the minimum-phase and maximum-phase channels, here too the performance of the proposed scheme is tested for its two properties. In the first set of experiments, the effect of inter symbol interference is studied and in the second set, the effect of additive white Gaussian noise is studied.

5.3.1 Effect of Inter Symbol Interference on the Performance of the Proposed Blind Equalizer

For the experiments carried out for mixed-phase communication channels, the channels are modeled as second-order mixed-phase FIR filters. To study the performance of the proposed scheme in the presence of different levels of inter symbol interference, 4

channels are considered. The simulation results for 2 of them are discussed in detail; however, the channel estimations obtained at the 2000th sample instant for all the 4 channels are depicted in a table.

In the first experiment, the channel is modeled as a second-order FIR filter with the transfer function given by

$$H(z^{-1}) = 0.6 + 1.4z^{-1} - 0.6z^{-2} \tag{5.8}$$

This channel has its roots at -2.7033 and 0.3699.

The plots for the adaptation of IIR predictor and adaptive FIR filter coefficients are shown in Fig. 5.11. From the plots of IIR predictor coefficients, it can be seen that the first and third coefficients of the IIR predictor have converged to 0, while the second one has converged to -0.3. From the plots of Fig. 5.11(d) and (e), it can be seen that three coefficients of the adaptive FIR filter are converging towards the desired channel parameter values, while the other two are converging to 0. The final channel estimate is obtained by multiplying the adaptive FIR filter coefficients by the gain G and it is shown in Fig. 5.11(f). The value of the gain is 1.2367 for this experiment. From the plots of Fig. 5.11(f), it is seen that the proposed blind equalizer has estimated the channel correctly.

In the second experiment, the amount of the inter symbol interference is increased by modeling the channel as a second-order mixed-phase FIR filter with the transfer function given by

$$H(z^{-1}) = 1.0 + 0.6z^{-1} - 0.72z^{-2} \tag{5.9}$$

This channel has its roots at -1.20 and 0.60, which are much closer to the unit circle as compared to the previous experiment.

For this experiment, the adaptation of the IIR predictor and adaptive FIR filter coefficients is shown in Fig. 5.12. From the plots of Fig. 5.12(a) and (b), it can be noticed that the first IIR predictor coefficient converges to a value of 0.2 and the second one to -0.5. The third coefficient of the IIR predictor, fluctuates around 0 with a small amplitude and in practice this coefficient can be switched off after the other coefficients have achieved their steady state. From the plots of Fig. 5.12(d) and (e), it can be observed that three of

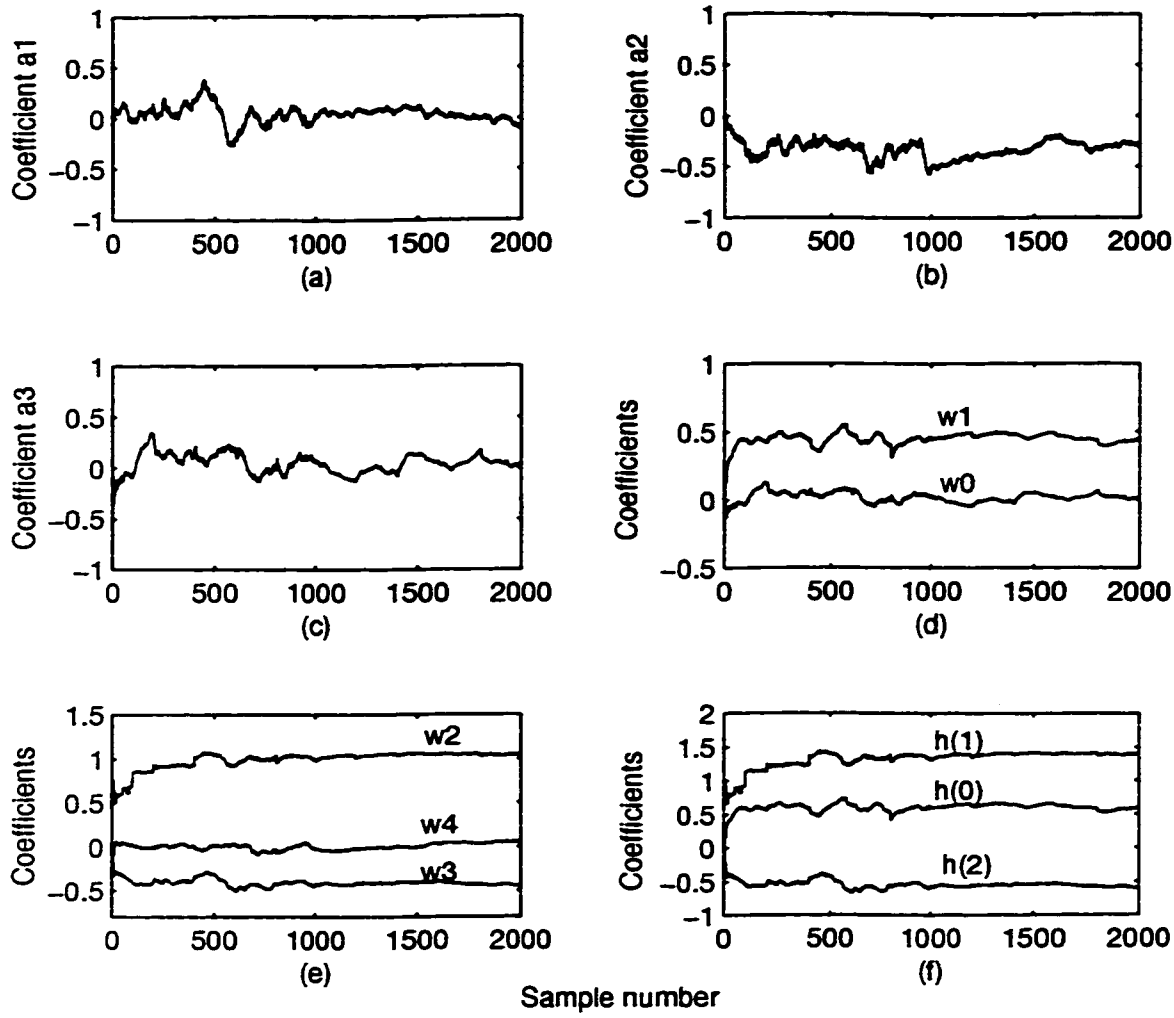

Figure 5.11: Equalizer coefficients for the channel with $H(z^{-1}) = 0.6 + 1.4z^{-1} - 0.6z^{-2}$. (a) First coefficient of the IIR predictor. (b) Second coefficient of the IIR predictor. (c) Third coefficient of the IIR predictor. (d) First and second coefficients of the adaptive FIR filter. (e) Third, fourth and fifth coefficients of the adaptive FIR filter. (f) Final channel estimate.

the coefficients converge to the channel parameter values and the remaining two fluctuate around zero, with a negligible amplitude. The final estimate of the channel is depicted in Fig. 5.12(f). From this plot, we can see that the proposed blind equalizer scheme estimates the unknown channel correctly. However, it now takes longer to achieve this estimate as compared to the channel of the first experiment. The value of the gain G for this experiment is 1.2872.

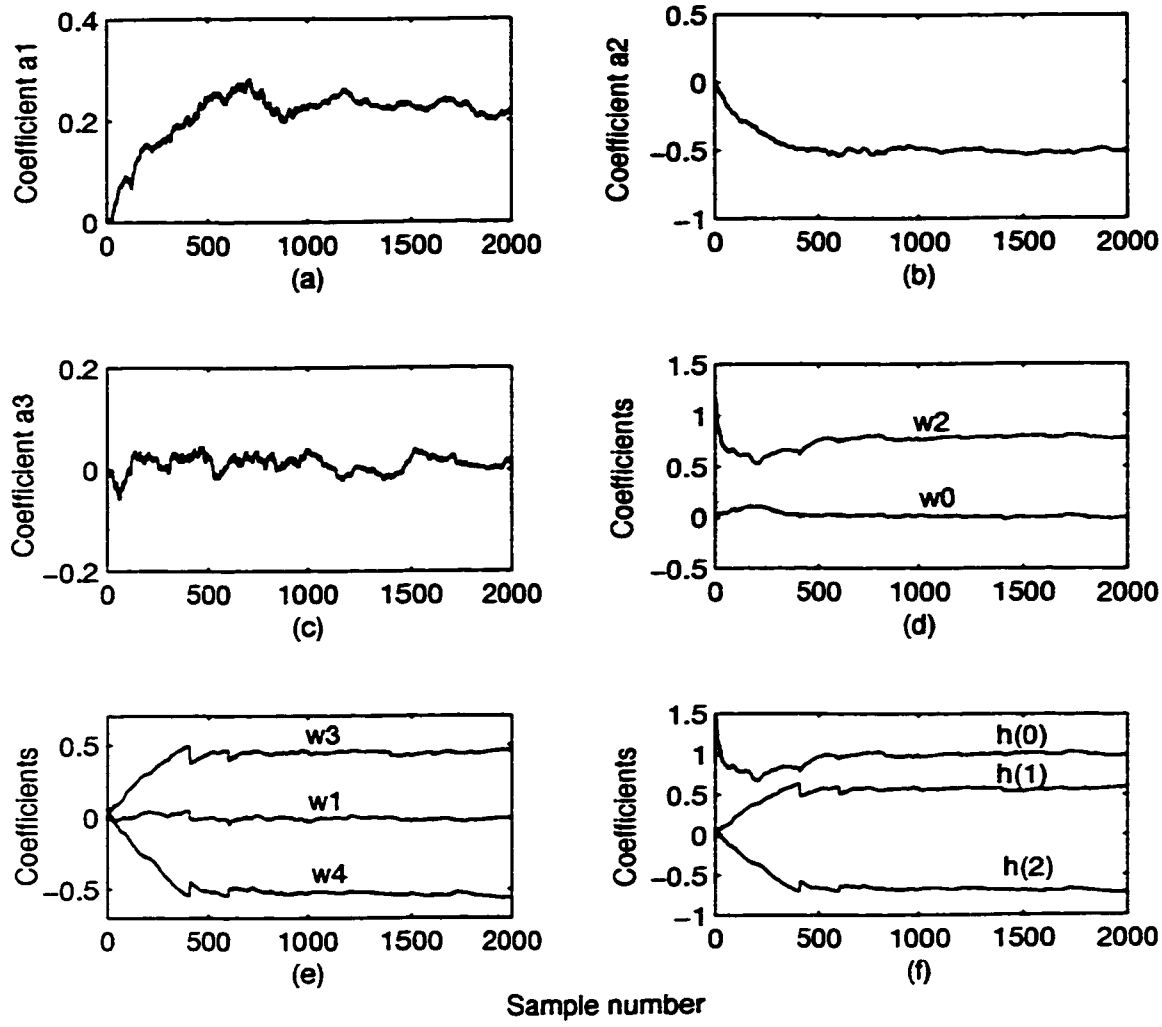

Figure 5.12: Equalizer coefficients for the channel with $H(z^{-1}) = 1.0+0.6z^{-1}-0.72z^{-2}$. (a) First coefficient of the IIR predictor. (b) Second coefficient of the IIR predictor. (c) Third coefficient of the IIR predictor. (d) First and third coefficients of the adaptive FIR filter. (e) Second, fourth and fifth coefficients of the adaptive FIR filter. (f) Final channel estimate.

For both the experiments described above, the data sequence $u(n)$ received at the input of the blind equalizer and the output $\overline{x}(n)$ of the second time reverser are plotted in Fig. 5.13. From the plots of data sequence $u(n)$, it can be observed that, as expected, for the first experiment, the amount of the inter symbol interference is smaller than that in the second experiment. From the plots of data sequence $\overline{x}(n)$, we can see that there is more

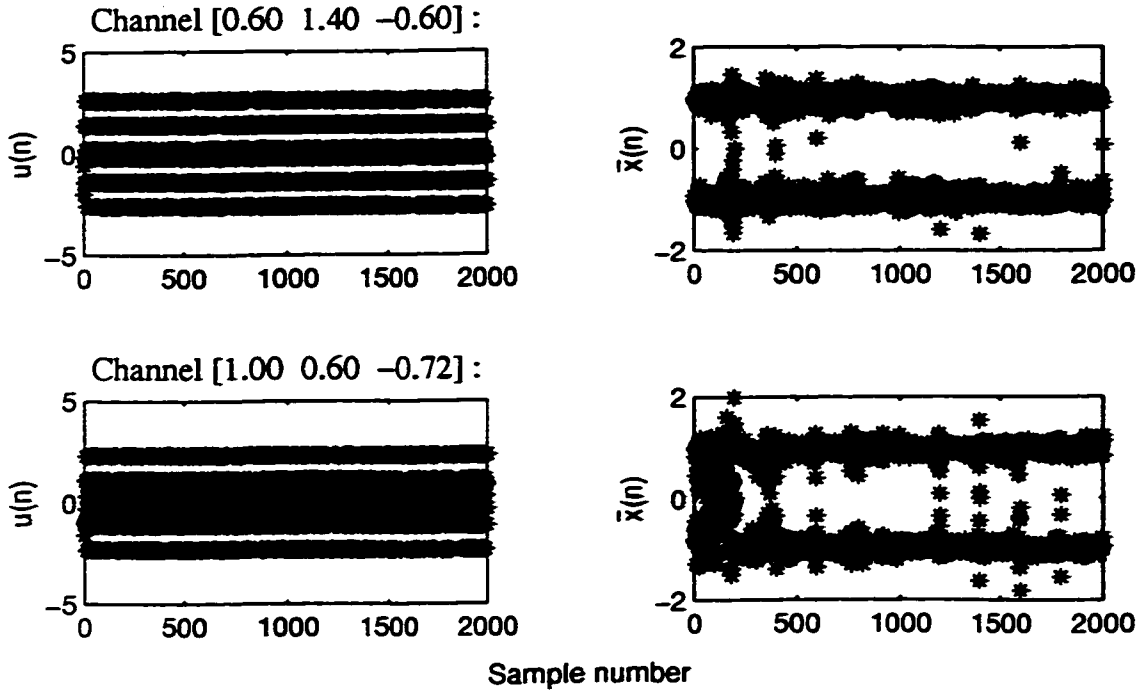

Figure 5.13: The data sequences $u(n)$ and $\bar{x}(n)$ at the input of the blind equalizer and at the output of the second time reverser, respectively for channels $H(z^{-1}) = 0.6 + 1.4z^{-1} - 0.6z^{-2}$ and $H(z^{-1}) = 1.0 + 0.6z^{-1} - 0.72z^{-2}$.

initial crowding of the data in the case of second channel which has a higher inter symbol interference. As a result, the blind equalizer now needs more number of samples, before it can estimate the channel correctly.

The values of the final channel estimate for all the 4 channels at the sample instant 2000 along with their standard deviations from the mean values are depicted in Table 5.3. To compare the performance of the proposed blind equalization scheme with the one introduced in [12], the results using the latter scheme are also presented in Table 5.4. From these tables it is noted that both the schemes estimate the unknown channel correctly. However, the proposed scheme has an advantage in that it has much smaller standard deviations from the mean values, thus making the proposed scheme more consistent in estimating the unknown channels.

Table 5.3: Blind estimate of second-order mixed-phase channels at the sample instant 2000 using the proposed blind equalization scheme.

Channel	Channel estimate $\{h(0)\ h(1)\ h(2)\}$	
	Mean	Std. deviation
{0.6000 1.4000 −0.6000}	{0.5928 1.3909 −0.6001}	{0.0007 0.0001 0.0001}
{1.0000 2.0000 −1.2500}	{0.9910 1.9991 −1.2517}	{0.0003 0.0008 0.0007}
{0.4000 1.2000 0.5000}	{0.3992 1.2030 0.5001}	{0.0006 0.0006 0.0003}
{1.0000 0.6000 −0.7200}	{0.9954 0.5987 −0.7201}	{0.0004 0.0001 0.0002}

Table 5.4: Blind estimate of second-order mixed-phase channels at the sample instant 2000 using the blind equalization scheme of [12].

Channel	Channel estimate $\{h(0)\ h(1)\ h(2)\}$	
	Mean	Std. deviation
{1.0000 2.0000 −1.2500}	{0.9875 1.9755 −1.2411}	{0.1338 0.0854 0.1136}
{0.4000 1.2000 0.5000}	{0.3984 0.1949 −0.4973}	{0.0208 0.0142 0.0275}
{1.0000 0.6000 −0.7200}	{0.9963 0.5928 −0.7158}	{0.0267 0.0310 0.0304}

From the above discussion, we can say that the proposed blind equalizer scheme estimates the unknown mixed-phase communication channel correctly for all levels of inter symbol interference and it gives better results than the scheme of [12], in terms of the standard deviations of the channel coefficients.

5.3.2 Effect of Additive White Gaussian Noise on the Performance of the Proposed Blind Equalizer

To study the performance of the proposed blind equalization scheme for mixed-phase communication channels under different levels of input signal-to-noise ratio, simulations are carried for all the 4 channels discussed in Section 5.3.1. A binary data sequence of 20000 samples has been transmitted in the range of 10 dB to 20 dB signal-to-noise ratio. The symbol error rate for all the 4 channels at 10 different values of the signal-to-noise ratio are plotted in Fig. 5.14.

From the plots of the symbol error rate it can be noticed that the maximum values of the symbol error rate themselves are very small for all the channels. However, the equalizer gives the best symbol error rate performance for the channel with its transfer

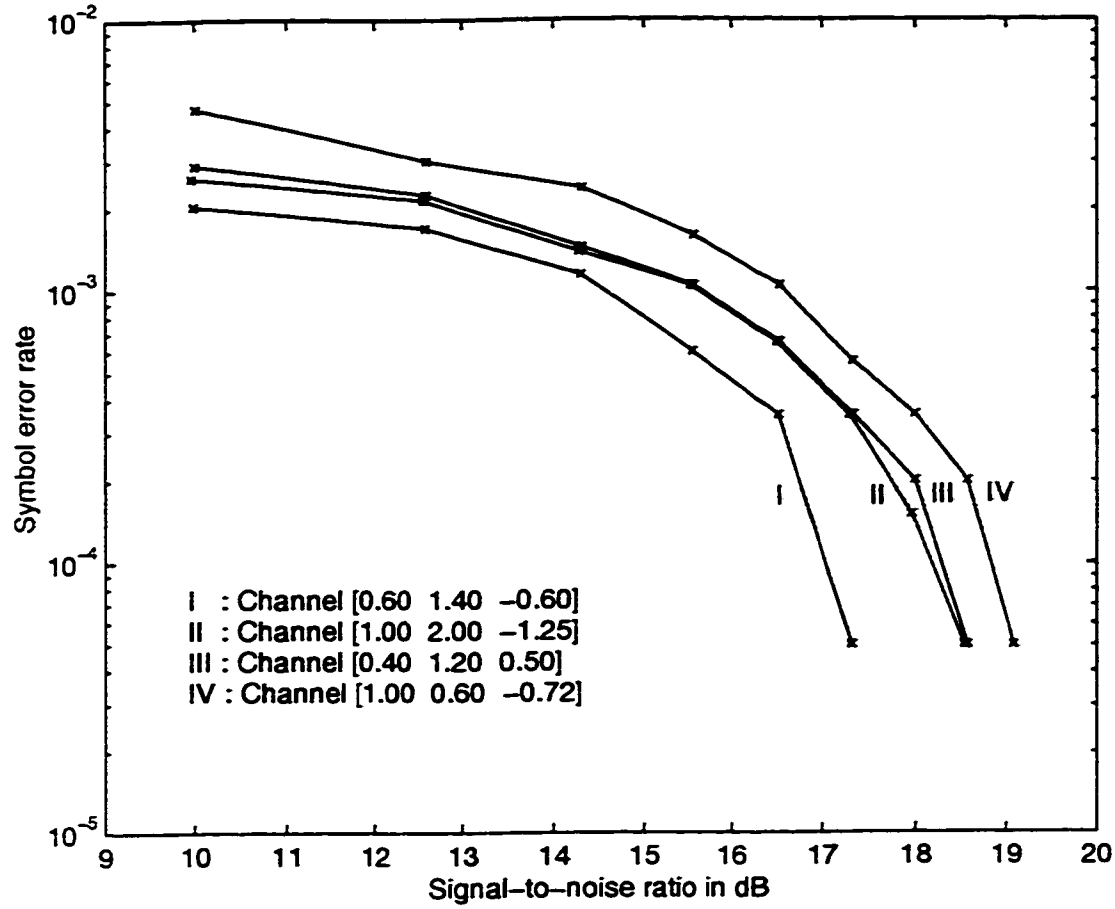

Figure 5.14: Symbol error rate for various mixed-phase communication channels.

function $H(z^{-1}) = 0.60 + 1.4z^{-1} - 0.60z^{-2}$. This is because of the fact that the roots of this channel being far away from the unit circle exert the least amount of the inter symbol interference amongst all. The symbol error rate plots of the channels with transfer functions $H(z^{-1}) = 1.0 + 2.0z^{-1} - 1.25z^{-2}$ and $H(z^{-1}) = 0.40 + 1.2z^{-1} + 0.50z^{-2}$ are almost overlapping. The reason for this is that the relative location of the zeros with respect to the unit circle are the same for both these channels.

From, the above discussions we conclude that the proposed blind equalizer works efficiently for the mixed-phase communication channels and gives very encouraging results even for lower values of the signal-to-noise ratio.

5.4 Experimental Results for Deep-Null Communication Channels

For a communication channel, the frequency-domain transfer function can be written as $H(e^{-j\omega})$. If at any frequency value, the spectral characteristic of $H(e^{-j\omega})$ possesses a zero or very low value, the signal power becomes negligible at that frequency. In other words, the signal-to-noise ratio becomes zero or very small whenever the spectral characteristic possesses nulls or assumes a small value [11]. In the z-domain, it means that zeros of the channel are either on or near the unit circle. The existing blind equalization algorithms, when applied to channels having deep spectral nulls, generally perform poorly for estimating the unknown channel. This is because of the fact that at or near the nulls, the signal power becomes negligible as compared to the noise power.

The performance of the proposed blind equalization scheme has already been studied for deep-null channels both in Chapter 4 and in this chapter in terms of estimation of the channel coefficients and symbol error rate. In order to make this study complete, we will now also consider the spectral performance of the blind equalization using the proposed scheme for deep-null channels. For this purpose, we attempt to obtain the estimate of a practical deep-null communication channel [12] characterized by the transfer function of a fourth-order maximum-phase FIR filter given by

$$H(z^{-1}) = 0.9413 + 0.3841z^{-1} + 0.5684z^{-2} + 0.4201z^{-3} + z^{-4} \tag{5.10}$$

This channel has complex zeros at $\frac{1}{0.98}e^{\pm j\pi/3}$ and at $\frac{1}{0.99}e^{\pm j3\pi/4}$. The length of the IIR predictor is taken as 5, while for the adaptive FIR filter as 9. The simulation is carried out for an equally probable binary data sequence of 3000 samples. The magnitude and phase responses of the estimated channel at the 1500th and 3000th sample instants along with the response of the actual channel is depicted in Fig. 5.15. From the magnitude and phase response plots, it can be seen that the proposed blind equalization scheme estimates the unknown channel completely despite the fact that it has deep spectral nulls. However, it takes it around 3000 samples to completely estimate such a deep-null communication channel.

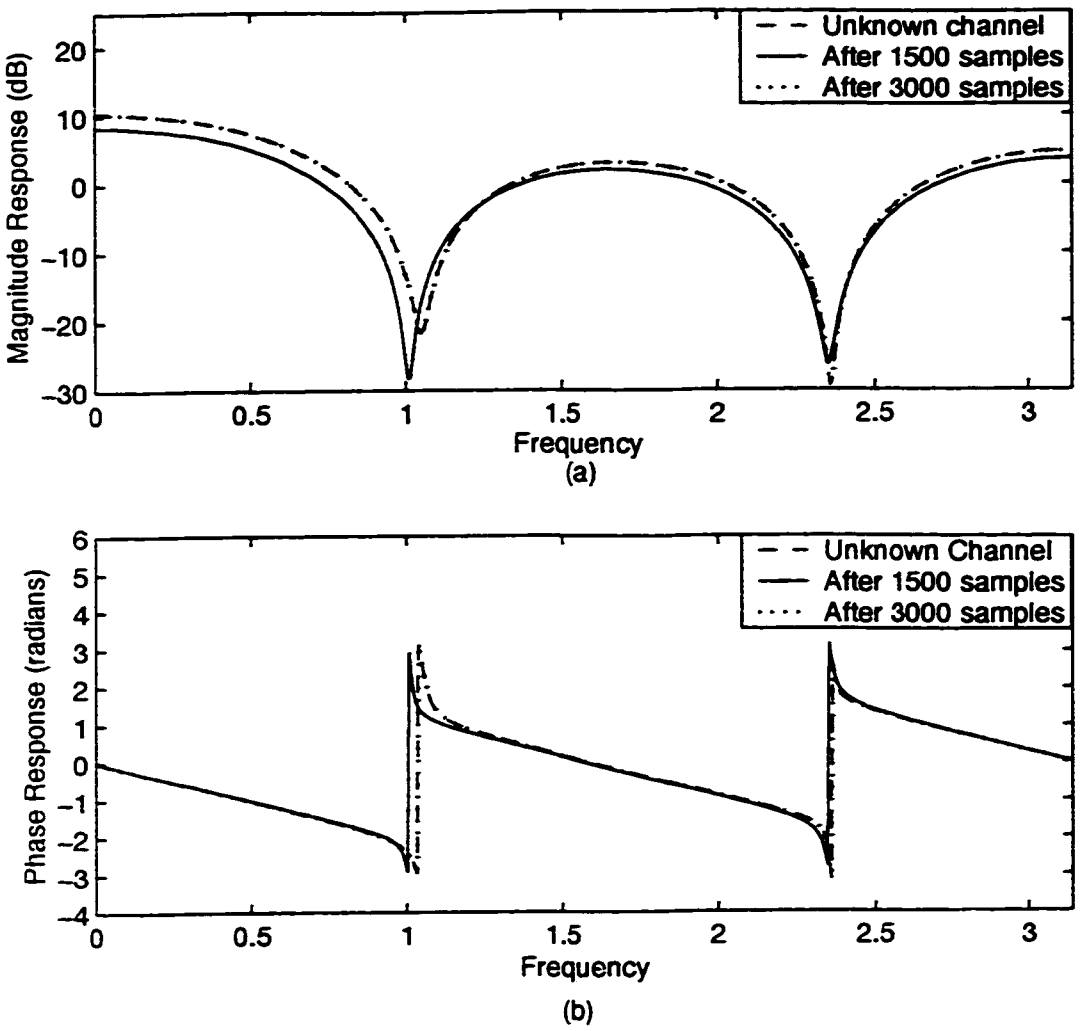

Figure 5.15: Frequency response of the estimated and the unknown deep-null channel. (a) Magnitude response. (b) Phase response.

5.5 Summary

In this chapter, the performance of the proposed blind equalization scheme has been studied for maximum-phase and mixed-phase communication channels.

Two types of experiments have been carried for the maximum-phase channels. In the first set of experiments, the performance test is carried out for different levels of inter symbol interference. Eleven channels have been used for this purpose. All the channels are modeled as first-order FIR filters to provide different levels of inter symbol interference.

From the experimental results, it is seen that as the amount of inter symbol interference increases, the convergence rates of the IIR predictor and FIR filter coefficients somewhat slow down. However, the proposed scheme estimates the unknown channel correctly. A comparison of the proposed scheme with the one presented in [12] has shown that the former scheme gives more consistent results.

In the second set of experiments, the symbol error rate of the proposed blind equalization scheme for different levels of the signal-to-noise ratio has been studied. The results have demonstrated that even for low levels of signal-to-noise ratio, the proposed scheme works efficiently and gives a very small value of the symbol error rate. It has been shown that with an increasing inter symbol interference, the symbol error rate increases and attains a negligible value at a higher value of the signal-to-noise ratio. A comparison of the proposed blind equalization scheme with the one given in [12] has also been carried out and it has been shown that the proposed scheme gives lower values of symbol error rate for all the levels of signal-to-noise ratio considered for this experimentation.

Next, the performance of the proposed blind equalization scheme for mixed-phase communication has been studied. Four channels, each modeled as a second-order mixed-phase FIR filter, were considered for this study. As was done in the case of maximum-phase channels, in this case also the convergence properties for estimating the unknown channel and the symbol error rate of the proposed blind equalization scheme were studied. It has been shown that the scheme works quite satisfactorily in both aspects of the performance.

Finally, to study the spectral performance of the proposed blind equalization scheme for the communication channels having deep spectral nulls a practical fourth-order mixed-phase channel has been taken. From the simulation results obtained, it is seen that the proposed scheme successfully estimates the channel for the entire frequency band including at frequencies having deep spectral nulls.

Chapter 6

Conclusion

6.1 Contributions of the Thesis and Concluding Remarks

This thesis has been concerned with the development of adaptive algorithms for the problem of blind equalization of communication channels with or without deep spectral nulls.

The traditional blind equalization schemes [1]-[9], employing only adaptive FIR filter-based structures, perform poorly for maximum-phase communication channels having deep spectral nulls. This problem is due to the difficulty of modeling the inverse of the maximum-phase communication channel with a finite-length adaptive FIR filter. An attempt has been made in [16]-[18] to solve this problem by using a blind equalization structure that makes use of an adaptive IIR predictor and an all-pass filter. This technique makes use of a fourth-order norm to estimate the unknown channel, thus requiring an extremely high computational complexity. A further attempt has been made in [12], to reduce this high computational complexity by using two block-based time reversers, in addition to IIR and FIR filters. However, this scheme reduces the computational complexity only to a certain extent. Moreover, the adaptive algorithm used for the adaptation of the IIR predictor may converge to an arbitrary point on the mean square output error surface, if the denominator polynomial of the IIR predictor does not satisfy a strictly positive real condition. This scheme also requires swapping of the IIR and adaptive FIR filters, for it to work satisfactorily at low levels of signal-to-noise ratio. Moreover, for the adaptation of the FIR filter, a normalized constant modulus adaptive-2 (CMA-2) algorithm has been used. A very high computational complexity of this algorithm makes the hardware implementation of the overall blind equalization scheme cost-ineffective.

In this thesis a new sufficient-order blind equalization scheme that attempts to address some of the above mentioned problems has been proposed. Similar to the scheme presented in [12], the proposed method uses a structure that is based on IIR and FIR filters and block-based time reversers. However, the new scheme incorporates simpler and more efficient algorithms for the adaptation of IIR predictor and FIR filter of the blind equalizer.

A new gradient-based adaptive algorithm to solve the convergence problem of the adaptive IIR predictor has been proposed. It has been shown that unlike the algorithm employed in [12], it does not require a test on the denominator polynomial of the IIR predictor transfer function to satisfy the strictly positive real condition. This adaptive algorithm is based on the well known least mean square error criterion.

A new constant modulus adaptive (CMA) algorithm for the adaptation of FIR filter of the blind equalization scheme has been proposed. It has been shown that the computational complexity of this algorithm is substantially lower than that of the CMA-2 algorithm used in [12]. It has also been shown that the proposed algorithm can be considered as an extension of the least mean square algorithm, thus making it well suited for an implementation using commercially available hardware.

Simulations have been carried out for a variety of minimum-phase, maximum-phase and mixed-phase communication channels with or without deep spectral nulls. The experimental results in terms of convergence of the adaptation coefficient, symbol error rate, and spectral response have demonstrated that even at the lower values of signal-to-noise ratio, the proposed blind equalization scheme works efficiently. Further, unlike the scheme of [12], it does not require the swapping of the IIR filter and the adaptive FIR filter, thus making the proposed scheme more versatile. It has also been shown that even in the presence of an intense inter symbol interference, the proposed blind equalization scheme estimates the channels correctly and yields better results than the existing schemes.

6.2 Scope for Future Investigation

In the proposed sufficient-order blind equalization scheme, two block-based time reversers have been used. These block-based time reversers store the output data sequences

of the IIR predictor and adaptive FIR filter, respectively. In the case of packet switching, the block length can be taken as equal to the length of each packet. However, in the case of circuit switching, this process may take a significant amount of time and reduce the data throughput of the channel. An investigation can be undertaken for finding an alternative of the block-based time reversers to improve the bandwidth efficiency.

The present investigation has been carried out for the development of a blind equalization scheme for an M-ary PAM system characterized by a baseband communication channel. In some applications, however, a passband quadrature amplitude modulation (QAM) system is used. In such an application, the proposed algorithm for the adaptation of the adaptive FIR filter can be used. However, an additional investigation would be required to extend the algorithm for the adaptation of the IIR predictor for a baseband communication channel for it to be used for QAM systems.

Finally, it may be worthwhile to look into the possibility of a hardware implementation of the sufficient-order blind equalization scheme proposed in this thesis.

References

[1] S. Haykin, *Adaptive Filter Theory*, 3rd ed. Upper Saddle River, NJ: Prentice-Hall, 1996.

[2] S.Haykin, *Communication Systems*. New York: John Wiley & Sons, 1988.

[3] R. W. Lucky, J. Salz, and E. J. Weldon Jr., *Principles of Data Communication*. New York: McGraw Hill, 1968.

[4] Y.Sato, "A method of self-recovering equalization for multilevel amplitude modulation systems," *IEEE Transactions on Communications*, vol. COM-23, no. 6, pp. 679-682, June 1975.

[5] A. Benveniste, M. Goursat, and G. Ruget, "Robust identification of a nonminimum phase system: Blind adjustment of a linear equalizer in data communications," *IEEE Transactions on Automatic Control*, vol. AC-25, no. 3, pp. 385-399, June 1980.

[6] A. Benveniste and M. Goursat, "Blind Equalizers," *IEEE Transaction on Communications*, vol. COM-32, no. 8, pp. 871-883, Aug. 1984.

[7] D. N. Godard, "Self-recovering equalization and carrier tracking in two-dimensional data communication systems," *IEEE Transaction on Communications*, vol. COM-28, no. 11, pp. 1867-1875, Nov. 1980.

[8] J. R. Treichler and B. G. Agee, "A new approach to multipath correction of constant modulus signals," *IEEE Transactions on Acoustics, Speech, and Signal Processing*, vol. ASSP-31, no. 2, pp. 459-472, Apr. 1983.

[9] J. R. Treichler and M. G. Larimore, "New processing techniques based on constant modulus adaptive algorithm," *IEEE Transactions on Acoustics, Speech, and Signal Processing*, vol. ASSP-33, no. 2, pp. 420-431, Apr. 1985.

[10] S. Haykin, *Blind Deconvolution*. Englewood Cliffs, NJ: Prentice-Hall, 1994.

[11] J. G. Proakis, *Digital Communications*, 2nd ed. New York: McGraw Hill, 1989.

[12] S. Lambotharan and J. A. Chambers, "A new blind equalization structure for deep-null communication channels," *IEEE Transactions on Circuits and Systems-II: Analog and Digital Signal Processing*, vol. 45, no.1, Jan. 1998.

[13] K. J. Astrom and T. Soderstrom, "Uniqueness of the maximum likelihood estimates of the parameters of an ARMA model," *IEEE Transactions on Automatic Control*, vol. AC-19, no. 6, pp. 769-773, June 1974.

[14] J. J. Shynk, "Adaptive IIR filtering," *IEEE ASSP Magazine*, pp. 4-21, 1989.

[15] P. S. R. Diniz, *Adaptive Filtering Algorithms and Practical Implementation*. Norwell, Massachusetts: Kluwer Academic Publishers, 1997.

[16] C. A. F. da Rocha, O. Macchi, and J. M. T. Romano, "An adaptive nonlinear IIR filter for self-learning equalization," *ITC, Rio de Janerio*, Brazil, pp. 6-10, 1994.

[17] C. A. F. da Rocha and O. Macchi, "A novel self-learning adaptive recursive equalizer with unique optimum for QAM," in *Proceedings of ICASSP-94*, Adelaide, Australia, pp. 481-484, 1994.

[18] J. A. Chambers and S. Lambotharan, "Phase inference and error surface analysis of a blind nonminimum phase channel equalizer," *IEE Colloquium Blind Deconvolution-Algorithms Applications*, Savoy Place, London, U.K., 1995.

[19] C. R. Johnson Jr., and M. G. Larimore, "Comments on and additions to, 'An adaptive recursive LMS filter'," in *Proceedings of IEEE*, vol. 65, no. 9, pp. 1399-1402, Sep. 1977.

[20] K. Binder, *Applications of the Monte Carlo Method in Statistical Physics*, vol. 36. New York: Springer-Verlag, 1984.

[21] L.R. Rabiner and R. W. Schafer, *Digital Processing of Speech Signals*. Englewood Cliffs, NJ: Prentice-Hall, 1978.

[22] L. R. Rabiner and B. Gold, *Theory and Application of Digital Signal Processing*. Englewood Cliffs, NJ: Prentice-Hall, 1992.

[23] A. V. Oppenheim and R. W. Schafer, *Digital Signal Processing*. Englewood Cliffs, NJ: Prentice-Hall, 1993.

[24] A. V. Oppenheim and R. W. Schafer, *Discrete-Time Signal Processing*. Englewood Cliffs, NJ: Prentice-Hall, 1989.

[25] J. G. Proakis, C. M. Rader, F. Ling and C. L. Nikias, *Advanced Digital Signal Processing*. New York: Macmillan Publishing Company, 1992.

[26] J. Das, *Review of Digital Communication*. New York: John Wiley & Sons, 1988.

[27] E. Biglieri and G. Prati, *Digital Communications*. New York: Elsevier Science Publishers B. V., 1986.

[28] J. G. Wade, *Signal Coding and Processing*. New York: John Wiley & Sons, 1987.

[29] M. S. Roden, *Digital Communication Systems Design*. Englewood Cliffs, NJ: Prentice-Hall, 1982.

[30] J. G. Proakis and M. Salehi, *Communication Systems Engineering*. Englewood Cliffs, NJ: Prentice-Hall, 1994.

[31] K. S. Shanmugan and A. M. Breipohl, *Random Signals: Detection, Estimation, and Data Analysis*. New York: John Wiley & Sons, 1988.

[32] *TMS320C54x DSP Applications Guide Reference Set*, vol. 4. Texas: Texas Instruments, 1999.

[33] B. Mulgrew and C. F. N. Cowan, *Adaptive Filters and Equalisers*. Norwell, Massachusetts: Kluwer Academic Publishers, 1988.

[34] M. L. Honig and D. G. Messerschmitt, *Adaptive Filters: Structures, Algorithms, and Applications*. Norwell, Massachusetts: Kluwer Academic Publishers, 1984.

[35] G. Picchi and G. Prati, "Blind Equalization and Carrier Recovery using a 'stop-and-go' decision directed algorithm," *IEEE Transactions on Communications*, vol. COM-35, pp. 877-887, 1987.

[36] O. Shalvi and E. Weindtein, "New criteria for blind deconvolution of non minimum phase systems (channels)," *IEEE Transactions on Information Theory*, vol. 36, pp. 312-321, 1990.

[37] S. Vembu, S. Verdu, R. A. Kennedy, and W. Sethares, "Convex cost functions in blind equalization," *IEEE Transactions on Signal Processing*, vol. 42, pp. 1952-1959, 1994.

[38] Y. Li and Z.Ding, "Global convergence of fractionally spaced Godard (CMA) adaptive equalizers," *IEEE Transactions on Signal Processing*, vol. 44, no. 4, pp. 818-826, 1996.

[39] B. Porat and B. Friedlander, "Blind Equalization of digital communication channels using high-order moments," *IEEE Transactions on Signal Processing*, vol. 39, pp. 522-526, 1991.

[40] D. Hatzinakos and C. L. Nikias, "Estimation of multipath channel response in frequency selective channels," *IEEE Journal on Selected Areas in Communications*, vol. 7, pp. 12-19, 1989.

[41] J. K. Tugnait, "Blind equalization and estimation of digital communication channel impulse response," *IEEE Transactions on Communications*, vol. 42, pp. 1606-1616, 1994.

[42] J. K. Tugnait, "Blind equalization and estimation of digital communication FIR channels using cumulant matching," *IEEE Transactions on Communications*, vol. 43, pp. 1240-1245, 1995.

[43] D. T. M. Slock, "Blind fractionally-spaced equalization, perfect-reconstruction filter banks and multichannel linear prediction," *in Proceedings of ICASSP-94*, Adelaide, Australia, pp. 585-588, 1994.

[44] S. C. Ng, C. Y. Chung, S. H. Leung, and A. luk, "Fast convergent genetic search for adaptive IIR equalizer," *in Proceedings of ICASSP-94*, Adelaide, Australia, vol. 3, pp. 585-588, 1994.

[45] L. Ljung and T. Soderstrom, *Theory and Practice of Recursive Identification*. Cambridge: MIT Press, 1983.